NOTE TO USERS

INVESTIGATION AND MODELLING OF THE HEAT TRANSFER PROCESS IN CARBON FIBRE/EPOXY COMPOSITE TOOLS

By

Magali Duval, B.Eng.

A thesis submitted to

The Faculty of Graduate Studies and Research

In partial fulfilment of

The requirements for the degree of

Master of Applied Science

Department of Mechanical and Aerospace Engineering

Ottawa-Carleton Institute

For Mechanical and Aerospace Engineering

Carleton University

Ottawa, Ontario

Your file Votre référence
ISBN: 0-494-13436-4
Our file Notre référence
ISBN: 0-494-13436-4

ABSTRACT

This research was focused on the understanding and modelling of the transient conductive heat transfer process in carbon fibre / epoxy composite tools. Using a comparative test method, the transverse and in-plane thermal conductivities of the 2/2 twill eight-ply laminate used in this research were determined as 0.57 W/mK and 1.87 W/mK respectively. These values were applied to the analytical and numerical models investigated. No simple closed form analytical solution was found that could accurately represent the problem. The finite element analysis software MSC Nastran Thermal Preference was used to carry out the numerical analysis of the problem. The modelling carried out indicated that the temperature gradients across the model were most affected by the applied convection and by the in-plane to transverse thermal conductivity ratio. Comparing modelling and experimental results showed that MSC Nastran was not flexible enough to allow accurate heater response predictions for use in advanced design of complex integrally heated composite tools.

À mes parents

ACKNOWLEDGEMENTS

I would like to acknowledge my supervisors, Professor P.V. Straznicky, for his invaluable help and advice given throughout the course of my research, and M. Donald Raizenne for providing the opportunity to carry out my research at the National Research Council Canada and for all the lessons learned in overcoming challenges.

I would also like to acknowledge the technicians at the Structures and Materials Performance Laboratory of the Institute for Aerospace Research, particularly the workers of the M-14 machine shop, without whom the experiments would not have taken place.

My appreciations also go to Comtek Advanced Structures Ltd who provided the carbon fibre prepreg for the research as well as ACG Ltd. who provided me with valuable information on the carbon fibre prepreg in question.

A particular thank you goes to Dr. Chun Li and Simon Hind whose support, advice and help were often key to understanding and improving results and simulations.

I also want to thank all those whose names are not mentioned but who contributed support and friendship. Most of all I would like to thank my parents for their unwavering support and belief in me throughout all of my education.

TABLE OF CONTENTS

LIST OF FIGURES

LIST OF TABLES

NOMENCLATURE

Acronyms:

AFP	Automated Fibre Placement
AFRP	Aramid Fibre Reinforced Polymer
ATL	Automated Tape Laying
CTC	Control Thermocouple
CTE	Coefficient of Thermal Expansion
CF/Ep	Carbon Fibre/Epoxy
CFRP	Carbon Fibre Reinforced Polymer
FEA	Finite Element Analysis
FEM	Finite Element Method
FG/Ep	Fibre Glass/Epoxy
GLARE©	GLAss REinforced aluminum laminate
GFRP	Glass Fibre Reinforced Polymer
HDPE	High Density Poly Ethylene
IAR	Institute for Aerospace Research
LCM	Liquid Composite Moulding
LE	Leading Edge
MLG	Main Landing Gear
NDI	Non-Destructive Inspection
NRC	National Research Council Canada
RFI	Resin Film Infusion
RTM	Resin Transfer Moulding
TC	Thermocouple
TE	Trailing Edge
VARTM	Vacuum Assisted Resin Transfer Moulding

Roman alphabet:

a	yarn width
A	cross sectional area
b	distance separating two fibre centres
c_p	specific heat
g	gap width
h	thickness, convection coefficient
h_c	interfacial thermal conductance
k	thermal conductivity
L	distance
p	proportional space occupied by the cylinders
q	heat
r	radius, radial distance
R	thermal resistance
S	area
t	thickness
T	temperature
$T_{\Lambda\Theta}$	transformation matrix
v	ratio of fibre to matrix thermal conductivity
v'	function of thermal conductivity
V_f	fibre volume fraction
x	spatial coordinate
y	spatial coordinate
z	spatial coordinate

Greek alphabet:

θ	angle, angular distance
Θ	temperature difference
ρ	density

Subscipts:

eff	effective
f	fibre, fill
HB	heater blanket
i	indice
l	longitudinal
r	radial
t	transverse
w	warp

1 Introduction

Modern aircraft are making more extensive use of advanced materials such as composites and hybrid materials. The interest in composite materials such as carbon fibre/epoxy (CF/Ep) or glass fibre/epoxy (GF/Ep) and hybrid materials such as GLARE© fibre metal laminates stems from their high strength to weight ratio. Composite and hybrid materials often have a lower density than metals, are capable of sustaining high tensile loads and are less prone to fatigue than metals. The degradation of strength at high temperatures restricts the use of most composites to temperatures below 150°C for structural applications [1][2]. The good load carrying capabilities of composites as well as their high resistance to fatigue make them ideal for many aircraft structural applications. The use of composites has been limited in the past due to their high costs and by the difficulties associated with inspection and damage assessment. New non-destructive inspection (NDI) techniques and better understanding of composites has led to improved manufacturing techniques and higher use of composites in aircraft. The weight reduction resulting from the use of composites in aircraft structures enables more efficient aircraft to be built.

In currently produced civil transport aircraft, use of composites has been restricted to primary empennage structures and to secondary structures in various parts of the aircraft. Composites were first used in flight surface primary structures on commercial aircraft on the Airbus A300. Boeing introduced composite flight surfaces in their 777 commercial aircraft. The use of composites on the Airbus A320 and Boeing 777 aircraft is shown in Figure 1-1 and Figure 1-2.

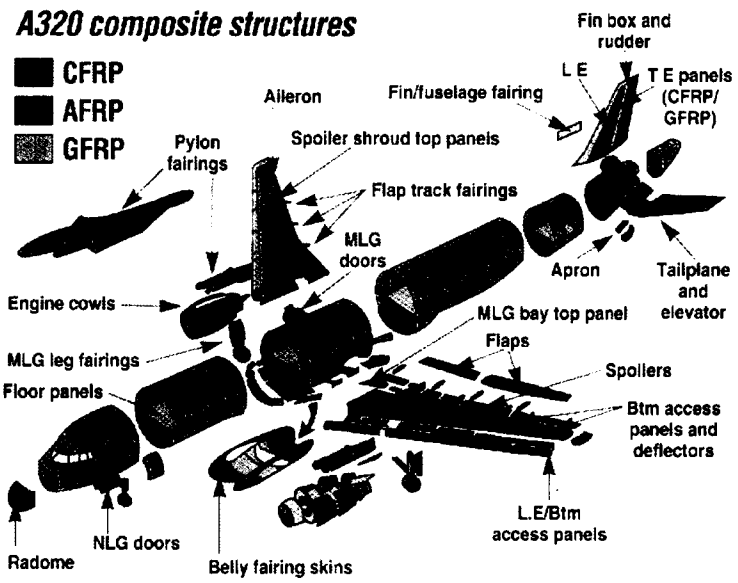

Figure 1-1: Composite Structures in the Airbus A320 [1]

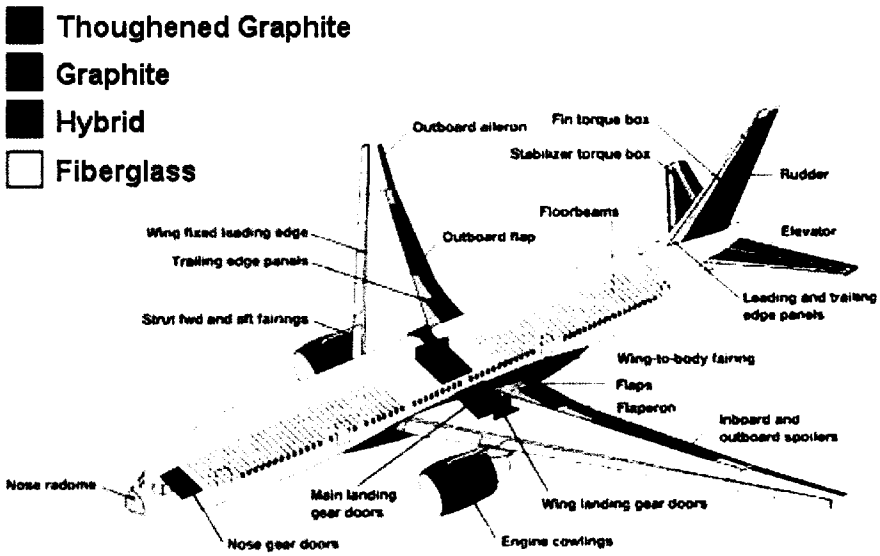

Figure 1-2: Composite Structures in the Boeing 777 [1]

New aircraft are making wider use of composites. Boeing's new 787 will have the most composite use of any commercial civil aircraft: 50% of its structure by weight is to be constructed of composites (Figure 1-3) [4]. Airbus is also increasing the amount of

advanced materials in their aircraft with the A380 having approximately 25% composite materials (Figure 1-4) [4].

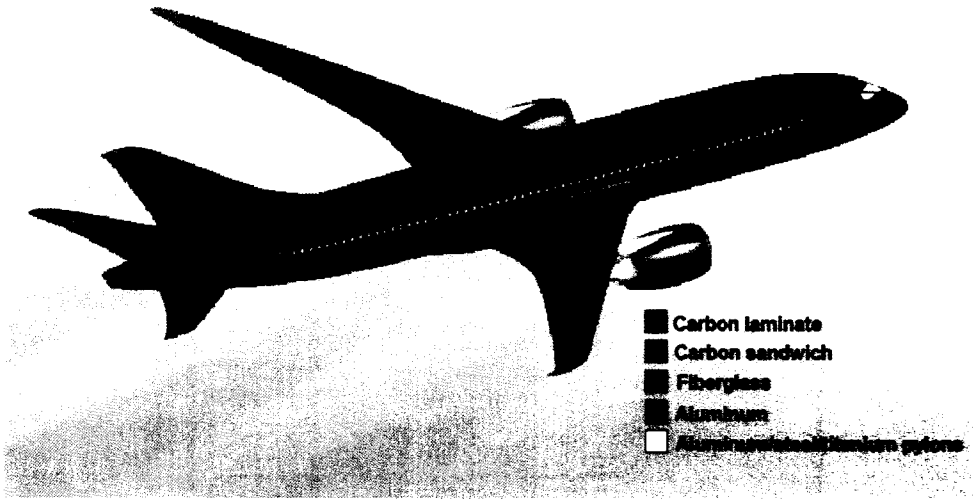

Figure 1-3: Exterior Material Composition for Boeing 787 Dreamliner [5]

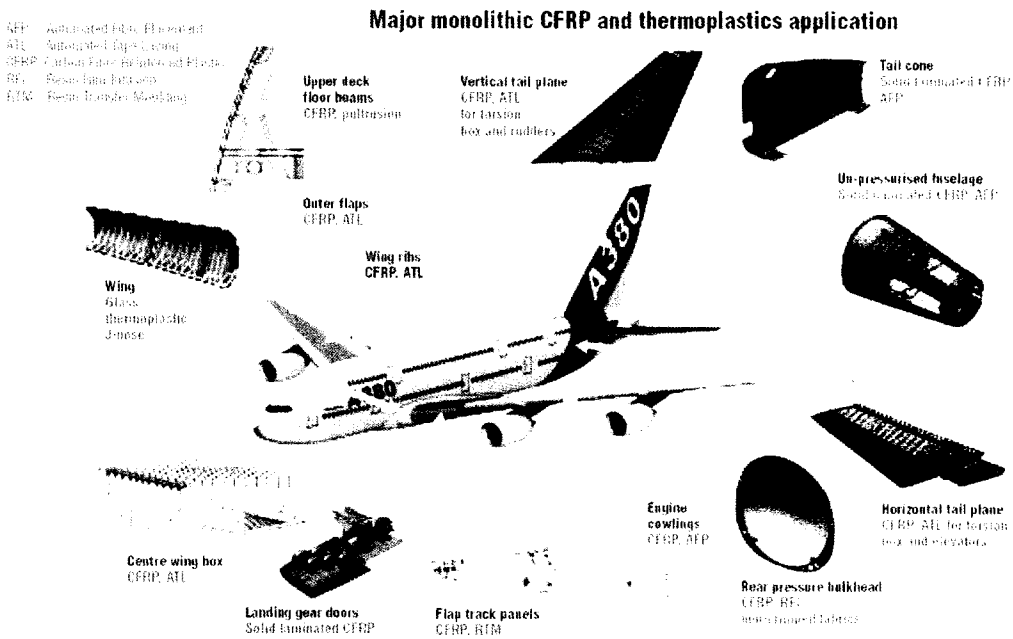

Figure 1-4: Composite Materials on the A380 [6]

Military aircraft, such as the Boeing F18, have made use of composites for a longer period of time, typically in control surface structures and aircraft skins. The use and experience gained in military application of composites has helped to increase their use in commercial aircraft.

Manufacturing of composites has typically been carried out by hand lay-up or automated fibre placement with autoclave curing. This results in expensive, high-energy consumption manufacturing processes. However, the increase in demand has been a driving factor in the emergence of low-cost composite manufacturing techniques for low to medium production industries such as the aerospace industry. Liquid composite moulding (LCM) techniques such as resin transfer moulding (RTM) or vacuum assisted resin transfer moulding (VARTM) can produce high quality parts out-of-autoclave, reducing manufacturing costs. Low-pressure processes such as VARTM have allowed lower cost composite tools to be used instead of the commonly used metallic tools. Aluminum, steel or Invar are typically used to manufacture composites, in order to sustain the high pressures encountered in autoclave and press manufacturing processes [7][8]. These tools or moulds are expensive to manufacture and can also prove difficult to modify or maintain. One major issue encountered when using aluminum and steel tools is that of mismatched coefficients of thermal expansion (CTE) between the substrate and the tool. This can lead to warping and dimensional inaccuracies in the finished product. Two methods of heating have been typically used for RTM and VARTM; convective heating using air-recirculation ovens and conductive

heating using integrally heated metallic tools. Radiation heating has also been used by means of heat lamps; however, this is typically used as a secondary rather than a primary heat source, usually for VARTM. Integral heating has also been reported for RTM applications to reduce processing times and increase initial resin flow. For these applications the metallic tools are heated using hot oil or electric cartridge heaters.

Conductive heating has been extensively used with composites, particularly in military applications, to repair both metallic and non-metallic structures. Heater blankets have been used to bond composite repair patches to the damaged structures. Despite the wide use of conductive heat transfer for bonded patch repair, little work has been reported on conduction heating of composites. Several issues are encountered when applying a conduction heating process to composite patches and to composites substrates. For example, direct conduction heating using uniform power density heaters can result in asymmetric temperature profiles in a CF/Ep composite laminate [9]. Uneven temperature distributions can lead to under-cured sections and to induced stresses due to mismatched coefficients of thermal expansion (CTE) between the composite patch and the patched structure and due to uneven degrees of cure obtained in the composite patch. This effectively reduces the load carrying capabilities and lifespan of the composite patch applied.

Based on its expertise with composite patch applications and with composite manufacturing, the National Research Council of Canada Institute for Aerospace Research (NRC-IAR) has developed a conduction-based heat transfer technique for use

with composite tooling. This integral heating technology uses heat transfer tiles coupled with multiple zones of closed loop temperature feedback control to ensure a uniform tool face temperature is achieved. NRC is currently applying this heating technology to VARTM and other resin infusion applications. The heating technique optimizes the cure cycle for each part, by using real-time temperature control and real-time epoxy cure kinetics and rheology to determine the optimum cure time based on the part's measured temperature. Applying this technology to LCM allows the processes to be made more cost effective by:

- Providing an accurate temperature distribution in the composite part being cured.
- Allowing epoxy cure cycle optimization through higher linear ramp rates, shorter soak times and epoxy cure kinetics optimization.
- Reducing the part scrap rate caused by epoxy under-curing.
- Optimizing the energy usage through conduction heat transfer.
- Increasing part throughput by providing more efficient manufacturing.

There has been very little reported work on the possibility of using integral tool heating with composite tools [9]. A number of process analysis studies have recognized that composite tools can be a cost-effective alternative to metallic tools for out-of-autoclave processes. The use of composite tools would result in similar CTE between the tool and the part, reducing the handling and post-processing costs associated to part machining [12]. Carbon Fibre/Epoxy (CF/Ep) and Glass Fibre/Epoxy (GF/Ep) woven prepreg composite systems are often used for composite tooling applications. Woven

materials offer more dimensional stability and are less prone to warping than the more traditional unidirectional materials used in composite structural applications. A composite tool heated with electric resistance heaters could produce good quality parts at lower energy consumption and with lower initial investment costs [9][11]

Tools for composite applications are often designed and made empirically, based on past experience. In order to further increase the efficiency of the composite manufacturing process, increased knowledge of the heat transfer process through the tool is required. This will allow for optimum placement of electric heaters, in order to achieve temperature homogeneity on the tool face. To date, all of the heat transfer work done at NRC has been based on experimentally derived data. The next step is to use this experimental data for the development of analytical and numerical models, which can be used to design integrally heated composite tools. This research is intended to contribute to the development of the design methodology for composite tooling and has the following objectives:

- to evaluate the use of commercially available finite element software for the purpose of modelling transient conductive heat transfer through a CF/Ep tool,
- to attempt developing a simple analytical model capable of predicting the transient conductive heat transfer process through a CF/Ep tool.

The initial phases of the thesis will focus on obtaining the thermal properties of the 2/2 twill CF/Ep composite prepreg used in this research in order to use these properties in the FEM and analytical models.

2 Literature Review

2.1 Background

The subject of composite tooling is not covered extensively in existing literature and none could be found regarding the heat transfer analysis of composites for tooling purposes.

In the current study, the composite tool to be investigated is a carbon fibre/epoxy (CF/Ep) 2/2 twill (Figure 2-1) woven laminate. This type of laminate is preferred to unidirectional laminates for tooling applications since it provides more strength and geometrical stability. The twill weave also offers more conformability than plain weave and unidirectional fabrics. The literature review will concentrate on this type of composite.

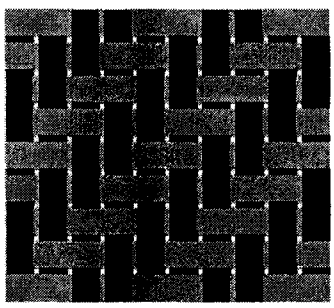

(a) Schematic representation

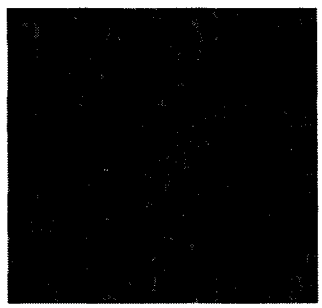

(b) Carbon fibre fabric

Figure 2-1: 2/2 Twill Weave Fabric

Most of the reported heat transfer analyses were carried out in order to better understand and improve the curing process of unidirectional laminate composites. The majority of these analyses focused on cure process parameters, such as degree of cure and reaction heat dissipation [13]-[18]. However, as composite tools are already cured, the cure information is not required for the heat transfer analysis considered in this thesis. The scale of the application is also important to consider; the CF/Ep tools are used to mould, heat up and cure large composite structures and the scale of interest is a macroscopic structural scale. Many models have been developed on sub-structural and microscopic scale in order to analyse the heat transfer process in composites [19],[20]. These models offer interesting information and knowledge of the processes involved, but are impractical to use in the analysis of large complex structures. Constitutive models such as the ones provided by Auriault et al. [21] and Graham et al. [22] yield valuable information, particularly in terms of transverse effective heat conductivity, and are more readily scaled up to structural scales.

2.2 Heat Transfer Processes for CF/Ep Tools

As with all heat transfer, three modes of heat transfer are possible for CF/Ep composites, namely convection, radiation and conduction.

In the case of CF/Ep tools, both the resin and reinforcing fibres are in solid state and neither undergoes a phase change to a fluid form. Consequently, the amount of heat transferred within the composite due to convection is negligible. The geometry and aspect ratios of the parts under consideration also render the amount of radiation heat transfer from and within the part negligible.

Within the CF/Ep tool, the primary form of heat transfer is conduction. The heat conduction occurs in three-dimensions; there is in-plane conduction in the x- and y-directions, and through-thickness conduction in the z-direction. In the case of unidirectional laminates, the longitudinal or y-direction has a different heat conduction rate than the x- and z-directions (Figure 2-2). In the case of a balanced woven fabric, if both the fill and warp are the same, it can be assumed that the two in-plane directions (Figure 2-3) have the same heat conduction characteristics while the transverse direction has a differing heat transfer rate.

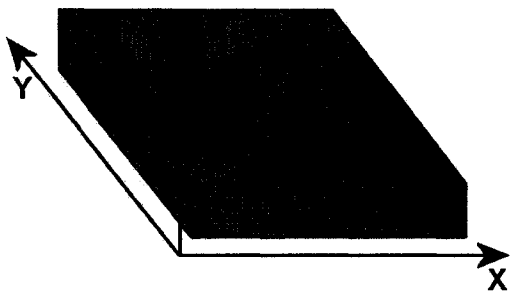

Figure 2-2: Unidirectional Laminate

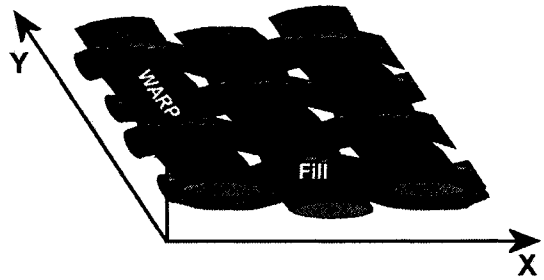

Figure 2-3: Plain Weave Fabric

The heat in the composite is conducted through the fibres and through the matrix. These components have differing thermal characteristics and the resulting composite material will have thermal properties between that of the fibre and that of the matrix. It should be noted that fibres are better heat conductors along their length than through their thickness. This results in a low through-thickness thermal conductivity that is further reduced by the thermal resistance at the fibre-to-matrix interface when the fibres are placed into a matrix. Although literature regarding the effects and determination of

thermal contact resistance between the fibre and the matrix is available [20]-[24], it has been shown that this thermal contact resistance can be assumed to have minimal influence on the effective thermal properties of the composite. Studies such as that of Ning et al. [25]-[26] as well as those of Zou et al., Kaminski and Roberts et al. [27]-[29], have shown that this assumption produces acceptable results for thermal models.

2.3 Required Physical Heat Transfer Parameters

In order to evaluate the heat transfer through a CF/Ep composite tool, knowledge of several physical parameters is required.

The composite tooling system is initially at room temperature and undergoes heating to a specified temperature, which is held for an optimal amount of time, before being brought back to room temperature. It is therefore subject to both transient and steady state heat transfer. The material properties needed to evaluate these heat transfer modes are:

- Fibre volume fraction
- Density
- Thermal Conductivity
- Specific Heat

Both the fibre volume fraction and the density of the composite prepreg material can often be obtained from the manufacturer. In cases where the fibre volume fraction is not known, James et al. [30] have shown it is possible to determine this through acid

digestion. Thermal conductivity and specific heat must be determined as they are required for steady-state and transient heat conduction analyses.

2.3.1 Steady-State Heat Conduction

For three dimensional conduction heat transfer, the following Laplace equation represents the temperature as a function of three spatial Cartesian coordinates [31][40]:

$$\frac{\partial^2 T}{\partial^2 x}+\frac{\partial^2 T}{\partial^2 y}+\frac{\partial^2 T}{\partial^2 z}=0 \qquad (2.1)$$

This equation can be solved analytically (for simple cases), numerically and graphically. The analytical solution is often carried out using the technique of separation of variables with known and homogenized boundary conditions. The solution to (2.1) is a function of all three spatial coordinates and is used to calculate the heat flow in the x, y and z directions with Fourier's Law [31]:

$$q_i = -kA_i \frac{\partial T}{\partial i} \qquad (2.2)$$

Where: q_i is the heat transfer rate in the i direction (W)

k is the thermal conductivity (W/mK)

A_i is the cross sectional area perpendicular to the heat flow q_i (m^2)

T is the temperature function (K)

i = x, y or z and is a spatial coordinate (m).

Four of these parameters are set by the geometry and operation settings, namely q, A, T and the spatial coordinate. The overall thermal conductivity, k, is a material property. In the case of a composite material, this property is a combination of the fibre

and resin's respective thermal conductivities. Due to the anisotropy of both the composite material and the fibres themselves, both the transverse and in-plane thermal conductivities need to be evaluated.

2.3.1.1 Thermal Conductivity in Unidirectional Laminates

Longitudinal Thermal Conductivity

In the case of a unidirectional laminate being subjected to a heat flow, the thermal conductivity in the direction of the fibre can be defined using the rule of mixtures approach. Hashin [32] and Halpin [33] have shown that:

$$k_l = V_f k_{l,f} + (1 - V_f) k_r \tag{2.3}$$

Where: k_l is the longitudinal thermal conductivity of the composite

V_f is the fibre volume fraction of the composite

$k_{l,f}$ is the longitudinal thermal conductivity of the fibre

k_r is the thermal conductivity of the resin.

It should be noticed that the resin is assumed to be isotropic, whereas here the fibre is assumed to be anisotropic.

Transverse Thermal Conductivity

The transverse thermal conductivity of a laminate is a function of the fibre and resin thermal conductivities, but it cannot be represented by a rule of mixtures approach. Several methods have been proposed to mathematically define the transverse conductivity of unidirectional composites. Some of these are discussed in this section.

The model proposed by Rayleigh [34] has inspired many representative volume element models. Rayleigh elaborated a mathematical model to describe the transverse

conductivity of a material containing a rectangular array of cylindrical inclusions as shown in Figure 2-4.

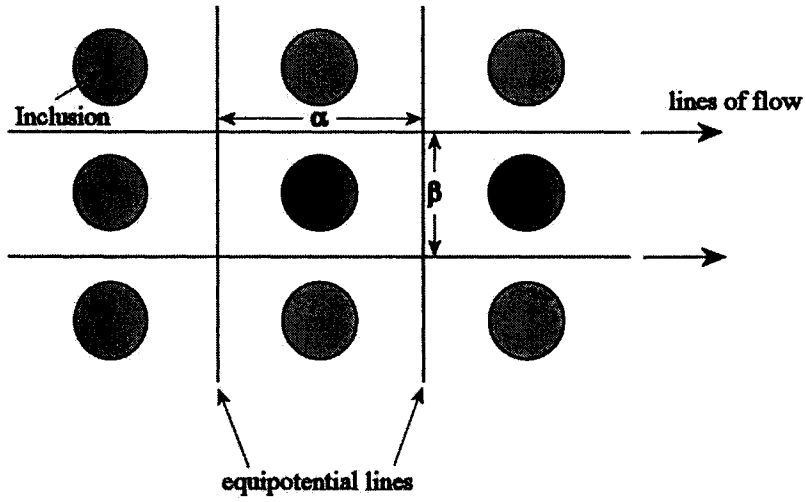

Figure 2-4: Rectangular array of cylindrical inclusions

To carry out his analysis he assumed that the inclusions and the medium possessed different thermal conductivities and derived the following expression for thermal conductivity [34]:

$$k_{t,eff} = k_r \left[1 - \frac{2p}{v' + p - \frac{3p^4}{v'\pi^4} S_4^2 - \frac{7p^8}{v'\pi^8} S_8^2} \right] \qquad (2.4)$$

Where: $k_{t,eff}$ is the effective transverse thermal conductivity

k_r is the matrix thermal conductivity

p is the proportional space occupied by the cylinders equal to $(\beta/\alpha)*V_f$ in the case of a rectangular arrangement.

v' is a function of conductivity of the cylinders such that v' = (1+v)/(1-v)

v is the ratio of fibre to matrix thermal conductivity

S_4 and S_8 are equation constants respectively equal to 3.1512 and 4.2557 in the case of a square arrangement where $\alpha = \beta$.

The thermal conductivity value found can be effectively interpreted as a ratio of the composite thermal conductivity over the resin thermal conductivity. This model has been found to represent the transverse thermal conductivity of materials with acceptable accuracy. It does not take into account the thermal contact resistance between fibres and resin.

Farmer et al. proposed a model that is based on Rayleigh's and that includes the effects of the thermal contact resistance between the matrix and the fibres. The modification made on Rayleigh's model concerns only the expression of the function of conductivities v':

$$v' = \frac{\left(v^{-1} + 1 + \frac{k_r}{ah_c}\right)}{\left(v^{-1} - 1 + \frac{k_r}{ah_c}\right)} \qquad (2.5)$$

Where: h_c is the interfacial thermal conductance across the fibre-matrix interface

The Hasselman-Johnson thermal conductivity model is also based on Rayleigh's findings and includes the thermal contact resistance between the matrix and the fibre. The resulting effective transverse thermal conductivity model is as follows:

$$k_{t,eff} = k_r \frac{\left[\left(\frac{k_f}{k_r} - 1 - \frac{k_f}{r_f h_c}\right)V_f + \left(1 + \frac{k_f}{r_f h_c} + \frac{k_f}{k_r}\right)\right]}{\left[\left(1 + \frac{k_f}{r_f h_c} + \frac{k_f}{k_r}\right)V_f + \left(1 + \frac{k_f}{r_f h_c} + \frac{k_f}{k_r}\right)\right]} \quad (2.6)$$

Where: $k_{t,eff}$ is the effective transverse thermal conductivity

k_r is the matrix thermal conductivity

k_f is the isotropic fibre thermal conductivity

r_f is the fibre radius

h_c is the interfacial thermal conductance across the fibre-matrix interface

The Hasselman-Johnson thermal conductivity model provides accurate representation of the thermal conductivity up to fibre volume fractions of 50% and is within a 5% error up to fibre volume fractions of 70%. Graham et al. created a finite element model that was verified against the Hasselman-Johnson model [22].

In order to apply the Farmer and Hasselman-Johnson thermal conductivity models, it is necessary to have a measure of the value of the thermal contact conductance. This makes the models difficult to use, as there are no methods to directly measure the thermal contact conductance; it has typically been back calculated from experimental results [20].

Cha et al. [24] developed a mathematical model using a similar approach but with a triangular fibre arrangement as opposed to a rectangular one. A set of equations were developed, and the effective thermal conductivity was defined as follows:

$$k_{t,eff} = \frac{q_0 L}{\overline{T_L} - T_0} \tag{2.7}$$

Where: $k_{t,eff}$ is the effective transverse thermal conductivity of the composite

q_0 is the is the uniform heat flux applied to the top boundary

L is the distance separating two fibre centres in the z-direction

T_0 is the uniform temperature of the bottom boundary

$\overline{T_L}$ is the is the average temperature at a horizontal plane and is expressed by: $\overline{T_L} = \frac{1}{b}\int_0^b T(x,L)dx$ where b is the distance separating two fibre centres in the x direction.

This model was solved numerically and the results obtained were compared to the Hasselman-Johnson model; it was found that the model proposed by Cha et al. produced valid results up to fibre volume fractions of 70%. The solutions obtained also allowed the estimation of the fibre's transverse conductivity [24].

Other methods, not based on the representative volume element approach have also been used to determine the transverse thermal conductivity of unidirectional laminates. One such method is that by James et al. [30] who proposes that transverse thermal conductivity cannot be obtained through one simple analytical expression due to the dependence of thermal conductivity on geometry and volume fractions. Instead, the

thermal conductivity can be bound by two equations. In this case, the higher bound would be provided by the rule of mixtures (equation (2.3)) and the lower bound would be given by the Thornburgh and Pears equation [30]:

$$\frac{1}{k_t} = \frac{V_f}{k_f} + \frac{(1-V_f)}{k_r} \tag{2.8}$$

The equations proposed effectively provide a lower and upper limit for transverse thermal conductivity.

Another approach is to use the analogy between thermal conductivity and in-plane shear. This is the approach that is proposed by Halpin [33] , leading to the following equation set for the determination of effective transverse thermal conductivity:

$$\frac{k_t}{k_m} = \frac{(1+\zeta\eta V_f)}{(1-\eta V_f)}$$

$$\eta = \frac{(k_f/k_m - 1)}{(k_f/k_m + \zeta)} \tag{2.9}$$

$$\zeta = \frac{1}{4-3V_m}$$

Where k_f is the isotropic thermal conductivity of the fibre. The results provided by this model were found to be in agreement with available experimental results.

Springer and Tsai also proposed a model for the transverse thermal conductivity of unidirectional laminates, as reported by Twardowski [39]. The Springer-Tsai model as corrected by Walker [39], is as follows:

$$\frac{k_t}{k_m} = \left(1 - 2\sqrt{\frac{V_f}{\pi}}\right) + \frac{1}{B}\left[\pi - \frac{4}{\sqrt{1-\left(\frac{B^2 V_f}{\pi}\right)}} \tan^{-1} \frac{\sqrt{1-\left(\frac{B^2 V_f}{\pi}\right)}}{1 + B\sqrt{\frac{V_f}{\pi}}}\right] \tag{2.10}$$

$$B = 2\left(\frac{k_m}{k_f} - 1\right)$$

Where k_f is the isotropic fibre thermal conductivity. This model was found to have a good accuracy and has been used to model experiments.

2.3.1.2 Woven Fabric Composites

Very little work has been reported regarding the heat transfer properties of woven fibre laminates. Dasgupta et al. [35] have proposed a model to evaluate the thermal conductivity of woven composites. Ning et al. [25][26] have developed closed-form solutions for the evaluation of the in-plane and transverse thermal conductivities of woven composite fabric. Both the model and the closed-form solutions are based on the thermal-electrical resistance analogy.

In-Plane Thermal Conductivity

Ning et al. [25] assumed a plain non-hybrid weave laminated composite. The warp and fill parameters are assumed to be different, yielding different thermal conductivities for the two in-plane directions. To carry out the analysis a unit cell is defined and idealized as shown in Figure 2-5.

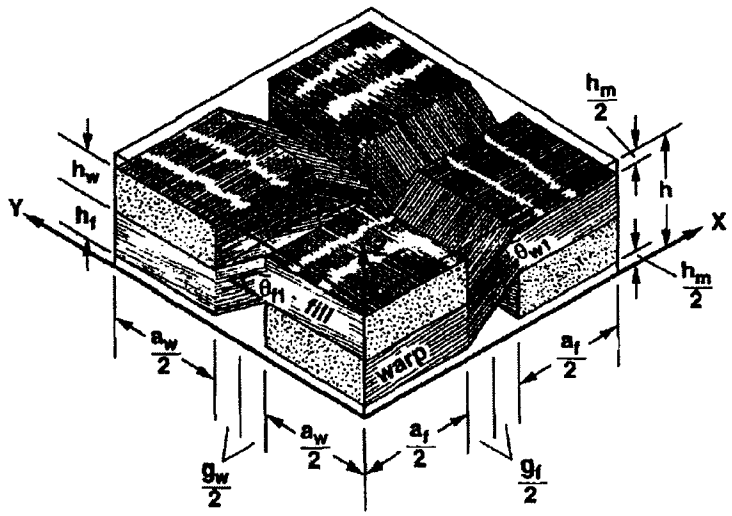

Figure 2-5: Idealized Unit Cell for Plain Weave Laminate [25]

The unit cell is sectioned into elements based on the properties of the materials present. The thermal resistance, R_i, of the *i*th conduction element is defined as:

$$R_i = \frac{L_i}{k_i S_i} \qquad (i = 1,2,...n) \tag{2.11}$$

Where: L_i is the length of the *i*th conduction element

k_i is the effective thermal conductivity of the *i*th conduction element

S_i is the area of the conduction element cross-section perpendicular to the heat flow.

All elements are evaluated and an overall equivalent resistance expression is derived using the effective in-plane thermal conductivity $k_{eff,w}$. Equating these, an expression for the effective thermal conductivity in the warp direction is obtained:

$$k_{eff,w} = \frac{1+\frac{g_f}{a_f}}{1+\frac{g_w}{a_w}} \left\{ \frac{k_r}{1+\frac{g_f}{a_f}} \left[\left(1+\frac{g_w}{a_w}\right)\frac{h_r}{h} + \frac{g_w}{a_w}\frac{h_w}{h} \right] + \frac{h_f}{h}\frac{g_w}{a_w}\left(\frac{1}{k_{f1}} + \frac{g_f}{a_f}\frac{1}{k_r}\right)^{-1} \right.$$

$$+ \frac{h_f}{h} \frac{1}{\frac{1}{k_{f2}} + \frac{g_f}{a_f}\left[\frac{1}{2}k_r + \left(\frac{1}{k_r} + \frac{1}{k_{w1}}\right)^{-1}\right]^{-1}} \qquad (2.12)$$

$$\left. + \frac{1}{\frac{1}{k_{w2}\frac{h_w}{h}} + \frac{g_f}{a_f}\left[k_{w1}\left(\frac{h_w}{h} - \frac{1}{2}\frac{h_f}{h}\right) + \frac{h_f}{h}\left(\frac{1}{k_{w1}} + \frac{1}{k_r}\right)^{-1}\right]^{-1}} \right\}$$

Where: g_f, g_w are the gap width between two neighbouring yarns

a_f, a_w are the width of the fill and warp yarns

h is the thickness of the lamina

h_f, h_w are the thicknesses of the fill and warp yarns

h_r is the thickness of the matrix

k_r is the thermal conductivity of the matrix

k_{di} are the thermal conductivities of the yarns with the fibres at an angle in the warp or fill direction (d = w,f ; i = 1,2).

Results of predictions done using this model were found to match up well with those found in other literature, namely those of Dasgupta et al. [35].

Dasgupta et al. [35] proposed an analytical model based on the thermal resistance of the components and their networking. Unlike Ning et al. [25],[26], the analytical model is not independent of heat transfer parameters, which are assumed uniform in order to

obtain a solution. Numerical analysis and experiments were also carried out to evaluate the accuracy of the model.

Transverse Thermal Conductivity

Ning et al. [26] followed the same partitioning of an idealized unit cell to develop an expression for the transverse effective thermal conductivity of a plain non-hybrid weave laminate:

$$k_{eff,t} = \frac{k_r}{\left(1+\frac{g_w}{a_w}\right)\left(1+\frac{g_f}{a_f}\right)}\left[\frac{g_w}{a_w}\frac{g_f}{a_f} + \frac{\frac{g_f}{a_f}}{\left(\frac{h_r}{h}+\frac{h_f}{h}\right)+\frac{k_r}{k_{w1}}\frac{h_w}{h}} + \frac{1}{\frac{h_r}{h}+\left(\frac{k_r}{k_{w2}}\frac{h_w}{h}+\frac{k_r}{k_{f2}}\frac{h_f}{h}\right)} + \frac{\frac{g_w}{a_w}}{\left(\frac{h_r}{h}+\frac{h_w}{h}\right)+\frac{k_r}{k_{f1}}\frac{h_f}{h}}\right] \tag{2.13}$$

Results obtained from Ning et al.'s transverse thermal conductivity model were compared with other existing models and experimental data. The results obtained were found to be in agreement with the pre-existing data.

It should be noted that both models proposed by Ning et al. [25][26] are developed using the geometry of the weave, and as such do not make any assumptions regarding boundaries or heat flow parameters.

Dasgupta et al. [35] also studied the transverse thermal conductivities of weaves. As the model for the in-plane and transverse thermal conductivities were developed

using a similar approach, the transverse thermal conductivity model is also dependent on the thermal boundaries applied.

2.3.2 Transient Heat Conduction

Transient heat conduction occurs as the material is being heated up or cooled down. In the case of composite manufacturing, the interest is on the heating, sometimes termed ramp-up, to the curing temperatures. For certain composites, it may be necessary to have multiple ramp-ups for the same cure, if different curing temperature levels are required for the properties expected of the finished product. Transient heat conduction is governed by [15],[36]:

$$\frac{\partial}{\partial t}\left(\rho c_p T\right) = \nabla\left(k \nabla T\right)$$

or: (2.14)

$$\frac{\partial}{\partial t}\left(\rho c_p T\right) = \frac{\partial}{\partial x}\left(k_x \frac{\partial T}{\partial x}\right) + \frac{\partial}{\partial y}\left(k_y \frac{\partial T}{\partial y}\right) + \frac{\partial}{\partial z}\left(k_z \frac{\partial T}{\partial z}\right)$$

Where: t is time (s)

c_p is the specific heat (J/kg-K)

k is the anisotropic thermal conductivity (W/mK)

T is temperature (K)

∇ is the gradient operator

In order to be able to evaluate this equation, the specific heat of the composite must be known. Unlike thermal conductivity, specific heat is not a directional property of the

material. If the specific heats for the matrix and the fibre are known, the value for the composite specific heat can be obtained using the rule of mixtures approach [14]:

$$\rho c_p = \rho_f V_f c_{p,f} + \rho_r (1 - V_f) c_{p,r} \tag{2.15}$$

Where: ρ is the density of the composite (kg/m^3)

ρ_f, ρ_r are the fibre and resin densities

$c_{p,f}$, $c_{p,r}$ are the specific heat of the fibre and resin (J/kg-K)

It should be noted that work has been reported in which transient heat conduction analysis was used to determine the thermal conductivity of the composite [28]. This does not seem to be the preferred method, as most research found in the literature indicates that the thermal conductivity was found using steady-state heat conduction analysis.

2.4 Experimental Determination of Thermal Properties

Many mathematical models have been developed to represent heat transfer through composites. However, few reported experiments have been carried out to verify these models. The observed trend is to verify the models by using a previously established model. Therefore there is little information in literature regarding the experimental procedures used to determine the thermal properties of composite materials.

Of the experimental procedures reported, the trend has been towards the use of smaller sized specimens, mostly due to concerns over the cost of manufactured composites. All experimental procedures reported make use of thermocouples to obtain

specimen temperature readings at steady-state. James et al. [30] noted that errors introduced in temperature measurement often amount to ±10% error in the value of thermal conductivity calculated. In order to remedy this problem, certain researchers use a correction factor in the calculation of the thermal conductivity [18].

Three types of apparatus for thermal conductivity measurement have been described in literature. Farmer et al. [20],[23] and Hsu [38] used a guarded hot plate apparatus, as shown in Figure 2-6, which is designed to measure the thermal performance of materials with low thermal conductivity. This apparatus can measure both the in-plane and transverse thermal conductivities of the composites, using plate specimens as shown in Figure 2-7. In order to obtain a thermal conductivity value, the apparatus measures and averages the properties obtained for two nearly identical specimens being tested simultaneously.

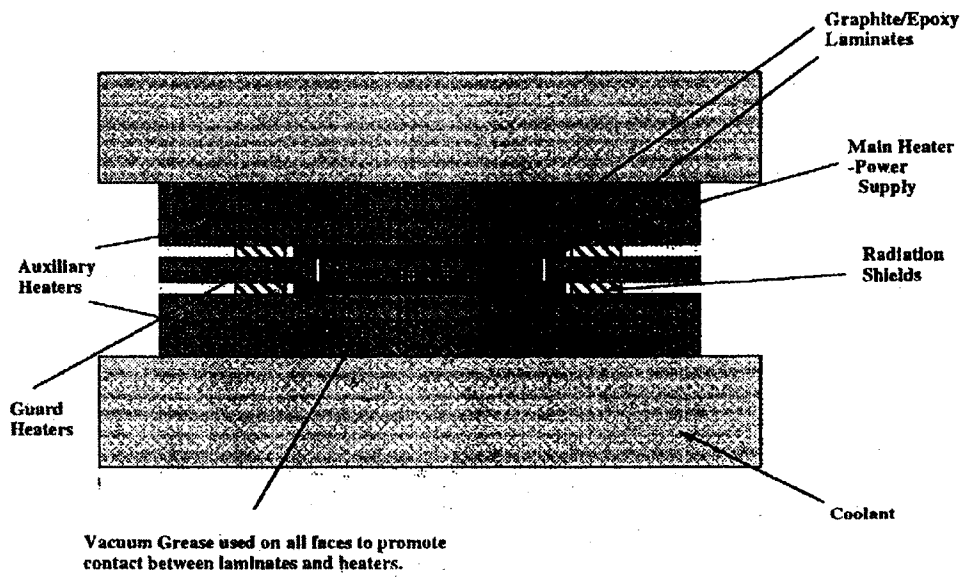

Figure 2-6: Guarded Hot Plate Apparatus with Experimental Setup Enclosed in a Vacuum [23]

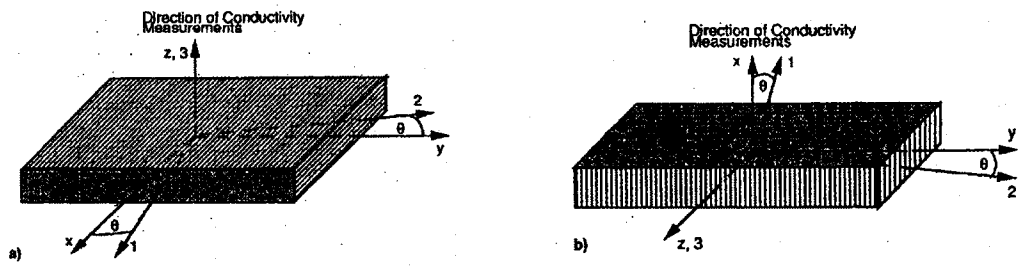

θ denotes the ply alignment in degrees

θ denotes the ply alignment in degrees

Figure 2-7: Specimens used by Farmer et al. for Thermal Conductivity Measurements a) in-plane and b) transverse [23]

Han et al. [37] used a similar concept. The apparatus used in this case consists of an electric foil heater centered between two aluminum faceplates, which constitutes the central heat source. The samples are placed on either side of the heat source, adjacent to the faceplates and are cooled on the outer edges by cooling plates. The cooling plates located on both external faces are cooled by means of cold water circulating within the plates. This apparatus is shown in Figure 2-8.

In order to adequately measure the heat flow, thermocouples are positioned in the faceplates, on the cooling plate surfaces and in the specimens along the heat flow axis.

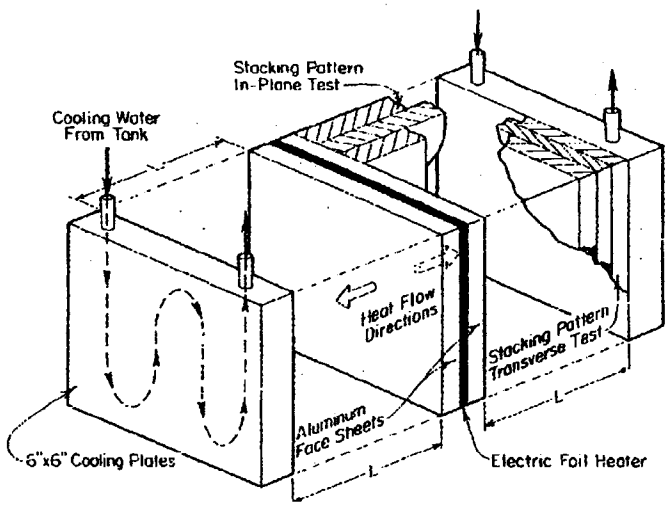

Figure 2-8: Thermal Conductivity Measurement Apparatus Used By Han et al. [37]

James et al. [30] chose a comparative approach for the measurement of thermal conductivity. Two standards of known thermal conductivity are used to measure the heat flow and once this heat flow has stabilised, the thermal conductivity of the samples can be determined. A schematic of the experimental set-up is given in Figure 2-9:

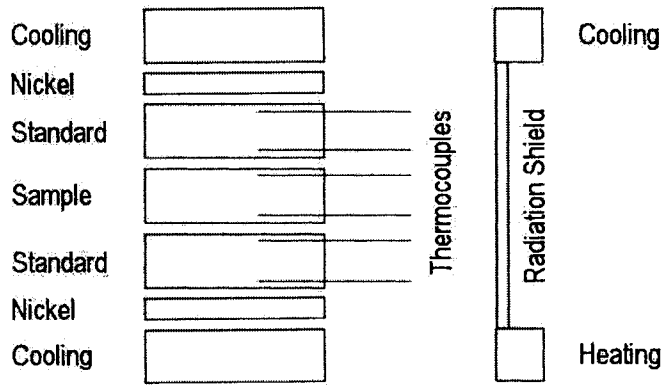

Figure 2-9: Typical Set-up Used in a Comparative Thermal Conductivity Measurement System [30]

Though the measurements obtained through the use of these experiments seem to yield results that are within an acceptable error range, the long time constant of low thermal conductivity materials remains a problem, as up to 10 hours may be necessary before steady state is achieved. This makes taking measurements a cumbersome process and has been noted by all researchers who perform this type of experiment.

2.5 Conclusions Drawn from the Literature Review

The heat transfer analysis of composites has largely been focused on improving the cure of composites, particularly unidirectional laminates. Few examples were found of heat transfer through cured composites and even fewer examples dealing with woven composites.

Many of the analytical models developed to represent the heat transfer process in composites, were developed at a micromechanical level. Very few of the models proposed were verified experimentally. Typically only models that had been developed for larger scale applications were backed by experimentation.

Several different methods have been proposed for the analytical evaluation of the thermal conductivities of composites, particularly for transverse conductivity. As many of these models were not verified experimentally, a comparative study will be necessary to determine the best approach to approximating the thermal properties of the composite material system particular to this study.

There are few reports of experiments performed to determine the thermal properties and behaviour of composites; only four reports detailing experimental works were

found. This trend had also been noted by Tucker in 1996 who remarked that though fibre and resin material properties could be obtained, little data was available on the effective conductivity of resin-saturated preforms [17].

3 Problem Statement

Currently, composite parts are typically manufactured using tools made from metals such as Invar or aluminum. Traditional processing of composite parts makes use of large ovens or autoclaves for curing: this is expensive due to the energy required to heat the oven and maintain the temperature required for the curing of the part. Integral heating of metallic tooling has been reported; hot oil is typically used as a heat transfer medium and the tool temperature is controlled through temperature feedback. However, these metallic tools are expensive and can result in composite part distortions due to the CTE mismatch between the tool and the composite part. Applying heat transfer tiles to composite tools would reduce the costs associated with heating and processing by providing an easily controlled electric heat source and by minimizing CTE mismatch to reduce part distortion.

The major objectives of this project are to understand and model the conductive heat transfer through a carbon fibre/epoxy composite and to evaluate if modelling could be used in the design of composite tools.

3.1 Objectives

The project was developed to fulfill the following major objectives by:

1. Evaluating the use of MSC Nastran finite element analysis (FEA) software as a predictive tool to model transient conductive heat transfer through CF/Ep tools.

2. Attempting to develop an analytical model capable of predicting the transient conductive heat transfer process through CF/Ep tools.

3.2 Approach

The proposed approach to meeting the tasks outlined above is to use finite element analysis and information existing in literature to evaluate the transient and steady state heat transfer through the carbon fibre tooling composite structure. Initial work will focus on obtaining the thermal properties of the tooling material: a comparative steady-state heat transfer test will be developed to evaluate the directional thermal conductivities of the CF/Ep tool material. The results are to be compared to values obtained from models found in literature and will be used in further modelling for this research.

Finite element models will be used to predict the dissipation of heat through a flat carbon fibre/epoxy plate. The finite element model is to be developed in three dimensions in order to explicitly model the ply orientations and material interactions. The FEA model will be used to evaluate the effect of varying material parameters such as specific heat, thermal conductivity as well as modified boundary conditions. Additionally, information found in literature will be used in the attempt to develop a simple, non-iterative analytical formula to describe the transient heat-transfer through a simple CF/Ep laminate tool.

The comparative test method to be used for the steady state measurement of thermal conductivity is based on methods described by James [30] and is detailed in Chapter 2. The specimens used for the thermal conductivity determination will be round in order to reduce the heterogeneity of any edge effects encountered. The experimental FEA heat transfer model validation will use a round specimen as well; however, these will be larger than those used for thermal conductivity determination to better observe the temperature gradients along the specimen. The experimental procedures developed for this research are based on previous heat transfer experiments carried out at NRC-IAR.

4 Determination of Thermal Conductivity

In order to carry out either an analytical or numerical analysis, the directional thermal conductivities of the composite system under consideration were necessary. An experiment was devised to obtain these properties experimentally.

4.1 Test Setup

To carry out predictive analysis of the heat transfer process through a composite, the directional thermal conductivities must be known. The composite used in this research was an eight-ply ACG LTM-33-CFO-700T 2/2 twill tooling laminate. The composite material was a balanced CF/Ep weave and the orthogonal in-plane directions were assumed to have the same directional properties. An experiment was devised based on the comparative testing method [30],[38],[45]. This experiment allowed measurement of thermal gradients across a column of materials thereby allowing the determination of the effective thermal conductivity of a CF/Ep laminate (Figure 4-1).

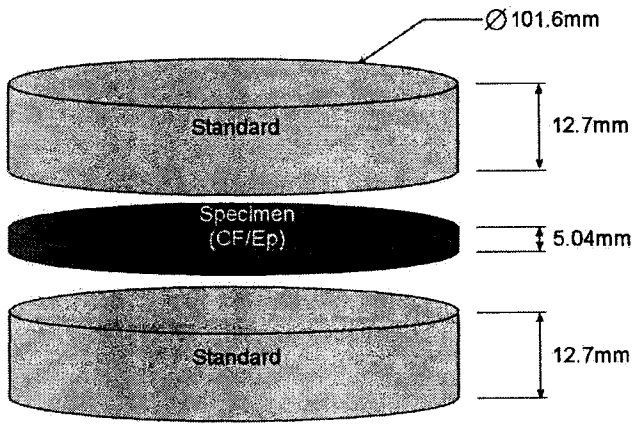

Figure 4-1: Measurement Column

To determine the thermal conductivity of the specimen, the magnitude of the heat flow passing through the column must be known. Two standards of known thermal conductivity were located at the top and bottom of the column. By measuring the temperature gradient across the standards, an estimate of the magnitude of the heat flow passing through the column was calculated. The specimen of unknown thermal conductivity was located between the standards and the temperature gradient across the specimen was also measured. Using the heat flow magnitude determined and the temperature gradient measured, the thermal conductivity of the specimen can be calculated.

The standards used in this experiment consisted of an isotropic metal alloy with known thermal conductivity. Both aluminum 6061 (Al 6061) and stainless steel 304 (SS 304) standards were used through the course of this experiment. The two materials for the standards were selected because they allow a broader spectrum of thermal conductivity to be covered; Al 6061 has a thermal conductivity of 154 W/mK whereas SS 304 has a much lower thermal conductivity of 16 W/mK. The standards are 12.7 mm (0.5 in) thick and have a 101.6 mm (4 in) diameter. The diameter was selected to obtain a large enough section in the center of the specimens that would be unaffected by edge effects, while keeping a small enough specimen to reduce manufacturing costs. The thickness of the standards was selected to allow vacuum bagging while allowing a temperature gradient to be measured across their thicknesses.

Specimens were required to have the same diameter as the standards as well as flat and parallel faces. The heat was applied by a 86.4 mm (3.4 in) diameter silicone rubber heater blanket. The heater blanket has a maximum power of 66.8 W and was located at the top of the column. In order to ensure proper surface contact between the heater blanket, the standards and the specimen, the column was placed under a vacuum bag. A vacuum of one atmosphere (-101.3 kPa or -14.7 psi) was applied and maintained for the duration of the measurements. In addition, IMS Infra-Kote thermal compound was applied in between the standards and the specimen contact faces as well as between the bottom face of the measurement stack and the aluminum. A layer of breather cloth was placed around the measurement column to prevent thermal grease from reaching the vacuum fitting.

The heat was drawn from this assembly by the means of two adjustable cold air guns. The air guns operate off compressed shop air and produce cold air by creating swirling vortices. Insulation was placed on top of the vacuum bagged assembly and weighed down with lead shot blankets to minimize heat losses. The experimental apparatus is schematically shown in Figure 4-2. The cold air flow temperature was monitored and the cold air stream was adjusted as required to produce a steady heat flow through the assembly.

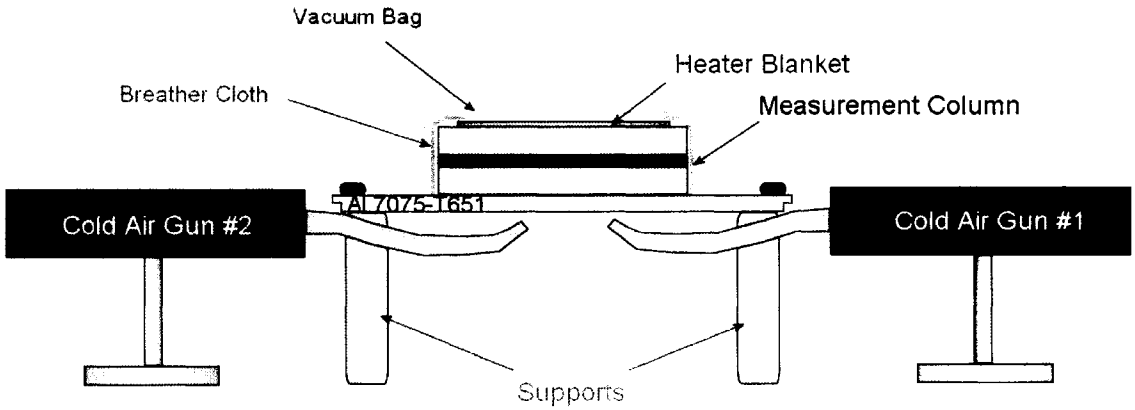

Figure 4-2: Thermal Conductivity Measurement Assembly

The cold air guns provided an effective means of drawing the heat from the apparatus. Although the temperature distribution across the base plate was not as homogeneous as it would have been if an ice bath had been used, the heater blanket used was not powerful enough to provide the heat required if such a cooling method had been selected. The temperature distribution was homogeneous over the centre of the lower face of the bottom standard, with only the outer edges (approximately 1 cm) being warmer. As the temperature readings used for the thermal conductivity determination were taken from the centre of the standards, the lack of homogeneity on the outer edges had negligible effects on the readings of interest in this research.

4.2 Temperature measurements

The temperature measurements were taken by means of spot-welded K-type thermocouples. The thermocouples have two metre leads and were calibrated using a Fluke 518 Dry Block Calibrator. Six slots 1.58 mm deep and 1.58 mm wide were machined into each standard in order to accommodate the thermocouples, as shown in Figure 4-3. In the case of the aluminum standards, the slots were mirrored on the top and

bottom surfaces, such that pairs of thermocouples were located along the same vertical axes. In the case of the stainless steel standards, the longer radial slot was mirrored; only one face contained the additional two thermocouple slots. The thermocouples were potted into the slots permanently with Omega CC High Temperature Cement Filler.

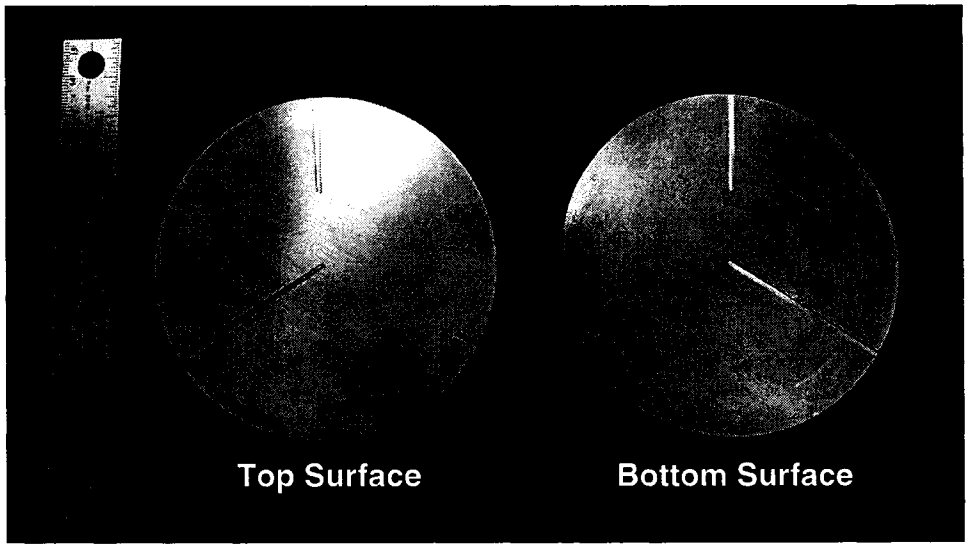

Figure 4-3: Thermocouple Slots on Aluminum Standards

In order to allow adequate temperature control of the heater blanket a thermocouple was placed on the heater blanket. This thermocouple monitored the heater blanket temperature to prevent over-heating. A thermocouple was placed on the bottom the aluminum base plate to monitor the temperature of the incident cold air stream produced by the cold air guns. A total of 14 thermocouples were connected to the assembly. However, only eight thermocouples could be connected to acquire data at once; due to this limitation initial tests were conducted using only the four central embedded thermocouples, the heater blanket monitor thermocouple and the cold air monitor thermocouple.

The thermal conductivity measurement experiment devised was found to be nearly identical to the experiment suggested in the ASTM E1225-04 [45]. This standard was not obtained until after the experiment for this thesis had been devised and started. It is therefore only used as a reference tool to assess the performance of the experiment devised.

4.3 Specimen Description

To measure the in-plane and the transverse thermal conductivities, two types of CF/Ep specimens were required (Figure 4-4). Both a transverse thermal conductivity specimen and an in-plane thermal conductivity specimen were manufactured. Stainless steel, aluminum and polyethylene specimens were also produced in order to evaluate the accuracy of the apparatus (Figure 4-5).

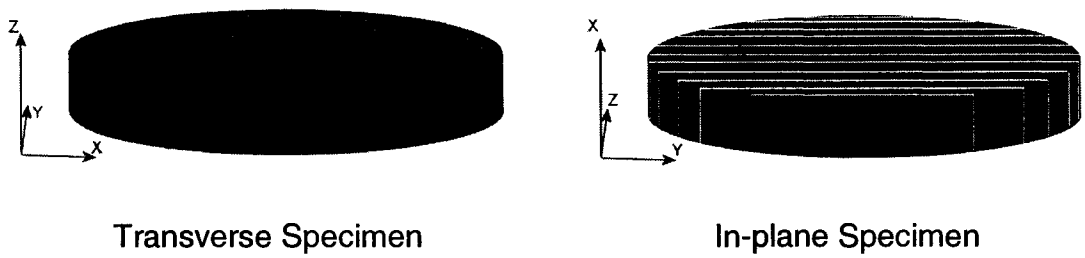

Figure 4-4: Composite Specimens

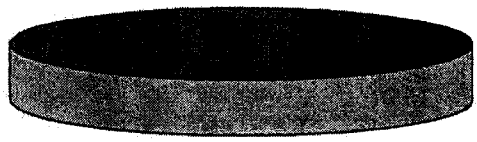

Figure 4-5: Isotropic Specimen

4.3.1 Transverse Thermal Conductivity Specimen

A transverse thermal conductivity specimen was manufactured using ACG LTM-33-CFO-700T carbon fibre tooling prepreg. The specimen was manufactured following the specifications and guidelines provided by the manufacturer [46]-[50].

The material was removed from the freezer 24 hours before layup in order to thaw. The composite material was cut into four 0/90° squares and four 45/-45° squares; the squares were cut to be 178 mm square. The eight cut pieces were laid up in two four-layer assemblies having orientations of [0/45/-45/90]. The two resulting layups were debulked at room temperature for 25 minutes. The two layups were then assembled to obtain the final layup of $[0/45/-45/90]_s$. The final layup was debulked for 25 minutes before being trimmed to a 140 mm square. The composite layup was then vacuum bagged. The manufacturing procedure and vacuum bag assembly are schematically shown in Figure 4-6. All composite manufacturing operations were carried out in a clean room environment.

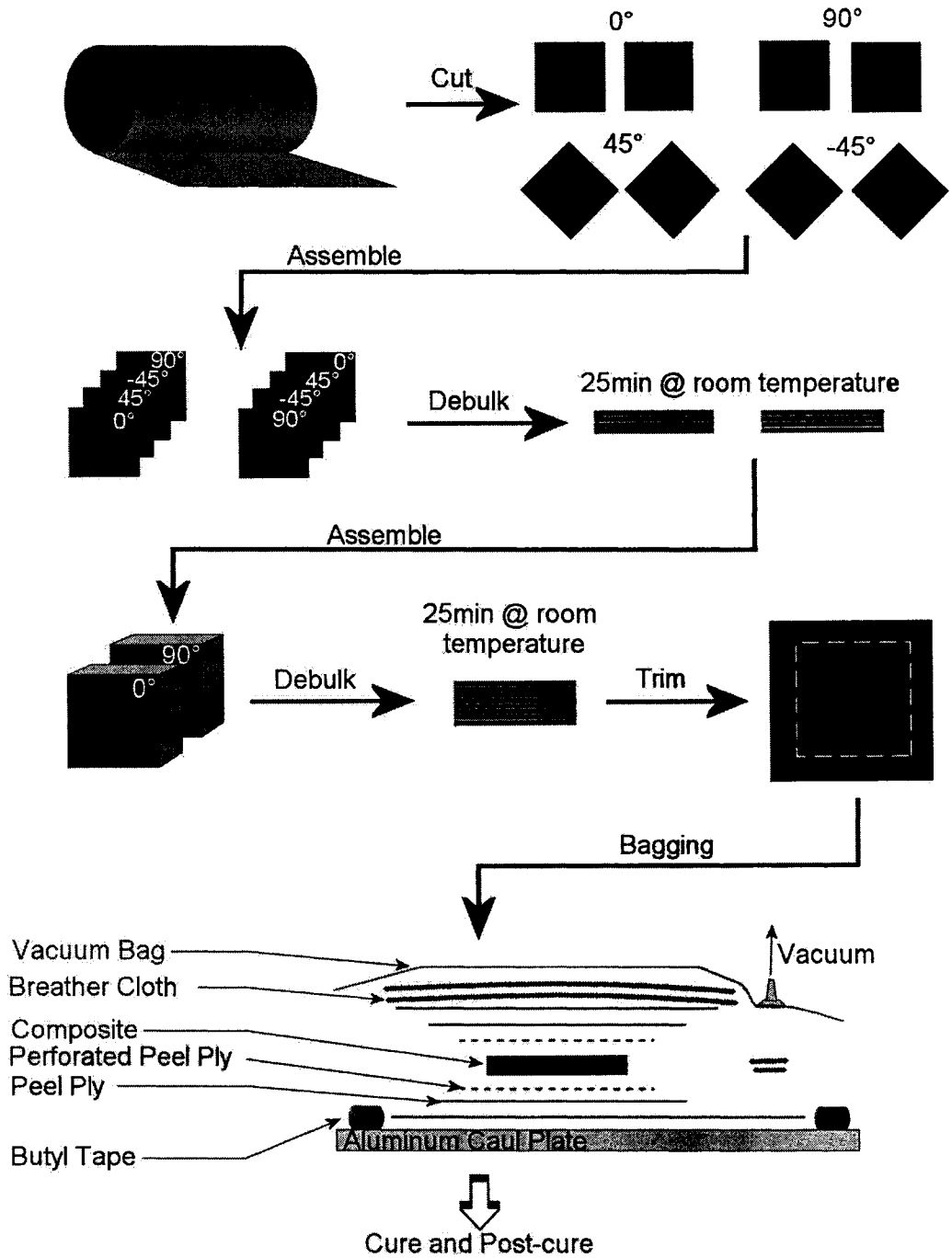

Figure 4-6: Schematic Representation of Layup Process for Transverse Specimen

The vacuum bag assembly was placed in the autoclave (Figure 4-7) and the composite was cured following the specifications established by ACG. The initial cure was carried out following the cure schedule shown in Table 4-1.

Table 4-1: Cure Schedule

Step No.	Temperature (°C)	Pressure (kPa)	Applied Vacuum	Operation	Dwell/Ramp Time (min)
1	25	0	27" Hg	Place Assembly in Autoclave	--
2	25	0-145	27" Hg	Ramp pressure up	3
3	25	145	Vent	Vent vacuum to atmosphere	--
4	25	145-620	Vent	Ramp pressure up	5
5	25-70	620	Vent	Ramp temperature up	32
6	70	620	Vent	Temperature dwell	180
7	25	620	Vent	Ramp temperature down	--
8	25	0	Vent	Ramp pressure down	--

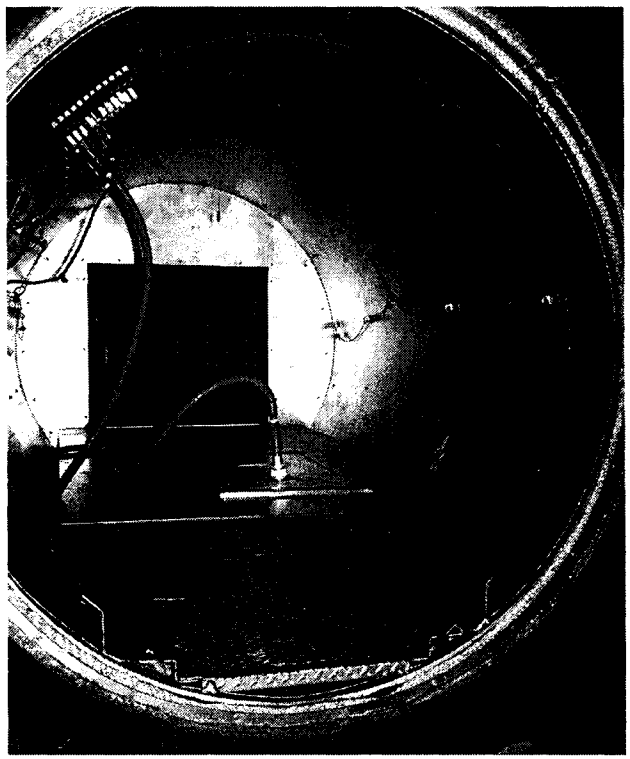

Figure 4-7: Vacuum Bag Assembly in Autoclave

A post-cure was required to obtain the optimum properties of the material. The post-cure was carried out in a programmable air-recirculation oven following the post-cure schedule shown in Table 4-2.

Table 4-2: Post-Cure Schedule

Step No.	Temperature (°C)	Ramp Rate (°C/min)	Dwell/Ramp Time (min)
1	25-170	0.3	484
2	170	--	15
3	170-160	-5	2
4	160	--	480
5	160-25	-2.5	64

Following the post-cure in the oven, the fully cured square composite plate was water-jet cut to a 102 mm (4 in) diameter disk (Figure 4-8). The final thickness of the disk was 5.5 mm.

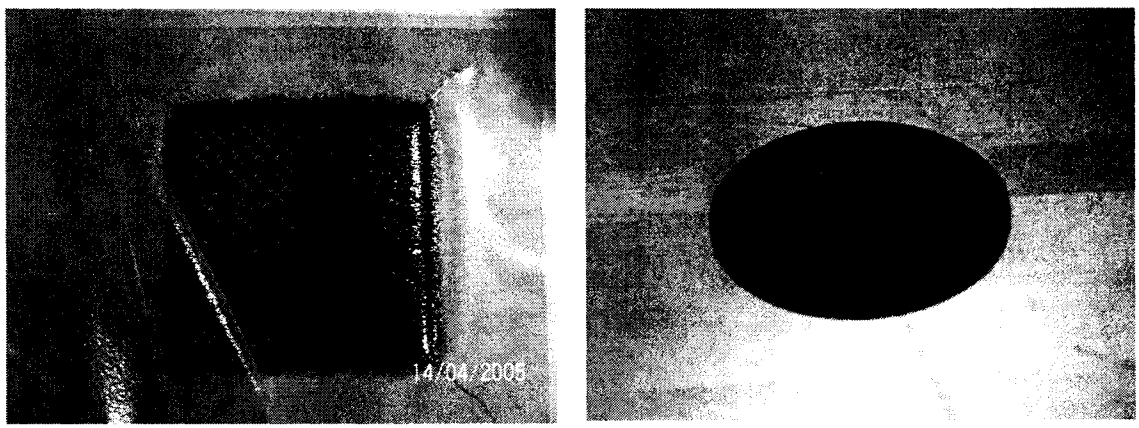

(a) (b)

Figure 4-8: Fully Cured Composite: (a) Immediately After Cure and (b) After Water-jet Cutting

4.3.2 In-plane Thermal Conductivity Specimen

To test for the in-plane thermal conductivity another specimen was manufactured. The initial manufacturing process used is similar to the process used for the transverse thermal conductivity; two composite sections eight inches square were laid up with ply orientations of $[0/90/0/90]_s$. Thirty 12.7 mm strips were then cut from the debulked eight-ply composite sections. The strips were then stacked to obtain a 12.7 mm thick plate. The plate was debulked and vacuum bagged (Figure 4-9) as with the transverse thermal conductivity specimen. A schematic of the procedure is shown in Figure 4-10.

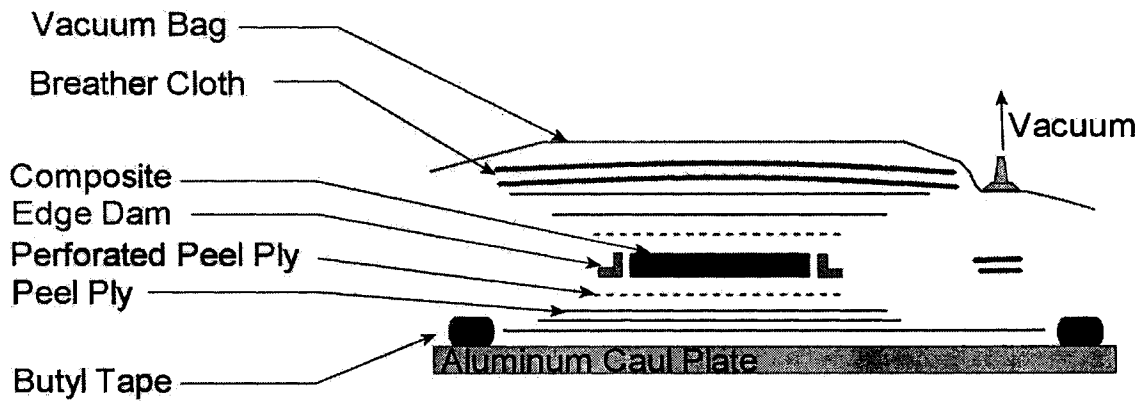

Figure 4-9: Schematic of the In-plane Composite Specimen Vacuum Bag Assembly

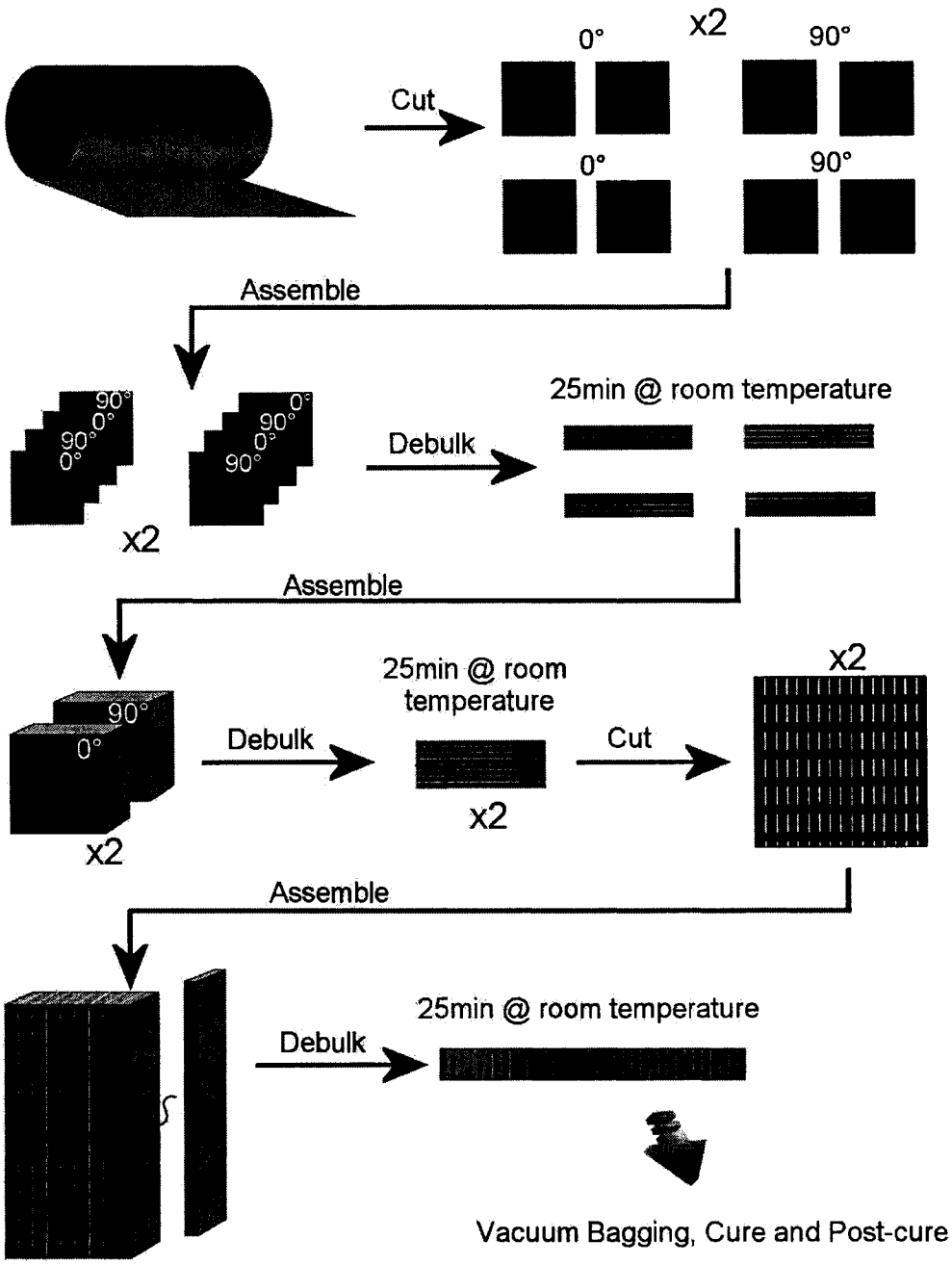

Figure 4-10: Schematic Representation of Layup Process for In-plane Specimen

The cure and post-cure operations were identical to those used for the transverse thermal conductivity specimen and are detailed in section 4.3.1. The specimen was then

water-jet cut and one side was faced using an end mill in order to have flat and parallel faces. The final specimen thickness was 9.8 mm.

4.3.2.1 Calibration Specimens

Isotropic calibration specimens were manufactured to assess the accuracy of the apparatus. Three types of materials of known thermal conductivity were used, namely Al 6061, SS 304 and high-density polyethylene (HDPE). These materials were selected because their thermal conductivities range from 0.46 to 153 W/mK. The materials were machined to be four inches in diameter with parallel, flat surfaces. The Al 6061 and SS 304 specimens were manufactured to a 12.7 mm thickness and the HDPE was manufactured from a 6.35 mm thick sheet. The specified thermal conductivity for each material is given in Table 4-3.

Table 4-3: Calibration Specimen Thermal Conductivities

Material	Thermal Conductivity @ 25°C (W/mK)	Source
Al 6061	153	MIL-HDBK_5H
SS 304	15.58	MIL-HDBK_5H
HDPE	0.46	Poli HI SOLIDUR

4.4 Data Acquisition

4.4.1 Hardware and Software

In order to operate the heater blanket and to acquire thermocouple readings the following hardware was used:

- A ToolSmart™ four-channel heater relay module,
- A National Instruments SC 2345 connector block with eight K-type thermocouple connectors and a heater relay connector,
- A laptop computer

The National Instruments connector block was connected to the computer via a National Instruments DAQ card. The Q420 ToolSmart™ software (Comtek V1.0) was used to acquire the thermocouple data and to control the heater blanket. The software allows the user to enter the desired heat-up rate, soak temperature, soak duration and cool down rate [44]. A thermocouple was configured as the control thermocouple for the heater blanket. The readings obtained from this thermocouple were compared to the desired temperature and the heater blanket was turned on and off as required. A second thermocouple positioned directly on the heater blanket was configured as a heater thermocouple and monitored the heater blanket temperature. If the heater blanket exceeded its specified maximum suggested operating temperature, the software would automatically turn off the heater blanket to avoid over-heating.

4.4.2 Settings

4.4.2.1 Calibration Thermal Conductivity Measurements

The isotropic specimens were tested at three different soak temperatures. The soak temperatures were adjusted depending on the material in order to remain within the heater blanket's heating capacity. The data acquisition rate was set to record ten data points per minute. The heat-up rate was specified as 1°C/minute for all heat trials the fall rate was specified as 3°C/min and the soak time as 30 minutes. For certain trials, the soak times were extended by "pausing" the soak phase during the trial in order to achieve steady-state conditions. The soak temperatures selected for each trial are given in Table 4-4.

Table 4-4: Soak Temperature Settings for Calibration Specimens

	Material	Trial	Soak Temperature (°C)		Material	Trial	Soak Temperature (°C)
Aluminum Standards	SS 304	5	43	SS 304 Standards	SS 304	33	50
		6	50			34	60
		7	55			35	70
		8	43			36	50
		9	50			37	60
		10	55			38	70
	Al 6061	11	45		HDPE	39	55
		12	50			40	65
		13	40			41	75
		14	40			42	55
		15	45			43	65
		16	50			44	75
	HDPE	17	45		Al 6061	45	50
		18	55			46	60
		19	70			47	40
		20	45			48	50
		21	55			49	60
		22	70			50	40
	SS 304 (New)	23	45				
		24	50				
		25	55				
		26	45				
		27	50				
		28	55				

4.4.2.2 CF/Ep Thermal Conductivity Measurements

Similarly, the CF/Ep specimens were tested at three different temperatures based on the capacity of the heater blanket. All settings but the soak time and temperature were identical to those used for the calibration specimens. The soak temperature settings for the CF/Ep specimens are given in Table 4-5. A nominal soak time of 45 minutes was used.

Table 4-5: Soak Temperature Settings for CF/Ep Specimens

Specimen	Test	Soak Temperature (°C)
Transverse	1	50
	2	70
	3	80
	4	50
	5	70
	6	80
In-Plane	7	50
	8	60
	9	70
	10	50
	11	60
	12	70

4.5 Results

Several heat trials were carried out in order to verify the accuracy of the apparatus used to measure the thermal conductivity of the CF/Ep specimens. The majority of the heat trials were carried out using isotropic dummy specimens of known thermal properties. The results obtained are shown in this section.

4.5.1 Results Obtained Using Al 6061 Standards

The temperature data obtained from the eight thermocouples were plotted against time to obtain the temperature profile of each trial. Based on the temperature profile, the steady-state heat transfer time and duration were determined: the temperature readings obtained over that time span were averaged and the average temperature gradients across the two standards and the specimens were calculated. The following equations were used

in order to obtain the heat flow across the top and bottom standards as well as to determine the average effective thermal conductivity of the specimen:

The heat flow through the apparatus was evaluated by:

$$\frac{q_x}{A} = \frac{k_{std}\left(T_{H\,Ave} - T_{C\,Ave}\right)}{\Delta x} \tag{7.1}$$

Where: q_x/A is either q_1/A or q_2/A the heat flow per unit area in the top and bottom standards respectively (W/m^2).

k_{std} is the thermal conductivity of the standard at the average temperature measured across the standard (W/mK).

$T_{H\,Ave}$ is the value of the hot side temperature measurements averaged over the steady-state period (°C).

$T_{C\,Ave}$ is the value of the cold side temperature measurements averaged over the steady-state period (°C).

Δx is the thickness of the specimen (m).

Based on the heat flow values obtained for the top and bottom standards, limit thermal conductivities were calculated:

$$k_x = \frac{q_x \cdot \Delta x}{(T_{H\,Ave} - T_{C\,Ave})} \tag{7.2}$$

Where: k_x is the thermal conductivity of the specimen based on q_x (x = (1,2)).

The effective thermal conductivity was calculated by taking the average of k_1 and k_2 as follows:

$$k = \frac{k_1 + k_2}{2} \tag{7.3}$$

Using these equations, the thermal conductivity of the specimens was evaluated.

Four sets of data were collected using the 6061-T651 aluminum standards. For each set, three temperature settings were investigated with two heat surveys carried out for each temperature setting. The temperature settings used for each specimen are summarized in Table 4-6.

Table 4-6: Temperature Set Points for Isotropic Material Specimens

Specimen Material	Temperature Set Points
SS 304	43°C, 50°C, 55°C
Al 6061	40°C, 45°C, 50°C
HDPE	45°C, 55°C, 70°C
SS 304 (new)	45°C, 50°C, 55°C

The values obtained were compared to the expected results for each material. The SS 304 and Al 6061 material properties were taken from Mil-HDBK-5H. The material properties of the HDPE were provided by the manufacturer.

The results are shown in Figure 4-11 to Figure 4-14.

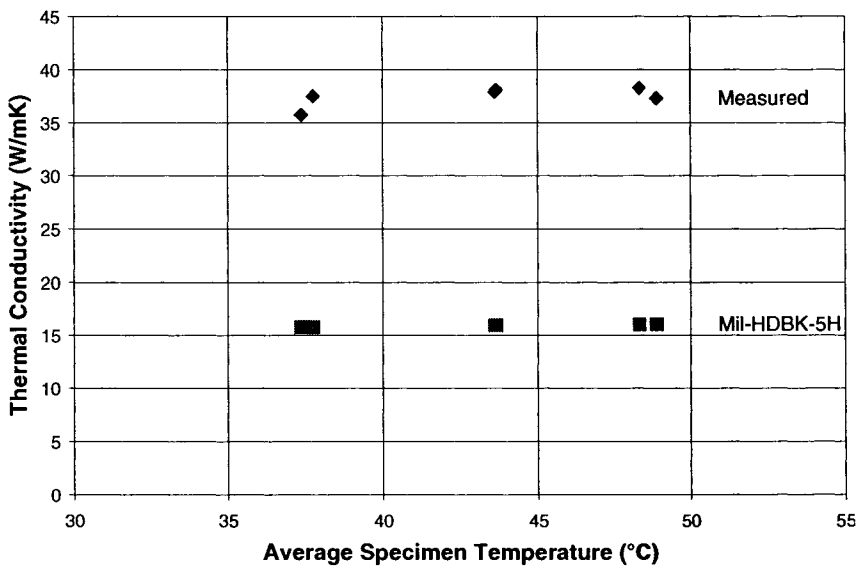

Figure 4-11: SS 304 Thermal Conductivity Measurement Results Using Al 6061 Standards

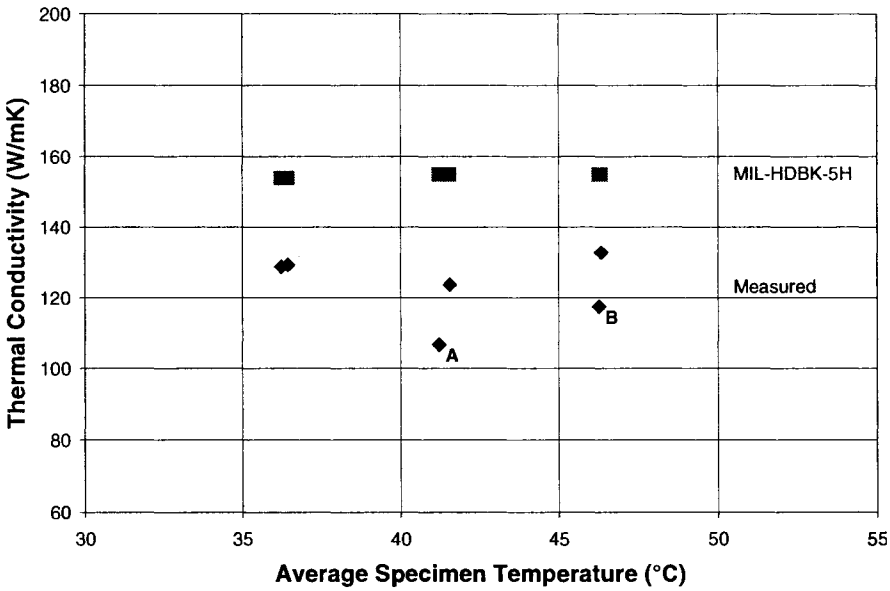

Figure 4-12: Al 6061 Thermal Conductivity Measurement Results Using Al 6061 Standards

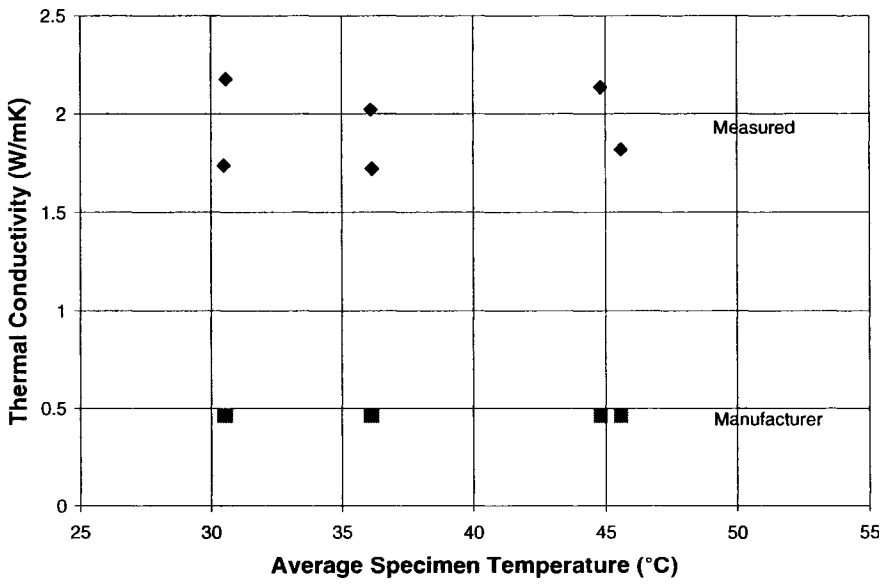

Figure 4-13: HDPE Thermal Conductivity Measurement Results Using Al 6061 Standards

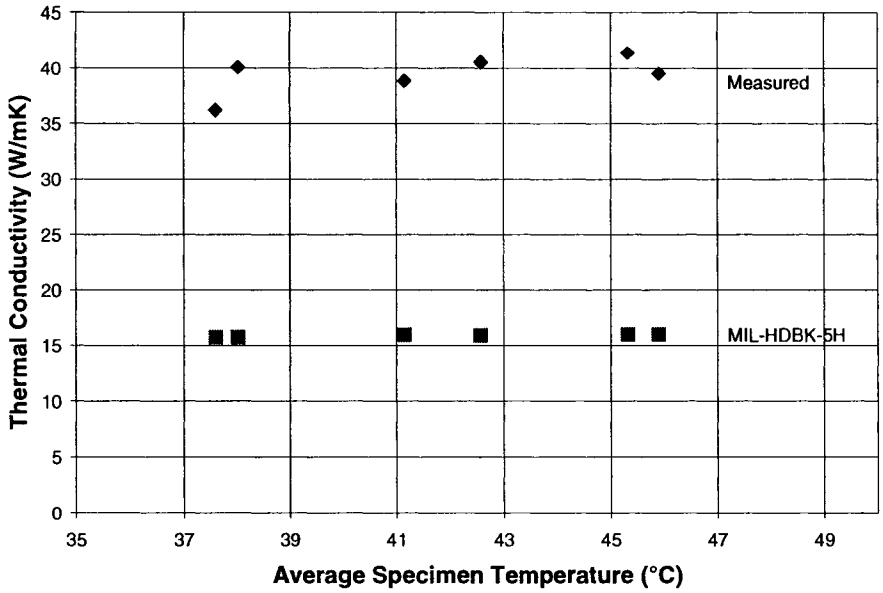

Figure 4-14: New SS 304 Thermal Conductivity Measurement Results Using Al 6061 Standards

The values measured experimentally showed a large and varying degree of error when compared to the expected thermal conductivity value. Two SS 304 disks from different manufacturing batches were used in order to ascertain the material type and conditioning. This approach verified that the errors recorded were due to the apparatus. In order to better measure the error encountered, the percent error was plotted against the expected thermal conductivity of each specimen (Figure 4-15). The percent error was calculated based on the average of all the thermal conductivity values measured for each specimen.

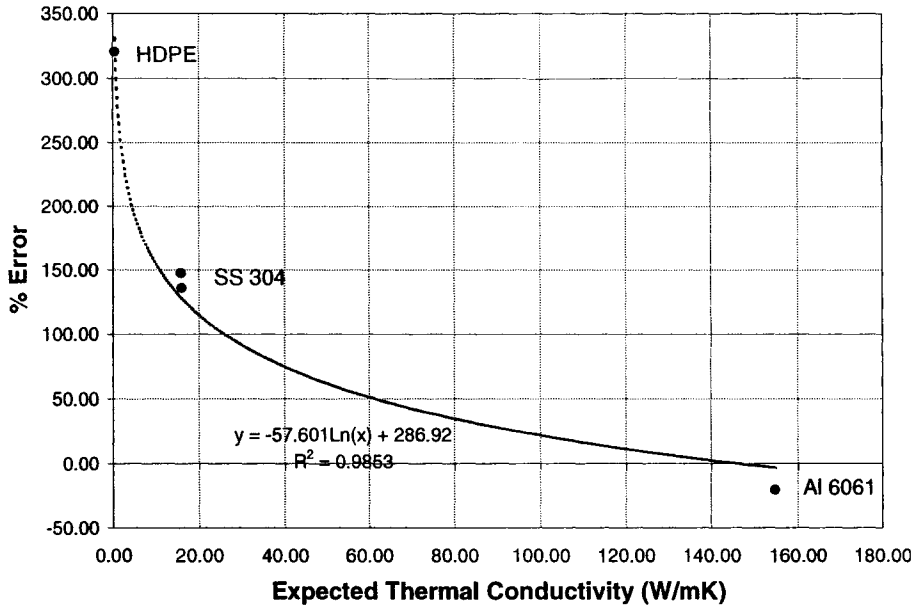

Figure 4-15: Percent Error as a Function of the Expected Material Thermal Conductivity Using the Al 6061 Standards

Though a negative error would be expected in the measured thermal conductivity due to heat loss in the system, negative error is only observed for the aluminum specimen. As the difference between the standard's thermal conductivity and the specimen's thermal conductivity increases, there is a logarithmic increase in the error measured. As the material of interest in this research has a thermal conductivity below that of SS 304, the aluminum standards would not be adequate to accurately measure the thermal conductivity due to the large error in that range of thermal conductivities.

In Figure 4-12, two sets of points (point A and B) were lower than the other data. Due to the relatively large error obtained with these first two trials, the insulation was improved around the measurement stack resulting in better thermal measurements.

To reduce the difference between the thermal conductivity of the standards and of the specimens, SS 304 standards were also used. The results for these are given in the following section.

4.5.2 Results Obtained Using SS 304 Standards

The thermal conductivity of the specimens were calculated in the same manner as that described in section 4.5.1 .

The temperature set points used for testing with the SS 304 standards are summarized in Table 4-7.

Table 4-7: Temperature Set Points for Isotropic and Composite Material Specimens Used with SS 304 Standards

Specimen Material	Temperature Set Points
SS 304	50°C, 60°C, 70°C
HDPE	55°C, 65°C, 75°C
Al 6061	40°C, 50°C, 60°C
CF/Ep Transverse	50°C, 70°C, 80°C
CF/Ep In-Plane	50°C, 60°C, 70°C

As with the trials carried out with the Al 6061 standards, the thermal conductivity values obtained for the isotropic materials were compared to their expected thermal

conductivity values. The results obtained for each material are shown in Figure 4-16 to Figure 4-18.

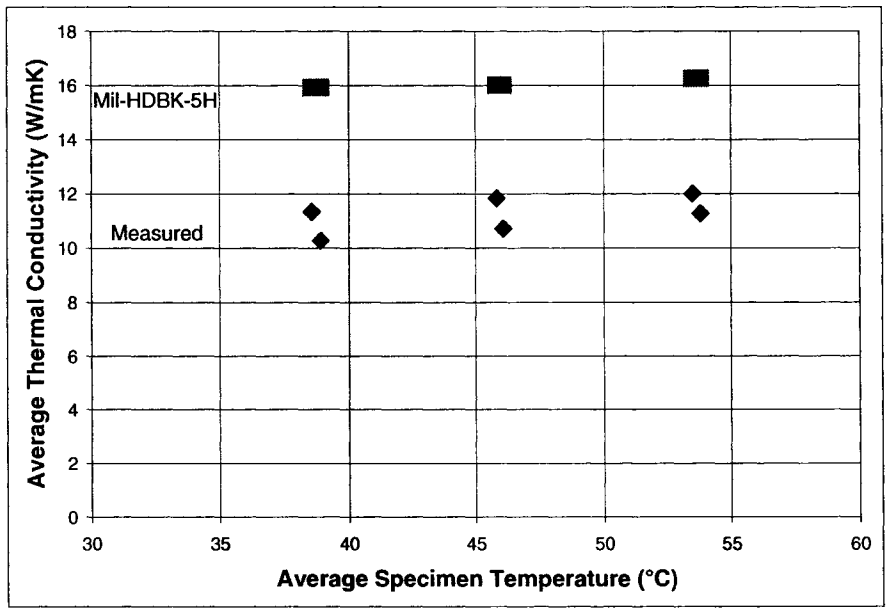

Figure 4-16: SS 304 Thermal Conductivity Measurement Results Using SS 304 Standards

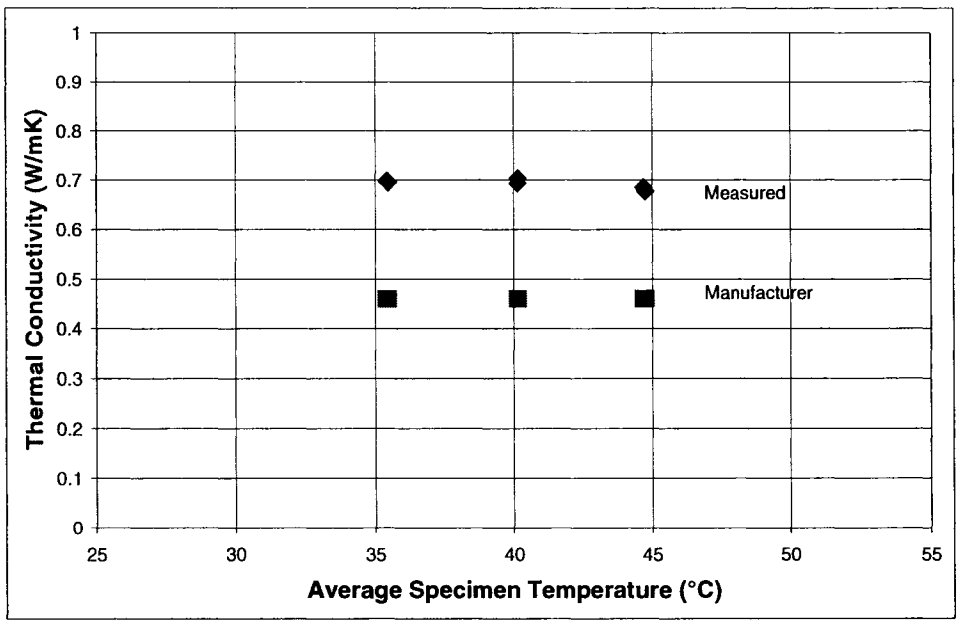

Figure 4-17: HDPE Thermal Conductivity Measurement Results Using SS 304 Standards

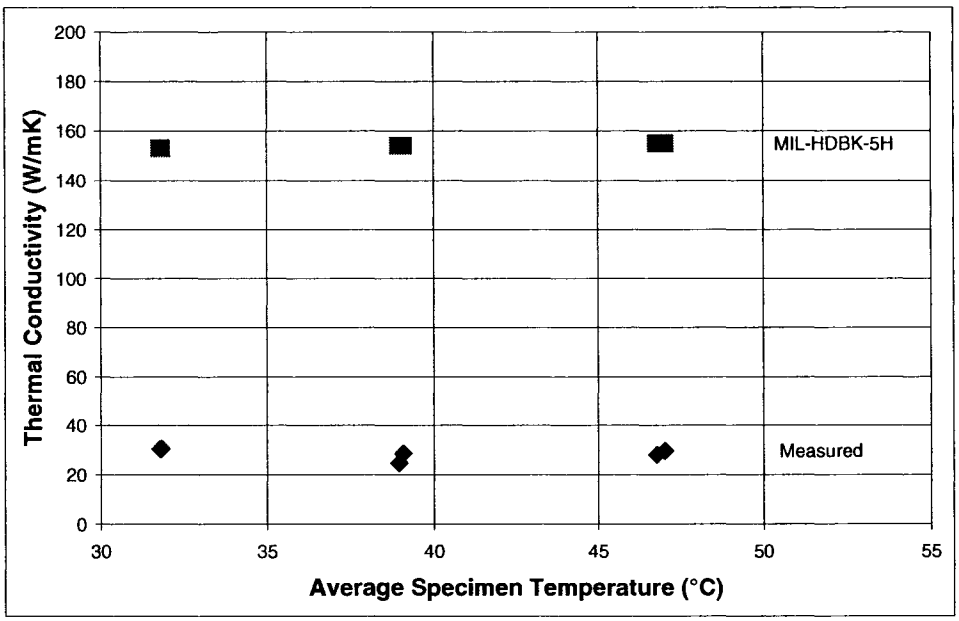

Figure 4-18: Al 6061 Thermal Conductivity Measurement Results Using SS 304 Standards

As with the Al 6061 standard, the error encountered in the thermal conductivity measurements varied depending on the specimen considered. The percent error was plotted against the expected thermal conductivity of each isotropic specimen (Figure 4-19).

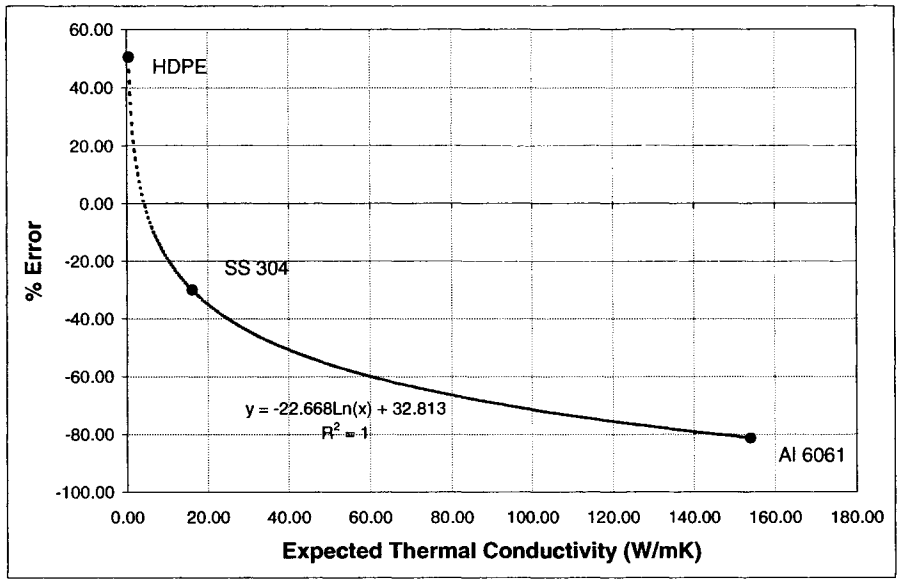

Figure 4-19: Percent error as a Function of the Expected Material Thermal Conductivity

When comparing the error obtained in the thermal conductivity values found for the SS 304 and the HDPE when using the SS 304 standards and the Al 6061 standards (Figure 4-15), the same trend can be noticed; however, the magnitude of the error was approximately seven times smaller when using the SS 304 standards.

Since the SS 304 standards offer better accuracy in the range between the HDPE thermal conductivity and the SS 304 thermal conductivity, these were used to determine the in-plane and transverse thermal conductivity of the composite laminate. The results obtained for the transverse and in-plane thermal conductivities are shown in Figure 4-20 and Figure 4-21 respectively.

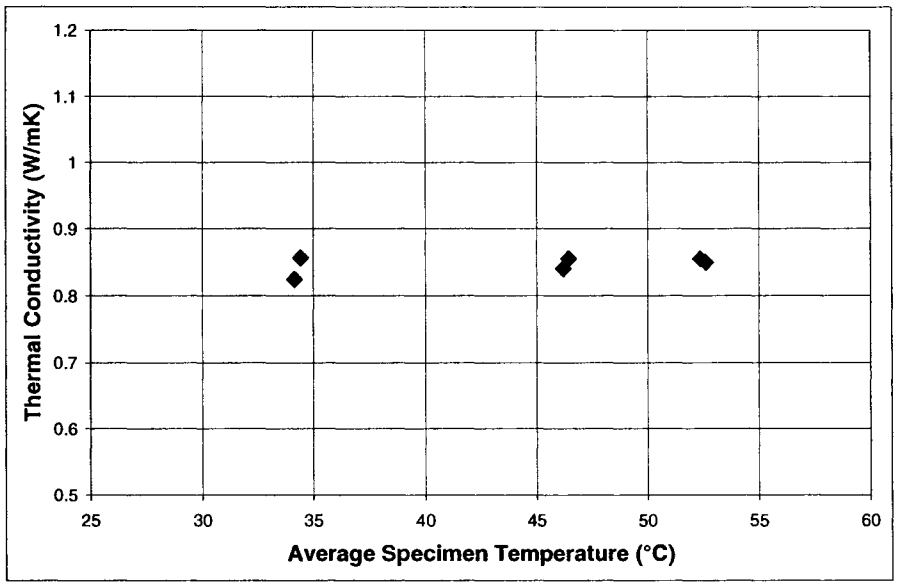

Figure 4-20: Measured Thermal Conductivity for the Transverse Thermal Conductivity CF/Ep Specimen

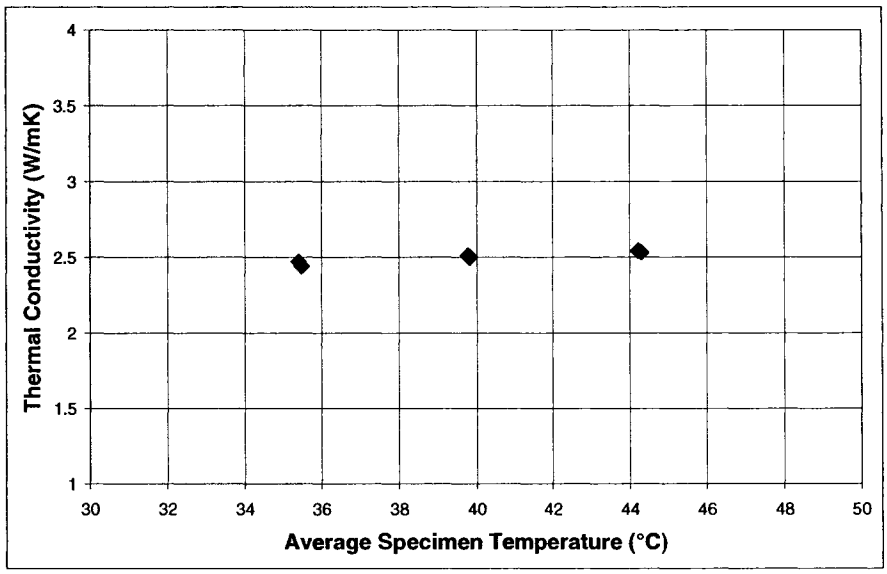

Figure 4-21: Measured Thermal Conductivity for the In-Plane Thermal Conductivity CF/Ep Specimen

The measured thermal conductivity was plotted against the error for the specimens of known thermal conductivity. Using the resulting curve, the expected error for the composite specimen was estimated. Based on the error, the transverse thermal conductivity was calculated as 0.57 W/mK and the in-plane thermal conductivity was calculated as 1.87 W/mK (Figure 4-22)

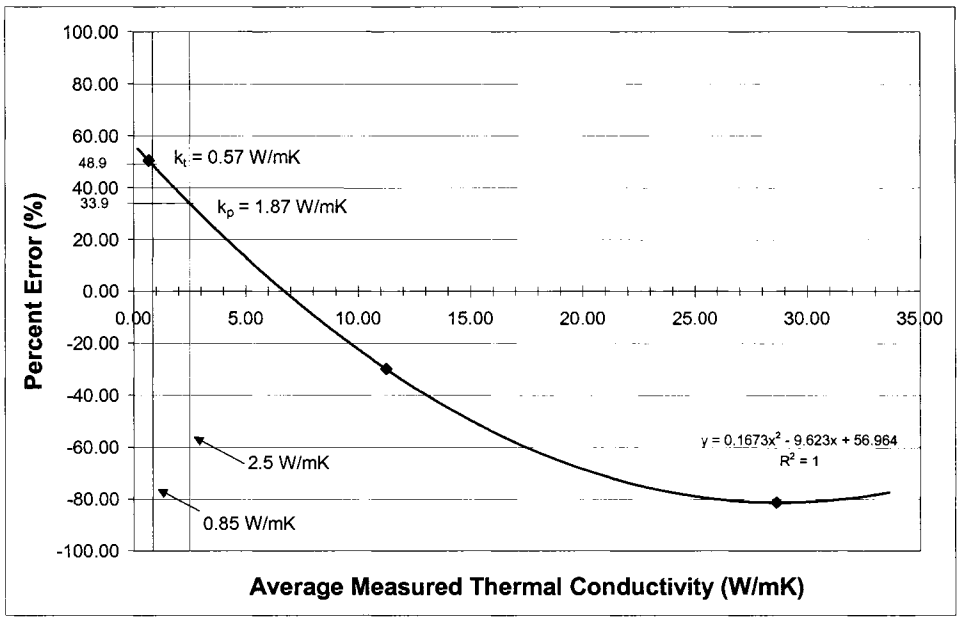

Figure 4-22: Error as a Function of the Calibration Specimens' Average Measured Thermal Conductivities

The value obtained for thermal conductivity was compared to the value estimated by the models found in literature. According to the manufacturer, the LTM 33 CFO 700T prepreg has a fibre volume fraction of 58%. This point was plotted against the curves obtained from six of the models for transverse thermal conductivity in literature as shown in Figure 4-23. As can be seen, there is good correlation between the value measured and Rayleigh, Farmer and Hasselman-Johnson's models.

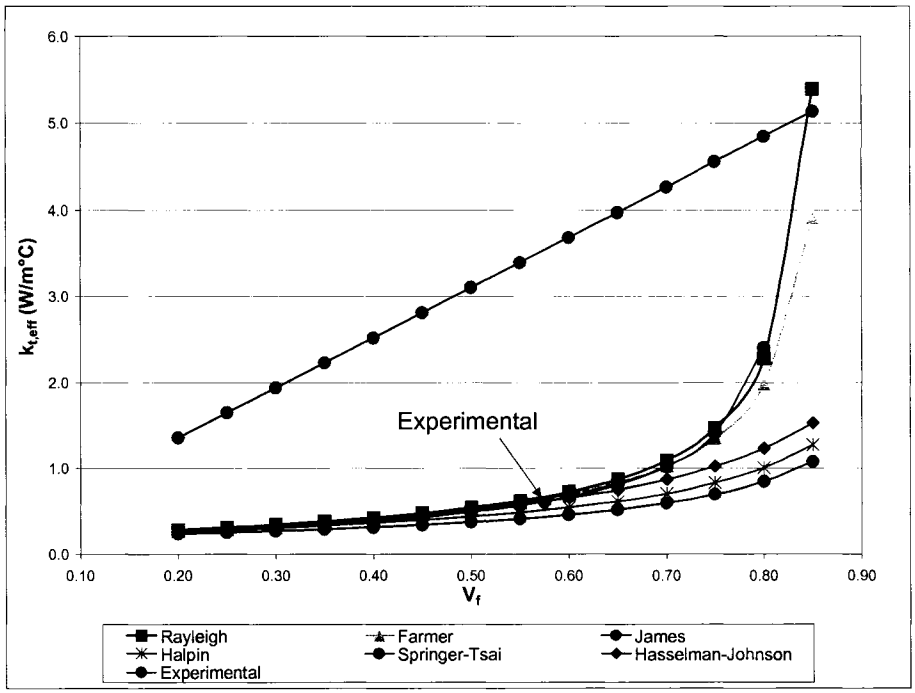

Figure 4-23: Experimental Point Compared to Literature Models

The values determined for the transverse and in-plane thermal conductivity of the composite were used in the FEM prediction analysis described in Chapter 6.

5 Analytical Approach

An analytical approach was sought to assess the possibility of using a relatively simple calculation method for predicting the conductive heat transfer characteristics within a composite tool. This would prove to be a valuable asset in the design and trade-off studies of composite tooling systems and processes, since it would provide a quick method of estimating the effectiveness of a system or process.

Although a number of numerical schemes can be used to solve this type of heat conduction problem, the focus here was on finding a closed-form solution, which could adequately be used to describe the conductive heat transfer process though a carbon fibre/epoxy, 2/2 twill, composite tool.

5.1 Conduction Heat Transfer

The conduction heat transfer process in itself is not complex; however, the anisotropic nature of composites causes the conductive heat transfer properties to vary widely depending on the orientation of the heat flux applied. In the application considered in this research, the heat is applied through a heater blanket or through a heat tile that is bonded to the tool; the heat tile consists of a heater blanket that is applied on a copper metal sheet. Both transient and steady-state heat transfer need to be considered for an accurate depiction to be obtained.

As stated in section 2.3.2, transient heat conduction obeys the energy equation (2.14). Fourier's law, equation (2.2) should also be respected when steady-state

conditions are attained. In order to obtain a valid solution, it is essential to know the boundary conditions that are applied to the part. In the case of the application considered, and assuming the heater blanket was centered on the composite plate, the known boundary conditions and initial conditions were as follows:

- At $z = 0 \; \forall \; (x,y) \in [0, (x^2 + y^2)^{1/2} = r_{HB}]$ — $q = n$ where n is a known value (W/in^2)
- At $z = 0 \; \forall \; (x,y) \notin [0, (x^2 + y^2)^{1/2} = r_{HB}]$ — $q = 0$ (assume perfect insulation)
- At $x = L$ and $z = -d$ — $q = 0$ (assume perfect insulation)
- At $x = l$, $y = 0$, $z = 0$ — $T = T_{setpoint}(t)$
- At $t = 0$ — $T = T_\infty$ where T_∞ is room temperature (°C)

The boundary conditions are shown schematically in Figure 5-1:

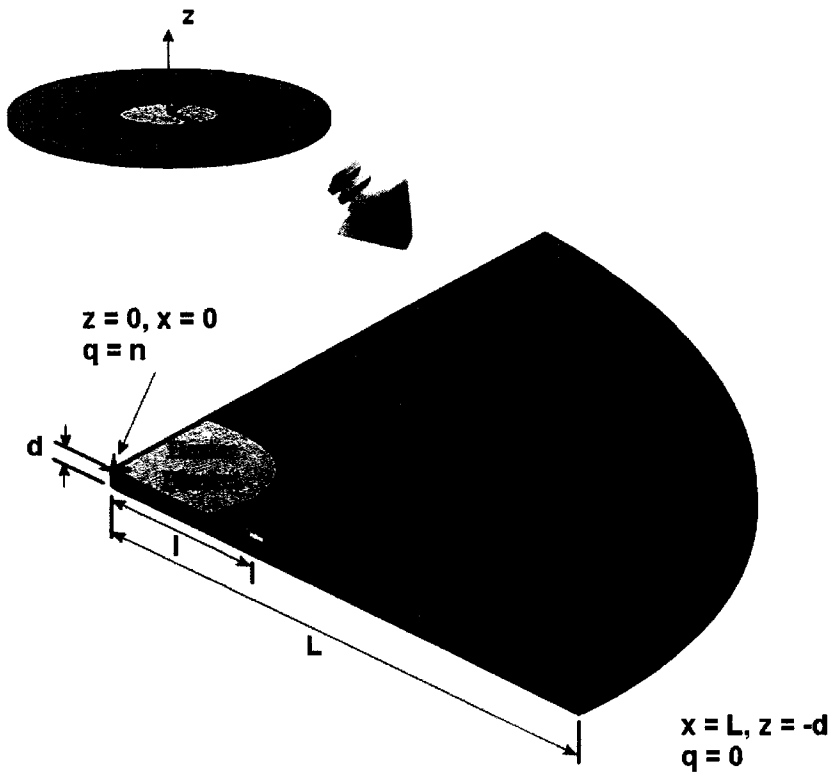

Figure 5-1: Known Boundary Conditions

These boundary and initial conditions are all directional and cannot be generalized due to the orthogonal properties of the 2/2 twill woven CF/Ep composite material used.

5.2 Temperature Field Determination

Transient conductive heat transfer can be described by equation (2.14):

$$\frac{\partial}{\partial t}\left(\rho c_p T\right) = \nabla\left(k \nabla T\right) \tag{2.14}$$

Due to the anisotropy of the material, the equation cannot be reduced to a two- or one-dimensional form. As such the thermal conductivity of the material is expressed as a 3 x 3 matrix of the form:

$$k = \begin{bmatrix} k_{xx} & k_{xy} & k_{xz} \\ k_{yx} & k_{yy} & k_{yz} \\ k_{zx} & k_{zy} & k_{zz} \end{bmatrix} \tag{4.1}$$

However, within a given ply, the matrix may be simplified to a diagonal matrix if no rotations about the z-axis are present:

$$k = \begin{bmatrix} k_{xx} & 0 & 0 \\ 0 & k_{yy} & 0 \\ 0 & 0 & k_{zz} \end{bmatrix} \tag{4.2}$$

If the ply is rotated by θ around the material z-axis and assuming that the out of plane heat flux is negligible, the off-axis ply properties are obtained by using the transformation matrix $[T_{\Lambda\theta}]$:

$$[T_{\Lambda\theta}] = \begin{bmatrix} \cos\theta & \sin\theta & 0 \\ -\sin\theta & \cos\theta & 0 \\ 0 & 0 & 1 \end{bmatrix} \tag{4.3}$$

Applying the transformation matrix yields the rotated thermal conductivity matrix k':

$$k' = [T_{\Lambda\theta}]^T \cdot k \cdot [T_{\Lambda\theta}]$$

$$k' = \begin{bmatrix} k_{xx}\cos^2\theta + k_{yy}\sin^2\theta & (k_{xx} - k_{yy})\cos\theta\sin\theta & 0 \\ (k_{xx} - k_{yy})\cos\theta\sin\theta & k_{xx}\cos^2\theta + k_{yy}\sin^2\theta & 0 \\ 0 & 0 & k_{zz} \end{bmatrix} \tag{4.4}$$

The temperature gradient ∇T is represented by a 3 x 1 matrix:

$$[\nabla T] = \begin{bmatrix} \partial T/\partial x \\ \partial T/\partial y \\ \partial T/\partial z \end{bmatrix} \tag{4.5}$$

The heat flux applied is related to equation (2.14) by the Fourier equation for heat conduction in anisotropic materials [40]:

$$q_i = -\sum_{j=x,y,z} k_{ij} \frac{\partial T}{\partial x_j} \qquad i = x, y, z \tag{4.6}$$

The heat flux can also be expressed in matrix form, $[q_i]$:

$$[q_i] = \begin{bmatrix} q_x \\ q_y \\ q_z \end{bmatrix} \tag{4.7}$$

Equation (4.6) can then be written as:

$$[q_i] = -[k] \cdot [\nabla T] \tag{4.8}$$

There are various methods which have been proposed by authors to obtain solutions to these equations. The methods include Laplace transforms, separation of variables and superposition methods, as shown in a number of heat transfer references such as Holman [31], Poulikakos [40] and Kutateladze and Borishanskii [41]. The methods proposed all provide a set of equations to which the initial and boundary conditions may be applied.

The most commonly used method is the method of separation of variables. In the case of three-dimensional analysis, the temperature field as a function of position and time can be determined by solving equation (4.9):

$$\frac{\partial^2\Theta}{\partial x^2}+\frac{\partial^2\Theta}{\partial y^2}+\frac{\partial^2\Theta}{\partial z^2}=\frac{1}{\alpha}\frac{\partial\Theta}{\partial t} \tag{4.9}$$

Where: Θ is the homogenized temperature function $\Theta = T - T_\infty$

In order to separate the variables, the homogenized temperature function is expressed as follows:

$$\Theta = X(x)Y(y)Z(z)S(t) \tag{4.10}$$

Through mathematical manipulations, a set of four equations is obtained:

$$\begin{aligned} X'' + \lambda^2 X &= 0 \\ Y'' + \beta^2 Y &= 0 \\ Z'' + \gamma^2 Z &= 0 \\ S' + \alpha\left(\lambda^2 + \beta^2 + \gamma^2\right)S &= 0 \end{aligned} \tag{4.11}$$

Solving these equations for each variable and back substituting into equation (4.10) yields an equation with eight unknown constants, which are determined using the boundary and initial conditions.

5.3 Temperature Prediction

In order to accurately predict temperature in the composite laminate, the initial temperature distribution in the body, as a function of x, y and z, must be known. The boundary conditions can be of different types, but must be known in three dimensions and as a function of time. As in most practical problems, the known boundary

conditions are incomplete for the tool heating process of interest for this research; obtaining a closed-form solution is not possible. These types of problems are common in practical models and are typically referred to as ill-posed problems.

Ill-posed problems are typical in engineering and applied sciences. A branch of mathematics has developed, whose field of study is the solution of ill-posed problems. Authors such as Hào [42] and Ang [43], have proposed solutions to a range of ill-posed conduction heat transfer problems; however, the understanding and proper application of these solutions require extensive mathematical knowledge and the application of such solutions is typically restricted to simple part geometries and to simple heat flow applications. As such, the practical use of these solutions is tenuous for the objectives of this research.

The possibility of obtaining an approximate solution was also investigated. Due to the nature of the composite laminate of interest in this research, the problem may be assumed two-dimensional and the analysis could be carried out in cylindrical coordinates:

$$\frac{\partial^2\Theta}{\partial r^2}+\frac{1}{r}\frac{\partial\Theta}{\partial r}+\frac{\partial^2\Theta}{\partial z^2}=\frac{1}{\alpha}\frac{\partial\Theta}{\partial t} \tag{4.12}$$

And manipulating:

$$\begin{aligned} &R''+\frac{1}{r}R'+\lambda^2R=0\\ &Z''-\beta^2Z=0\\ &S'+\alpha\left(\beta^2-\lambda^2\right)S=0 \end{aligned} \tag{4.13}$$

This dimension reduction is possible due to the fact that the laminate layup leads to quasi-homogeneous in-plane heat transfer properties; the assumption that temperature at a given radius does not vary with angular displacement is acceptable. This reduces the amount of boundary conditions required. Translating the known boundary conditions to cylindrical coordinates yields:

- At $z = 0 \; \forall \; r < r_{HB}$ — $q = n$ where n is a known value (W/in^2)
- At $z = 0 \; \forall \; r > r_{HB}$ — $q = 0$ (assume perfect insulation)
- At $r = L$ and $z = -d$ — $q = 0$ (assume perfect insulation)
- At $r = l, z = 0$ — $T = T_{setpoint}(t)$
- At $t = 0$ — $T = T_{setpoint}(t)$ $T = T_\infty$ where T_∞ is room temperature (°C)

In order to solve this analytically, further assumptions are required. The following simplifying assumptions could be made:

- The heater blanket could be assumed as a point load and located at $r = 0, z = 0$
- The control thermocouple location could be assumed to be at the heater blanket point load location.

The resulting boundary conditions are represented schematically in Figure 5-2:

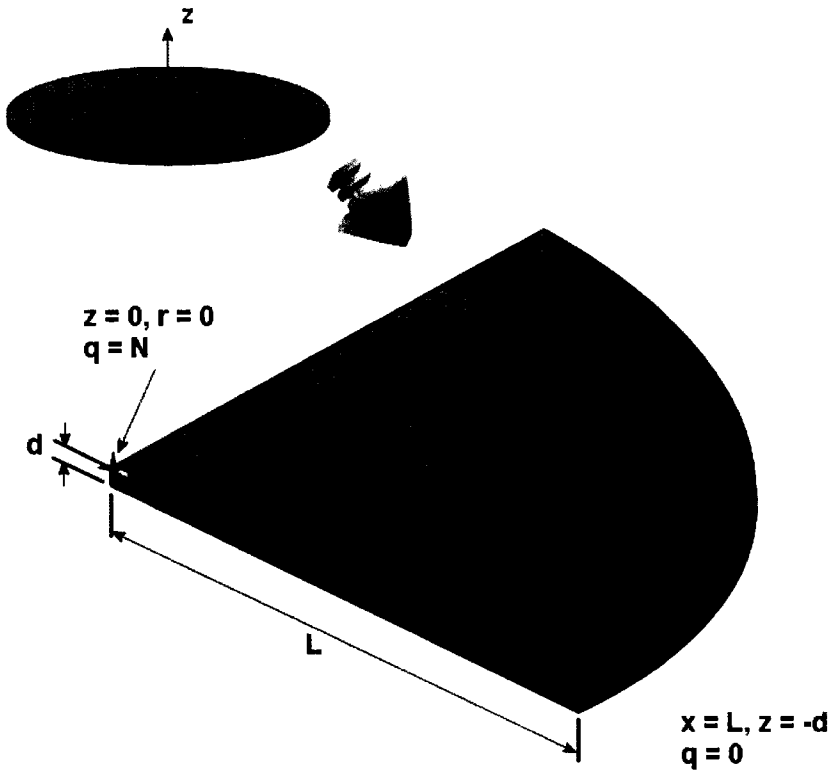

Figure 5-2: Simplified Boundary Conditions

These simplifying assumptions increase the amount of known thermal boundaries; however, further simplifying assumptions would be required to facilitate the evaluation of the equations. Though additional simplifying assumptions are theoretically possible, the system obtained by making these assumptions is no longer representative of the physical system of interest. Furthermore, the simplifying assumptions made do not allow a proper representation of the temperature variations which occurs in composites nor do they allow manipulation of the control thermocouple location, heater blanket and power density.

Therefore, although simplification of the problem described is possible it would render the analysis unrepresentative of the current physical system studied.

5.4 Conclusion

No closed-form solution has been found that could be applied to the physical model of interest in this research. This is due to incomplete knowledge of boundary conditions and to the anisotropy of the material studied. Though an analytical solution could be found if further simplifying assumptions were considered, the analysis would no longer be representative of the physical model studied. The usefulness of such a model would be limited since it would not be applicable to real-life problems, which are typically more complex than well-defined and controlled laboratory experiments.

The interest is now to investigate the possibility of using off-the-shelf numerical analysis software in order to predict the thermal behaviour of a composite whose basic thermal properties are known.

6 Finite Element Modelling

Finite element analysis can be used to discretize and analyze the system numerically. In this project, the MSC Patran pre- and post-processor was used to define the geometry, mesh and boundary conditions and to view the results. MSC Nastran Thermal solver was used to carry out the analysis.

A description of the thermal problem and the modelling parameters used are described in Section 6.1. The test program is detailed in Section 6.3 and the modelling results are presented in Sections 6.4 and 6.5.

6.1 Model Description

6.1.1 Thermal Problem

A number of simplifications were used to allow modelling of the heated composite tooling system. Two tooling system heating configurations were investigated; one configuration used the heater blanket as the heating medium while the second configuration included a copper heat tile to distribute the heat over the substrate. These tooling system configurations were based on the composite systems that are being investigated at the NRC-IAR.

The substrate is a circular flat plate composed of eight plies of woven composite, which has a symmetric lay-up of $[0, 45, -45, 90]_S$. The heat is provided by a silicone heater blanket 62 mm in diameter, which has a uniform power density of 9.3×10^{-3} W/mm^2. The heat is conducted into and through the composite. A control

thermocouple is placed on the composite to provide the temperature feedback necessary for the controlled ramp and soak of the part: the software uses the temperature feedback to turn the heater blanket on or off as required. Schematics of the two problem configurations are shown in Figure 6-1 and Figure 6-2.

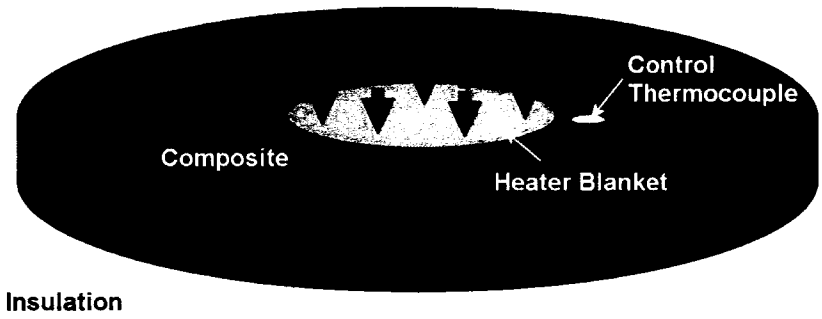

Figure 6-1: Thermal Problem Using Heater Blanket

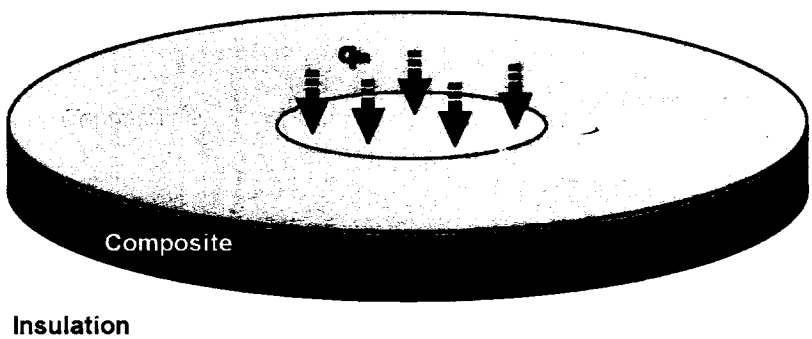

Figure 6-2: Thermal Problem Using Heater Blanket With Copper Tile

6.1.2 Methodology

Due to the symmetry of the problem studied, only a quarter of the physical model was represented in finite element.

The model was evaluated using three-dimensional HEX8 hexagonal elements and WEDGE6 wedge elements. The eight-noded hexagonal elements were selected as they offer good accuracy in thermal model calculations. The six-noded wedge elements were chosen in order to obtain a radiating pattern of elements. To orient the ply material according to the lay-up, each ply was modelled as an independent set of geometrical solids. Figure 6-3 and Figure 6-4 shows the mesh created to represent a thermal problem similar to the schematic of Figure 6-1.

A mesh of 15 concentric quarter-circles of elements was generated. The 14 outermost quarter circles are composed of hexagonal elements whereas the innermost quarter circle of elements is composed of wedge elements. All element thicknesses correspond to the thickness of the solids to which they are associated. Each layer, with the exception of the heater blanket, is composed of two geometric solids.

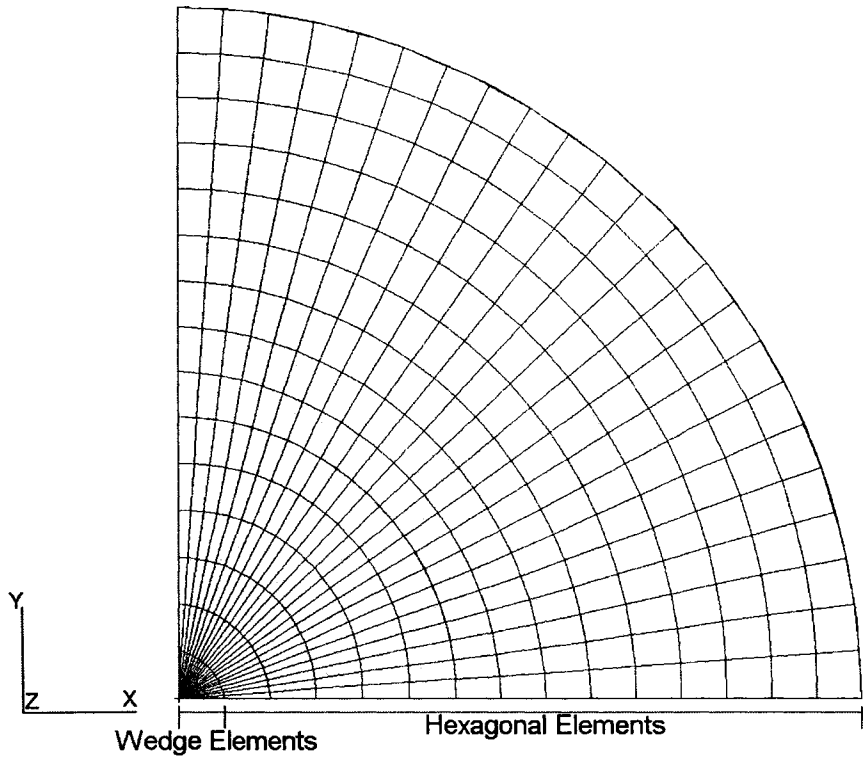

Figure 6-3: Specimen Mesh – Top View

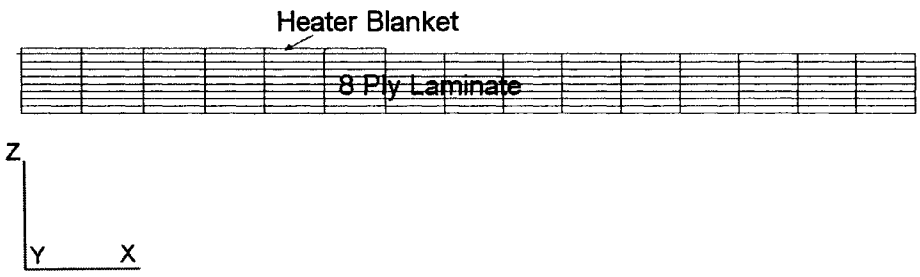

Figure 6-4: Specimen Mesh – Side View

In the case of the configuration with the heater blanket and the copper tile, an additional layer of elements is included between the heater blanket and the top laminate layer.

The elements were separated into groups, based on their assigned properties and orientation with respect to the main material axes. The groups are shown in Figure 6-5 for the heater blanket configuration. A list of the groups is given in Table 6-1.

Table 6-1: Element Property Set Groups

Group	Property Set	Group	Property Set
1	Silicone Rubber	4	CF/Ep Weave – orientation –45°
2	CF/Ep Weave – orientation 0°	5	CF/Ep Weave – orientation 90°
3	CF/Ep Weave – orientation 45°	6	Copper*

* for heater blanket and heater tile configuration

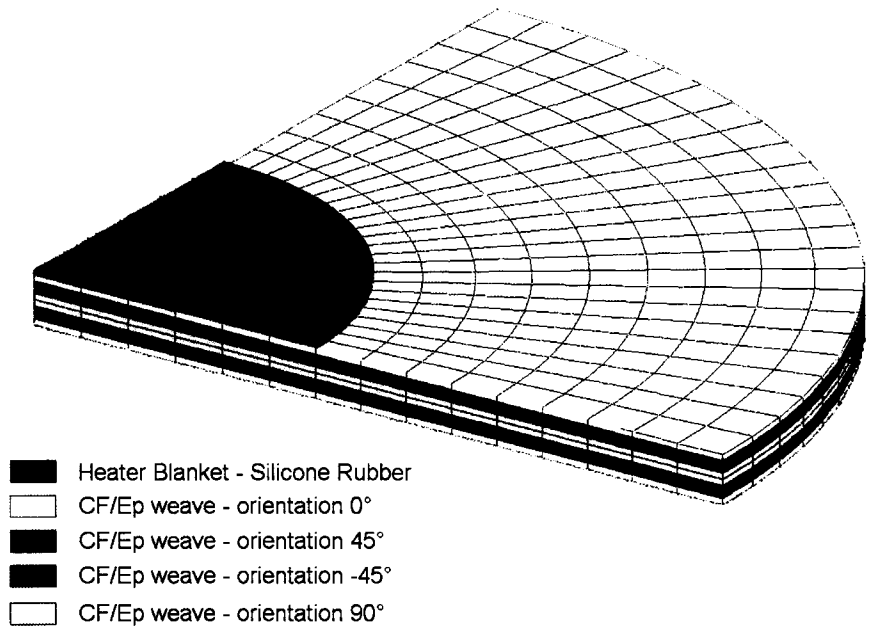

Figure 6-5: Element Groups

Three types of materials were used for these models, namely carbon fibre/epoxy (CF/Ep) 2/2 twill composite, silicone rubber and copper. The CF/Ep directional

material properties were rotated as required by the ply orientations. The material properties used for the parametric studies are given in Table 6-2 [30][36][44][49]. The material properties were drawn from literature and were not used in the final predictive model.

Table 6-2: Nominal Material Thermal Properties**

Property	CF/Ep	Property	Copper	Silicone Rubber
k_{11}, k_{22} (W/mm·K)	0.1	k (W/mm·K)	0.391	0.00022
k_{33} (W/mm·K)	0.002	ρ (kg/mm^3)	8.9×10^{-6}	1.249×10^{-6}
ρ (kg/mm^3)	1.4×10^{-6}	c_p (W/kg·K)	385	1880
c_p (W/kg·K)	800			

** These values were used for the parametric studies

A volumetric heat generation load of 0.0164 W/mm^3 (268 W/in^3) was applied to the heater blanket. This corresponds to a power of 24.95 W for the heater blanket. The volumetric heat generation function was controlled by a material property field which caused the volumetric heat generation to be on when the overall average temperature of the heater blanket was below 100°C and off if this temperature was exceeded.

6.2 Mesh Sensitivity Study

In order to assess the accuracy of the mesh used, a mesh sensitivity study was carried out. The model was analysed using adiabatic boundary conditions and a varying mesh size.

6.2.1 Model Mesh Variations

Three mesh sizes were used in the sensitivity study:

- A coarse mesh of 708 elements and 868 nodes.
- A nominal mesh of 2898 elements and 3394 nodes.
- A refined mesh of 11224 elements and 12841nodes.

The mesh sizes were based on the global element edge length used to generate the mesh. For the coarse mesh a global edge length of 10.4 was used, 5.2 was used for the nominal mesh and 2.6 was used for the refined mesh. The global edge length is the length of the edge of elements located along the x-axis. In all cases the thicknesses of the elements were equal to the thickness of the geometric solids they were associated to. The three meshes generated for this study are shown in Figure 6-6.

A volumetric heat load of 0.0041 W/mm^3 was applied to the heater blanket solid and adiabatic boundary conditions were applied to the models.

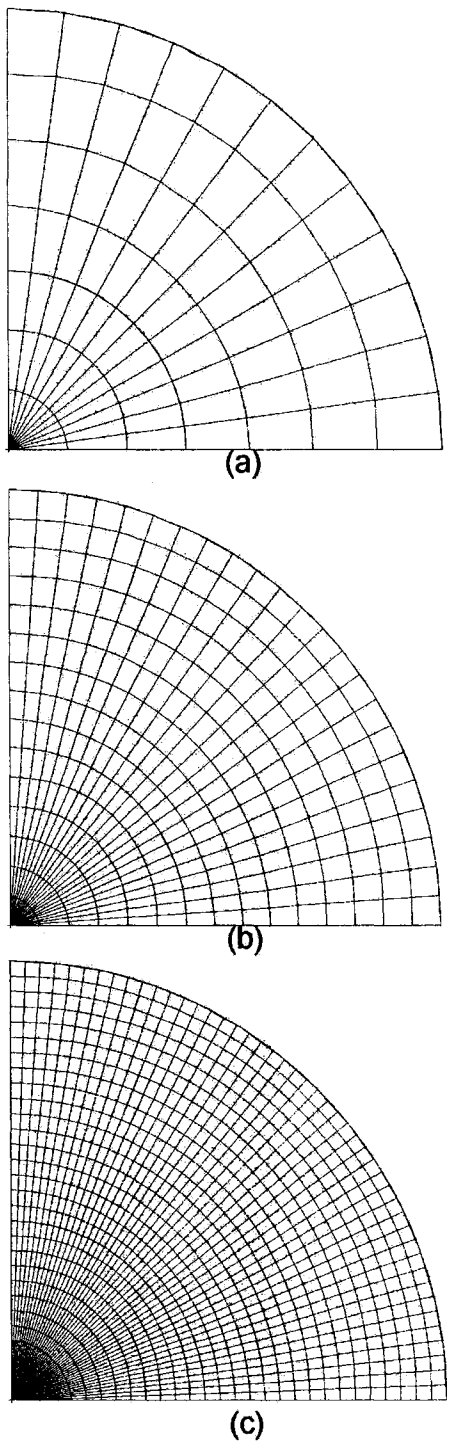

Figure 6-6: Top View of Meshes Generated (a) Coarse Mesh, (b) Nominal Mesh and (c) Refined Mesh

6.2.2 Sensitivity Study Results

The temperature results obtained were plotted as a function of time. Figure 6-7 shows the location of the nodes for which the temperature data were taken. It can be seen in Figure 6-8 and Figure 6-9 that the results for the nominal and refined mesh are very close. There is little or no difference in the amplitude and oscillations between the nominal and refined mesh whereas the coarse mesh typically shows larger amplitude in oscillations when transferring from the ramp-up to the soak segment of the temperature profile.

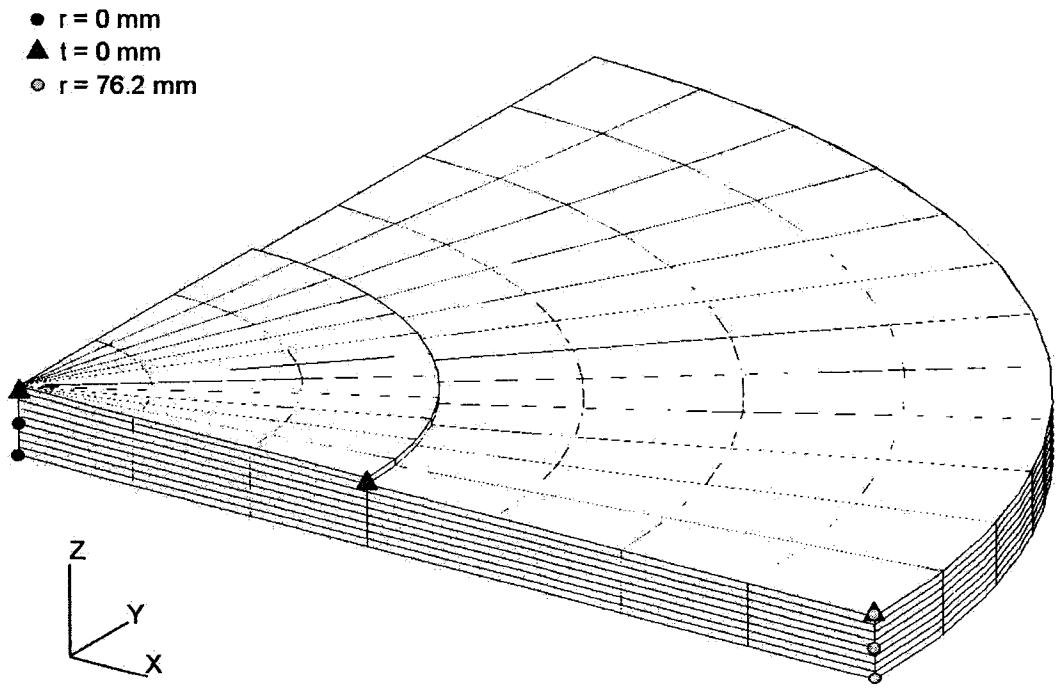

Figure 6-7: Node Locations for Temperature Measurements for Mesh Refinement Analysis

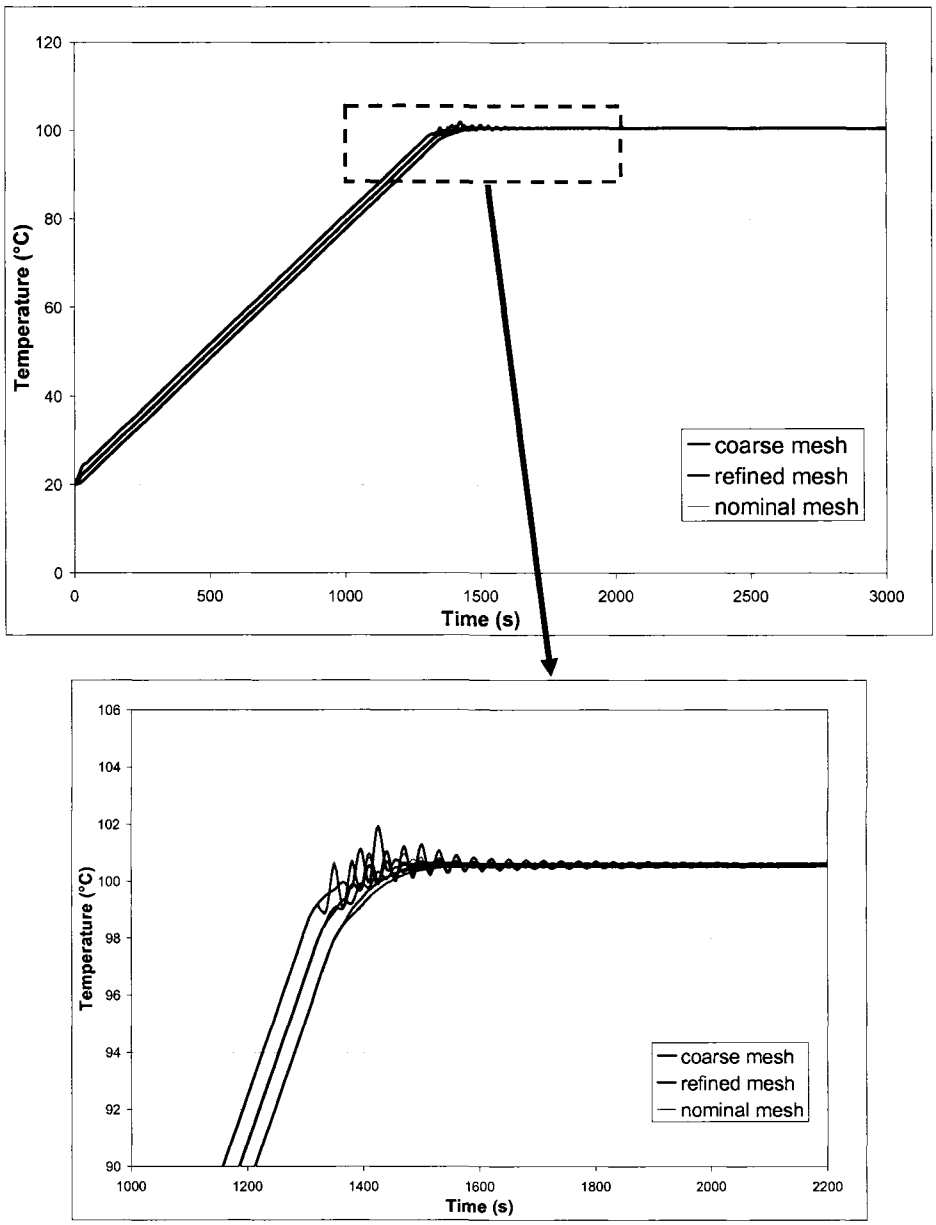

Figure 6-8: Temperature Profiles for Various Mesh Sizes at the Top Surface (t = 0, 3 points)

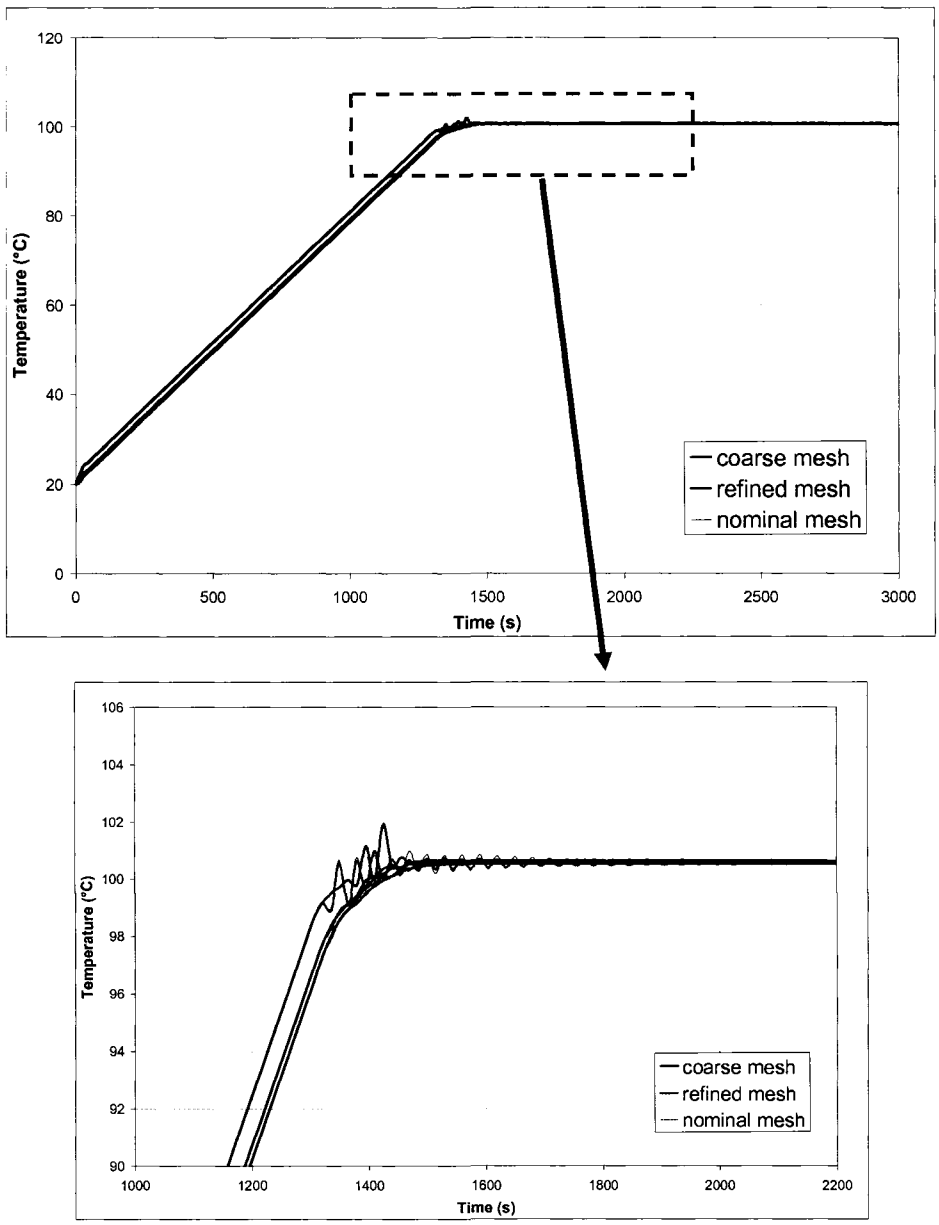

Figure 6-9: Temperature Profiles for Various Mesh Sizes at the Central Axis (r = 0, 3 points)

Based on these results, the nominal mesh was selected for modelling; the increase in node numbers and calculation time when using the refined mesh would not be justified

given the very minor differences in the results obtained between the nominal and refined meshes.

6.3 Modelling Test Program

Two modelling phases were carried out for this research; the first modelling phase consisted of parametric studies and the second phase consisted of predictive modelling of the specified heat transfer problem (Section 6.1.1).

The parametric studies were carried out in order to assess the effects of the variation of thermal conductivity, specific heat and copper tile thickness on the results. This also allowed an evaluation of the sensitivity of the model to these parameters. Nominal material properties drawn from literature were used for this phase of the modelling as the trends observed during the parametric studies are not linked to a particular numerical material property value.

6.4 Parametric Studies

6.4.1 Model Descriptions

Four test case configurations were used to carry out the parametric studies for this model. The difference in the model configurations stemmed from the presence or absence of a copper heater tile between the heater blanket and the CF/Ep substrate as well as from the boundary conditions imposed. In all cases, the initial temperature was set to 20°C and a volumetric heat generation load of 0.0041 W/mm^3 (67.13 W/in^3) were applied to the heater blanket. This corresponds to a power of 6.24 W for the heater blanket. The volumetric heat generation function was controlled by a material property

field which caused the volumetric heat generation to be on when the overall average temperature of the heater blanket was below 100°C and off if this temperature was exceeded. In two configurations adiabatic boundary conditions were applied and in the remaining configurations very small convection was applied to the free surfaces to mimic imperfect insulation. The convection coefficient was varied from 0 to 2 W/m^2K with 2 W/m^2K being the lowest value typically attributed to free convection [36]. In the adiabatic cases, the surrounding environment is assumed to have no effect on the heat transfer occurring within the system under consideration ($q = 0$ and $h = 0$). The four model configurations are outlined in Table 6-3.

Table 6-3: Model Configurations

Configuration	Boundary Condition	Heating Configuration
A	Adiabatic	Heater Blanket
B	Adiabatic	Heater Blanket & Heat Tile
C	Convection	Heater Blanket
D	Convection	Heater Blanket & Heat Tile

Using these different configurations, the effects of various parameters were evaluated. The effects due to variations of in-plane and transverse thermal conductivity were observed, in addition to the effects due to changes in specific heat. The heater tile thickness and convection coefficient were also varied where applicable. A test matrix was established for these tests; this matrix is shown in Table 6-4.

Table 6-4: FEM Test Matrix

Test Configuration	ID #	Composite Properties			Heater Blanket		Convection	Heater Tile
		k_{xx}, k_{yy} (W/mm.K)	k_{zz} (W/mm.K)	c_p (J/Kg.K)	Diameter (in)	Power Density (W/mm^2)	Convection Coefficient (W/mm^2K)	Thickness (mm)
A	1	0.1	0.002	800	62.2	0.00928		
	2	0.1	0.02	800	62.2	0.00928		
	3	0.1	0.02	700	62.2	0.00928		
	4	0.4	0.02	700	62.2	0.00928		
	5	0.1	0.0002	800	62.2	0.00928		
	6	0.025	0.02	700	62.2	0.00928		
	7	0.1	0.02	900	62.2	0.00928		
B	1	0.1	0.002	800	62.2	0.00928		0.5
	2	0.1	0.02	800	62.2	0.00928		0.5
	3	0.1	0.0002	800	62.2	0.00928		0.5
	4	0.1	0.0002	800	62.2	0.00928		1
	5	0.1	0.002	800	62.2	0.00928		1
	6	0.1	0.002	800	62.2	0.00928		1.5
	7	0.1	0.002	800	62.2	0.00928		2.25
C	1	0.1	0.002	800	62.2	0.00928	2.00E-06	
	2	0.1	0.002	800	62.2	0.00928	5.00E-07	
	3	0.1	0.002	800	62.2	0.00928	1.00E-06	
	4	0.1	0.002	800	62.2	0.00928	1.50E-06	
D	1	0.1	0.002	800	62.2	0.00928	5.00E-07	1.5

In the case of configurations A and C, the mesh generated (Figure 6-3 and Figure 6-4) is composed of a total of 2898 elements, 2691 of which are hexagonal and 207 of which are wedge elements. These models contain 3394 nodes and are composed of 17 geometric solids to which the material properties were assigned. The models used to evaluate configurations B and D contain 3243 elements, with 3013 elements being hexagonal and 230 elements being wedge elements. These models contain 3755 nodes and are composed of 19 geometric solids.

The hexagonal elements used in these models are 8-noded elements are Patran HEX8 that are analysed by Nastran Thermal as CHEXA elements. The wedge elements containing 6 nodes are Patran WEDGE6 elements that are analysed by Nastran Thermal as CPENTA elements [53]. All analysis except cases C1 and C4, were analysed using

200 15-second time steps, for a total time of 3000 seconds (50 minutes). The convection coefficients used in cases C1 and C4 caused the applied heat load on the heater blanket solid to turn on with increased frequency; the time step of 15 seconds was too large for this type of load analysis and 600 time steps of 5 seconds were used to obtain improved results.

In all cases, perfect contact was assumed between all layers of the model. No contact resistances were modelled.

6.4.2 Results

In the following sections, the results for the four test configurations are discussed. The results for each configuration set are given in Table 6-5 to Table 6-8. Each table summarizes the parameters varied and provides the magnitude of the temperature gradient (ΔT) during the ramp up phase as well as during the hold phase of the FEM analysis test. The temperature gradient at r = 0 is the difference in temperature between the composite laminate's bottom and top face nodes at the specified time. The temperature gradient at t = 5.04 mm is the difference in temperature between the composite laminate's outer radius (r = 76.2 mm) and centre axis (r = 0 mm) nodes. The heat-up rate is also provided in the summary table. This indicates the maximum heat-up rate achieved assuming that the heater blanket is always on during ramp-up. It is calculated as the slope of the curve during ramp-up.

6.4.2.1 Configuration A (Heater Blanket, Adiabatic)

Table 6-5: Result Summary for Configuration A Cases

Case ID	Material Properties			Results				
				ΔT (°C)				heat-up rate (°C/min)
				t = 1005s		t = 2205s		
	k_x (W/mm)	k_z (W/mmK)	c_p (J/KgK)	r = 0 mm	t = 5.04 mm	r = 0 mm	t = 5.04 mm	
A1	0.1	0.002	800	2.202	1.028	0.024	0.000	3.51
A2	0.1	0.02	800	0.249	1.628	0.000	0.000	3.51
A3	0.1	0.02	700	0.248	1.621	0.008	0.000	3.99
A4	0.4	0.02	700	0.242	0.346	0.003	0.000	3.99
A5	0.1	0.0002	800	11.691	0.055	0.025	0.000	3.51
A6	0.025	0.02	700	0.248	6.730	0.007	0.002	3.99
A7	0.1	0.02	900	0.250	1.634	0.059	0.001	3.13

From the results obtained in cases A1, A2, and A5 as well as cases A3, A4 and A6 (see Table 6-5) it can be observed that transverse and radial conductivities do not influence the heat-up rate. However, it can also be observed that an increase of the specific heat, c_p, for given transverse and in-plane thermal conductivities and for a fixed heat input, causes a decrease in heat-up rates. This can be seen in Figure 6-10. The decrease in heat-up rates is explained by the added energy storage capacity of the material. The heat-up rates are related by a quasi-linear relationship at the heat capacity range of interest (700J/kgK to 900J/kgK) as shown in Figure 6-11.

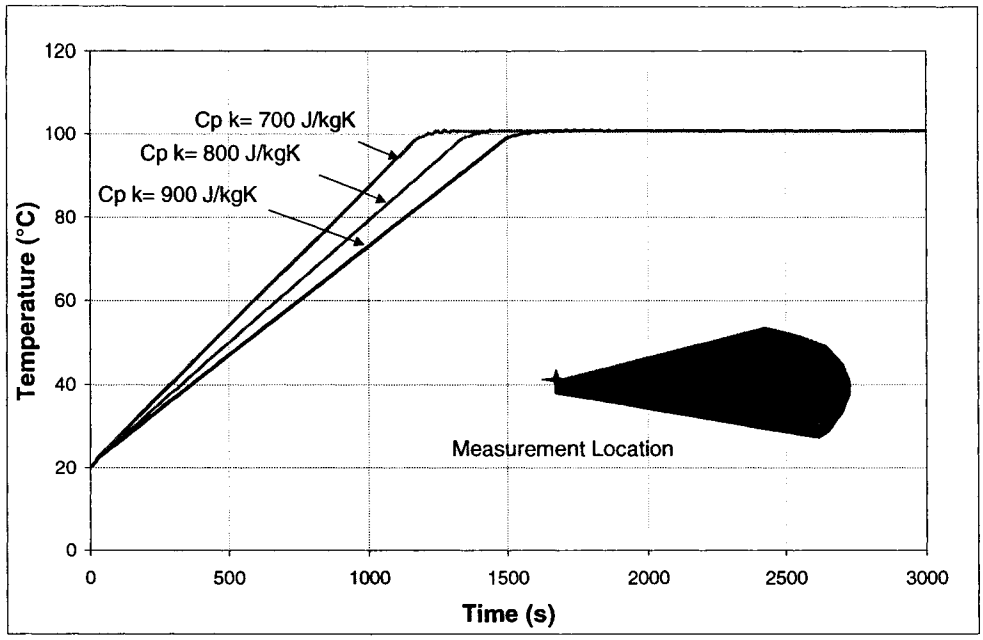

Figure 6-10 Temperature Profiles for Various Specific Heats (r = 0, t = 0)

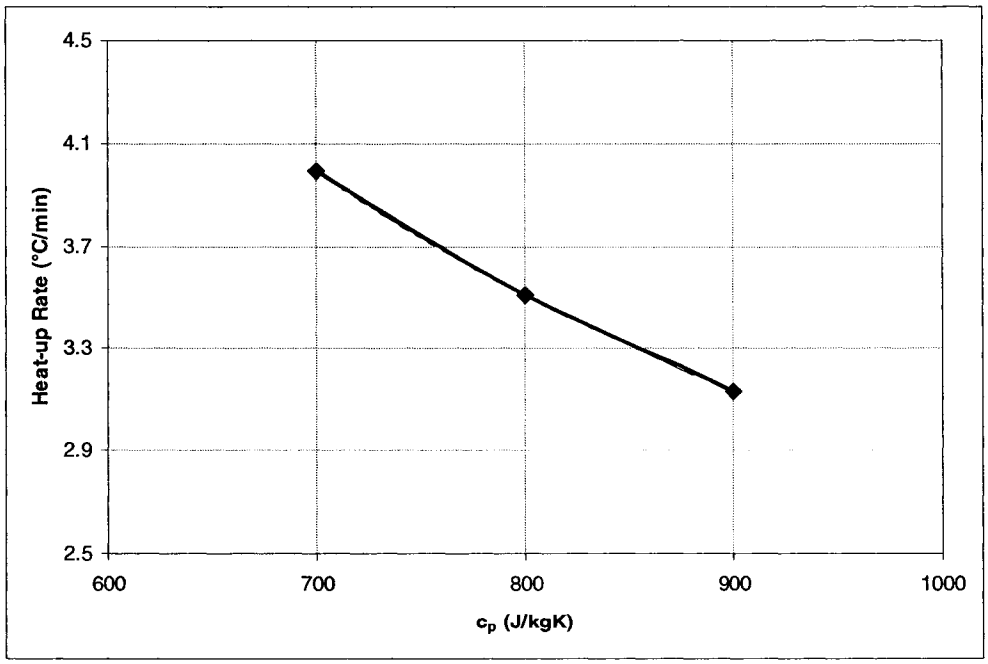

Figure 6-11: Heat-up Rate as a Function of Specific Heat

From the results obtained and shown in Table 6-5 and in Figure 6-12 it can be seen that the radial and transverse temperature gradients are not significantly influenced by changes in specific heat.

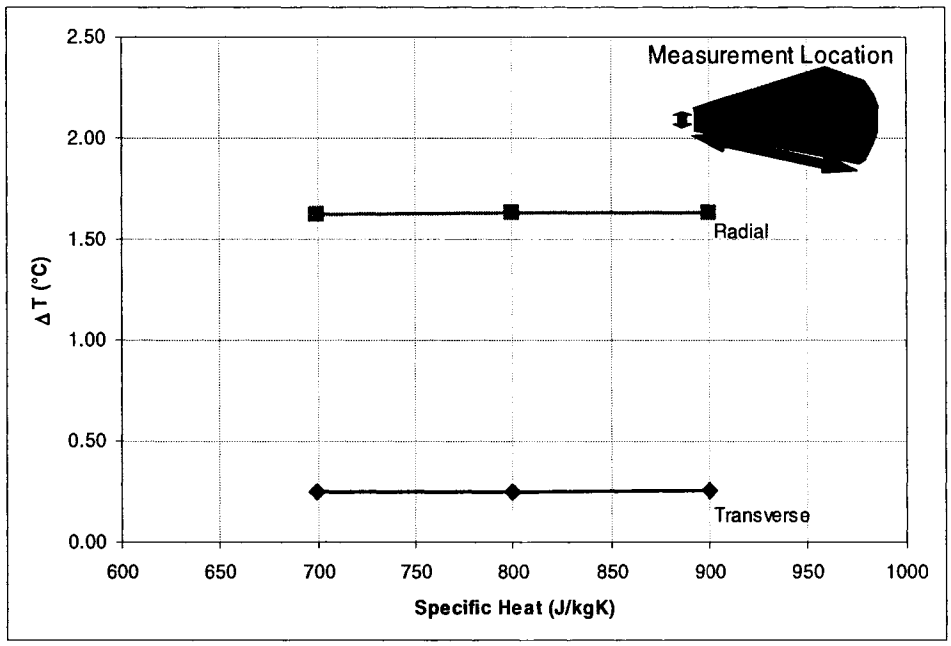

Figure 6-12: Radial and Transverse Temperature Differential as a Function of Specific Heat

During ramp-up, the transverse temperature differential decreases sharply as the transverse thermal conductivity increases from zero to approximately 0.0025 W/mmK. The decrease in temperature differential then remains low and tends to level off asymptotically. The radial temperature differential increases logarithmically with increasing transverse thermal conductivity; however, it remains low (below 2°C) at all values of transverse thermal conductivity observed in this study. This can be seen in Figure 6-13.

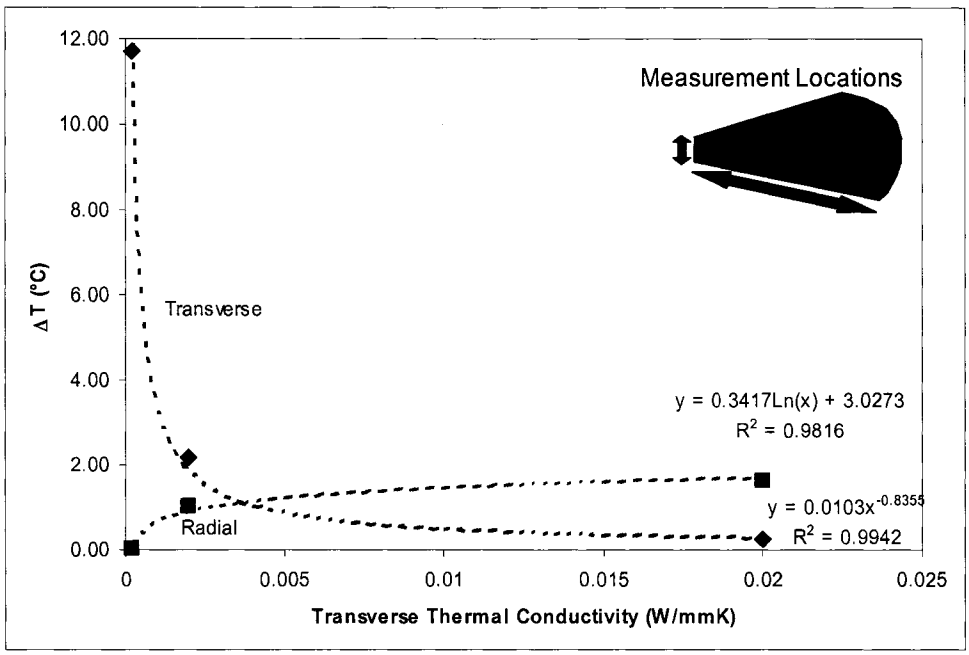

Figure 6-13: Transverse and Radial Temperature Differential as a Function of Transverse Thermal Conductivity During Ramp-Up

During ramp-up, the in-plane thermal conductivity has little effect on the transverse temperature differential. As the in-plane thermal conductivity is increased from zero to 0.4 W/mmK the radial temperature differential decreases following a decreasing power function. The temperature differential decreases rapidly from zero to 0.1 W/mmK, then has an asymptotical behaviour as shown in Figure 6-14.

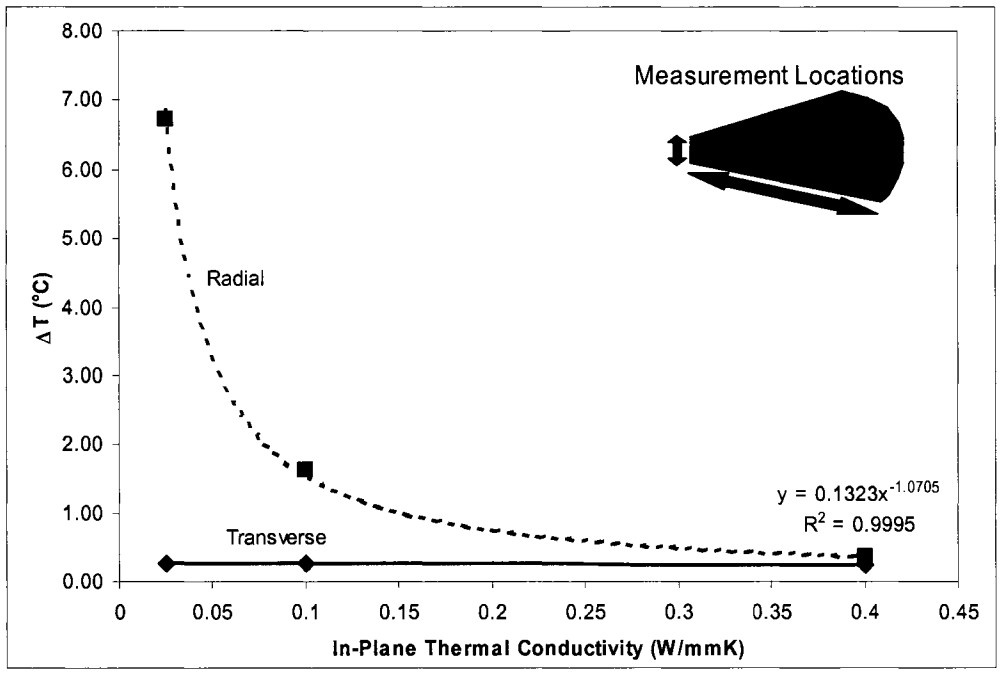

Figure 6-14: Transverse and Radial ΔT as a Function of In-plane Thermal Conductivity During Ramp-Up

6.4.2.2 Configuration B (Heater Blanket and Tile, Adiabatic)

For this configuration, the nominal properties values were used for the in-plane thermal conductivity and for the specific heat of the composite laminate.

The results for configuration B are given in Table 6-6.

Table 6-6: Result Summary for Configuration B Cases

Case ID	Material Properties		Results				
			ΔT (°C)				heat-up rate (°C/min)
			t = 1005s		t = 2205s		
	k_z (W/mmK)	t_{Cu} (mm)	r = 0 mm	t = 5.04 mm	r = 0 mm	t = 5.04 mm	
B1	0.002	0.5	1.365	0.594	0.025	0.000	2.71
B2	0.02	0.5	0.183	1.150	0.002	0.007	2.71
B3	0.0002	0.5	5.572	0.017	0.020	0.000	2.71
B4	0.0002	1	4.018	0.010	1.627	0.004	2.21
B5	0.002	1	0.993	0.418	0.179	0.181	2.21
B6	0.002	1.5	0.784	0.322	0.784	0.322	1.86
B7	0.002	2.25	0.597	0.240	0.597	0.240	1.51

From the results obtained in cases B1 to B3 (Table 6-6) it can be observed that transverse conductivity does not influence the heat-up rate; this agrees with previous results obtained for configuration A. However, it can also be observed that for a given transverse thermal conductivity k_z and a fixed heat input, an increase of the copper tile thickness, $t_{Cu,}$ causes a decrease in heat-up rates. This can be seen in Figure 6-15.

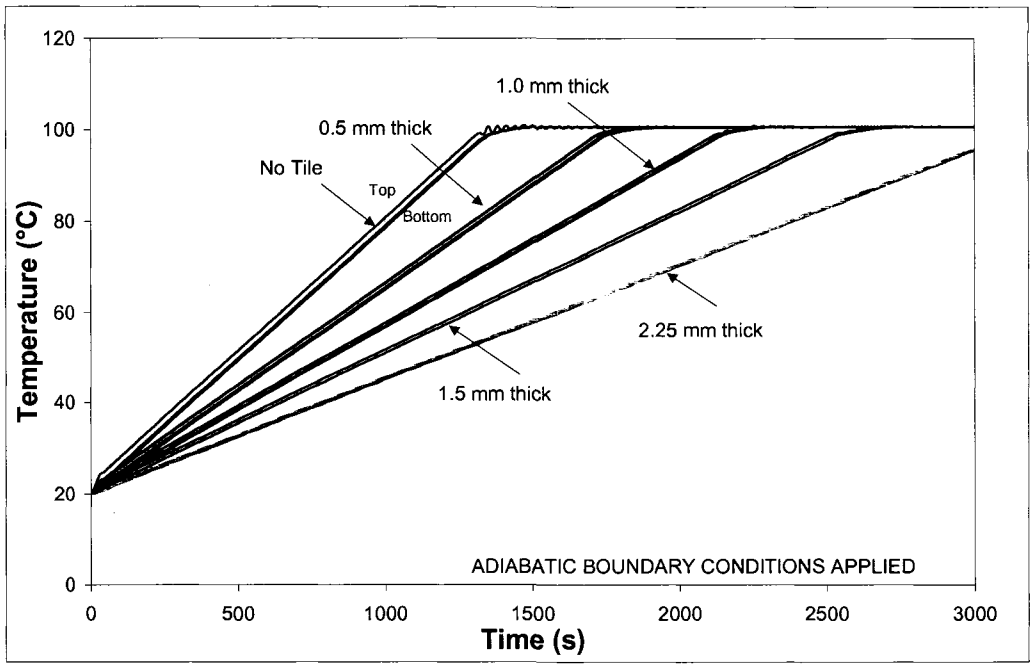

Figure 6-15: Temperature Profiles for Various Copper Tile Thicknesses (r = 0, 3 points)

The decrease in heat-up rates can be explained by the added thermal mass of the copper tile. The magnitude of the heat-up rate was plotted as a function of copper tile thickness (Figure 6-16): the initial section of the curve (t_{Cu} from zero to approximately 2mm) follows a third order polynomial trend, whereas the later section of the curve would tend to follow a logarithmic trend as seen in Figure 6-16 and Figure 6-17 respectively. It is important to note, that the work carried out with copper heater tiles at NRC to date used copper thicknesses ranging from 0.5 mm to 2 mm; therefore, the interest would lie in the initial part of the curve for tile thicknesses up to approximately 2 mm.

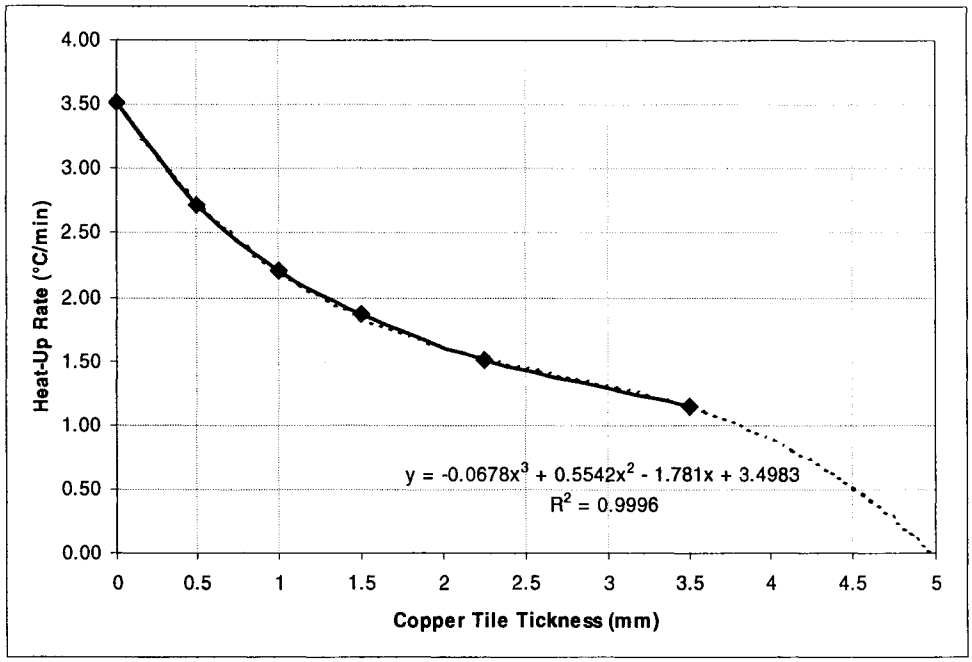

Figure 6-16: Heat-up Rate as a Function of Copper Tile Thickness with Polynomial Trendline

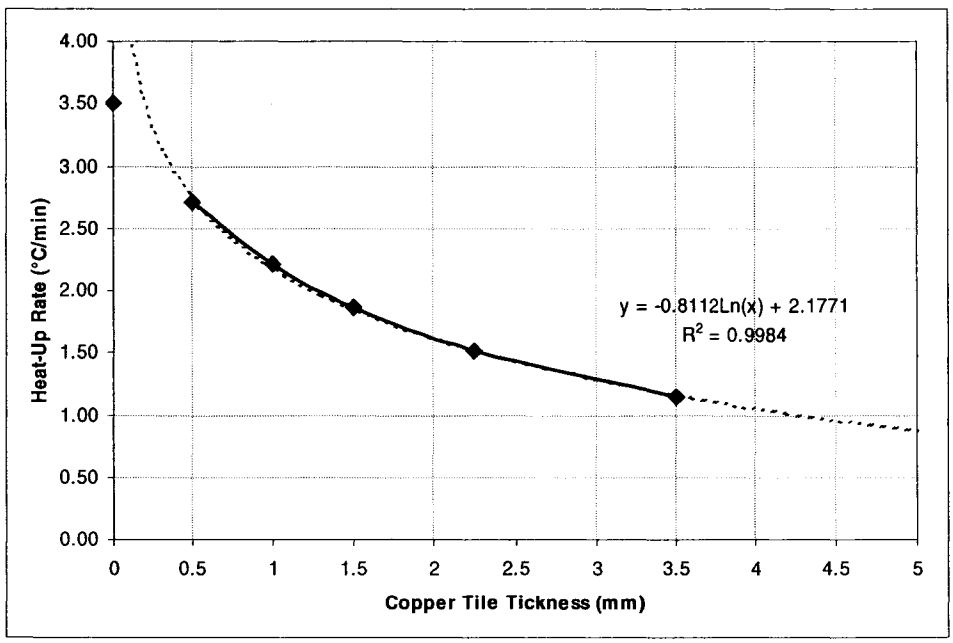

Figure 6-17: Heat-up Rate as a Function of Copper Tile Thickness with Logarithmic Trendline

The transverse temperature differential was found to decrease with increasing copper tile thickness (Figure 6-18). This can be explained by the slower heat-up rates encountered with increased copper tile thickness: this allows more time for the heat to travel through the substrate. However, the transverse temperature differential is also a function of the transverse thermal conductivity. The temperature differential decreases sharply as the transverse thermal conductivity increases from zero to approximately 0.0025 W/mmK. For all cases the temperature differential is low (below 2.5°C) and tends towards an asymptotical behaviour. This trend can be seen in Figure 6-19, and is comparable to the trend observed in Figure 6-13.

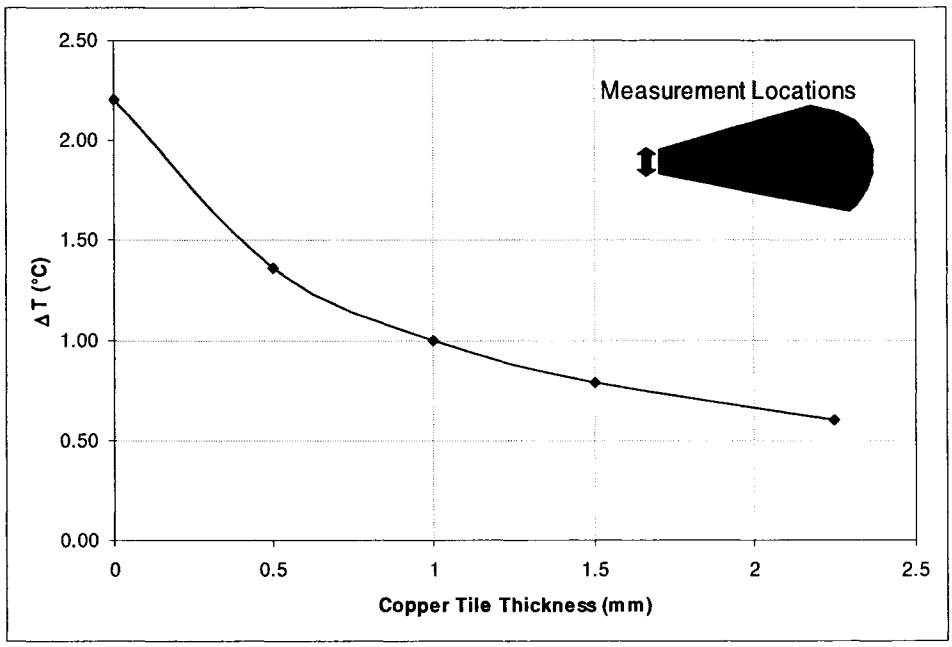

Figure 6-18: Transverse ΔT as a Function of Copper Tile Thickness During Ramp-Up

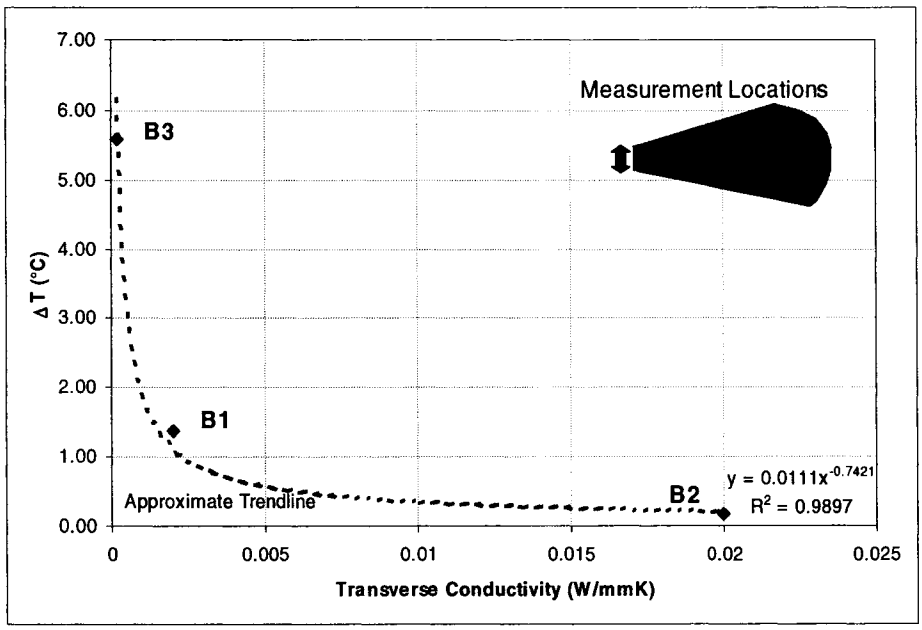

Figure 6-19: Transverse Temperature Differential as a Function of Transverse Thermal Conductivity for SS 304 Standards During Ramp-Up

These analyses indicate that the effectiveness of the copper tile is dependent on the transverse thermal conductive properties of the substrate. The lower the transverse thermal conductivity of the substrate, the more effective the copper tile will be in obtaining a low temperature gradient across the tool face. This can be seen in Figure 6-20. This behaviour is due to the high ratio of in-plane versus transverse thermal conductivity. The heat conducts quickly through the tile to produce a uniform heating along the top of the substrate. At high in-plane to transverse thermal conductivity ratios, the low transverse thermal conductivity, relative to the in-plane thermal conductivity, allows heat to distribute uniformly in-plane before significant transfer in the transverse direction occurs. As the ratio of in-plane to transverse thermal

conductivities decreases, so does the effectiveness of the copper tile as the heat begins to transfer through the thickness before it has spread uniformly in the in-plane direction.

The radial temperature difference is affected by the copper tile thickness; however, the most significant effect is obtained by the inclusion or absence of the copper tile. Increases of the copper tile thickness have little influence on the radial temperature spread (0.6°C at 0.5mm of thickness to 0.24°C at 2.25mm of thickness). This can be seen in Figure 6-21.

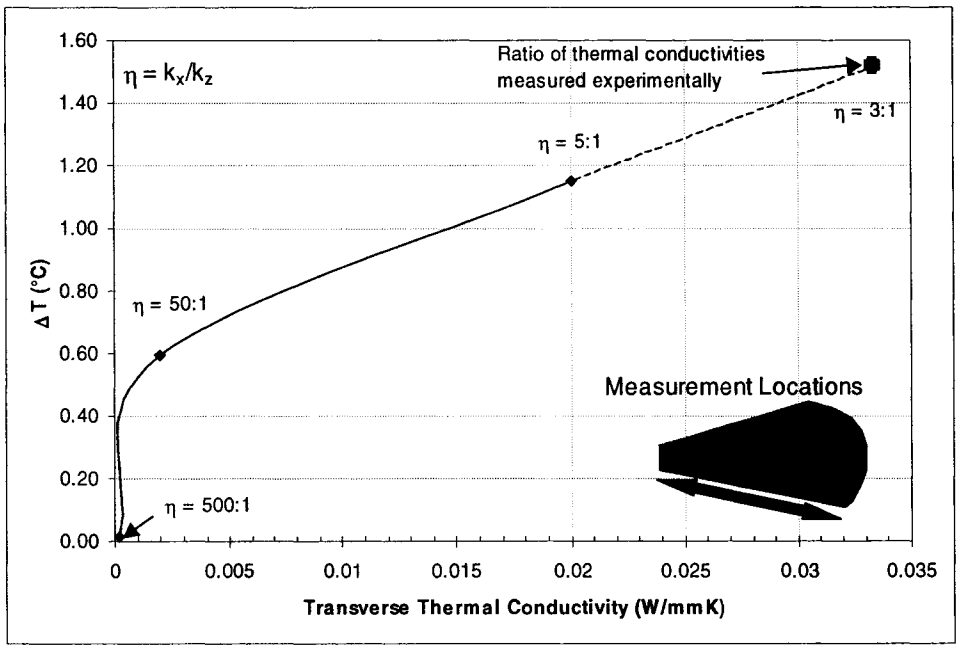

Figure 6-20: In-Plane Temperature Differential as a Function of Transverse Thermal Conductivity for a Set Copper Tile Thickness During Ramp-Up

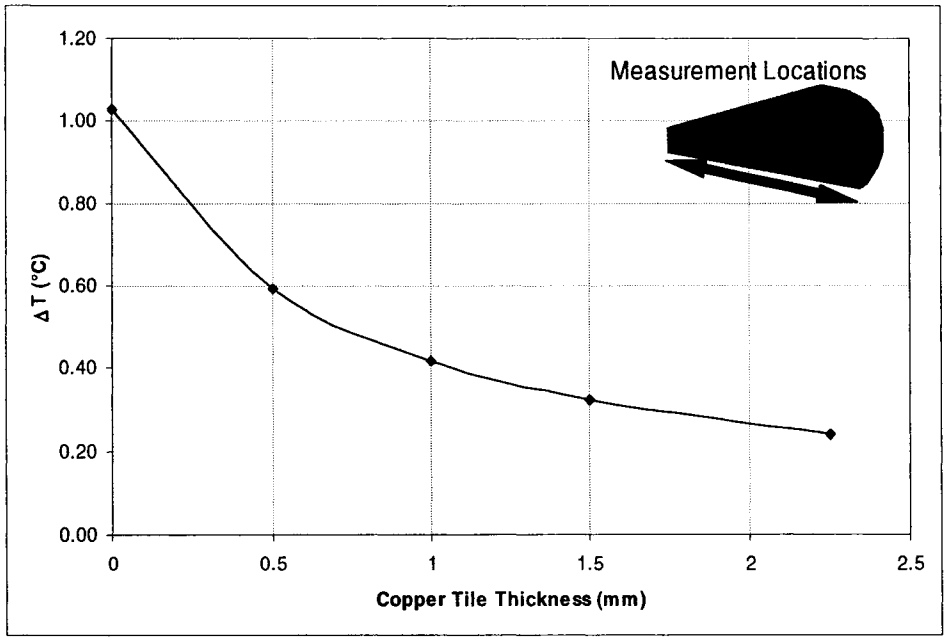

Figure 6-21: Radial Temperature Differential as a Function of Transverse Thermal Conductivity for a Set Transverse Thermal Conductivity During Ramp-Up

6.4.2.3 Configuration C (Heater Blanket, Convection)

Free convection to an air temperature of 30°C was applied to the model in addition to the volumetric heat generation load. The results are given in Table 6-7

Table 6-7: Result Summary for Configuration C Cases

Case ID	Boundary Condition	Results				
		ΔT (°C)				time to soak (sec)
	h	t = 1005s		t = 2205s		
	(W/m^2K)	r = 0 mm	t = 5.04 mm	r = 0 mm	t = 5.04 mm	
C1	2	2.223	1.057	2.250	1.091	2655.00
C2	0.5	2.209	1.037	0.427	0.251	1695.00
C3	1	2.214	1.045	0.957	0.499	1815.00
C4	1.5	2.219	1.052	1.790	0.750	2040.00
A1	0	2.202	1.028	0.024	0.000	1140.00

From the results obtained in cases C1 to C4 it can be observed that the convection coefficient highly affects the time required to reach soak conditions (Table 6-7). Figure 6-22 shows that an increase in convection coefficient from 0 to 2 W/m^2K increases the time required to achieve soak by approximately 1515 seconds or 130 %. It should be noted that past experience with heat transfer work at NRC-IAR has shown that the heat-up profiles obtained with heater blankets and adequate insulation are quasi-linear in nature. This would indicate that the typical convection losses would range between convection coefficients of 0.5 W/m^2K to approximately 1.5 W/m^2K.

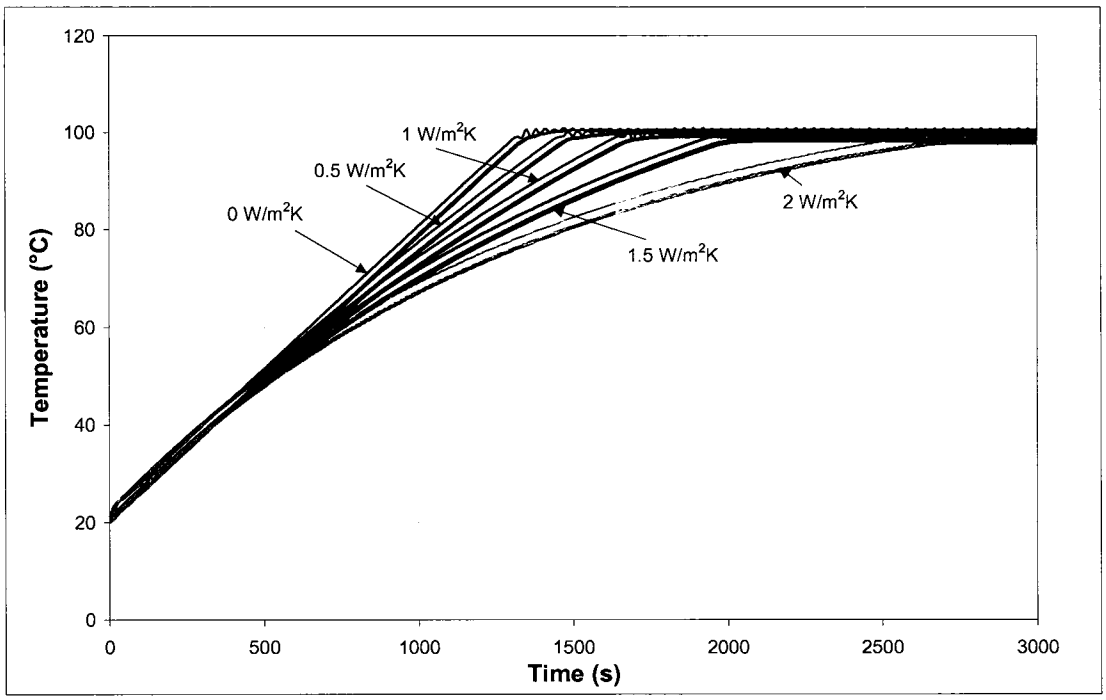

Figure 6-22: Temperature Profiles for Various Convection Coefficients

It was found that the convection coefficient has little influence on the transverse temperature gradient during the ramp-up phase. However a quasi-linear increase in temperature gradient is observed during the steady state or soak phase with increasing convection (Figure 6-23). It is important to note that the temperature gradients encountered are small at approximately 1°C.

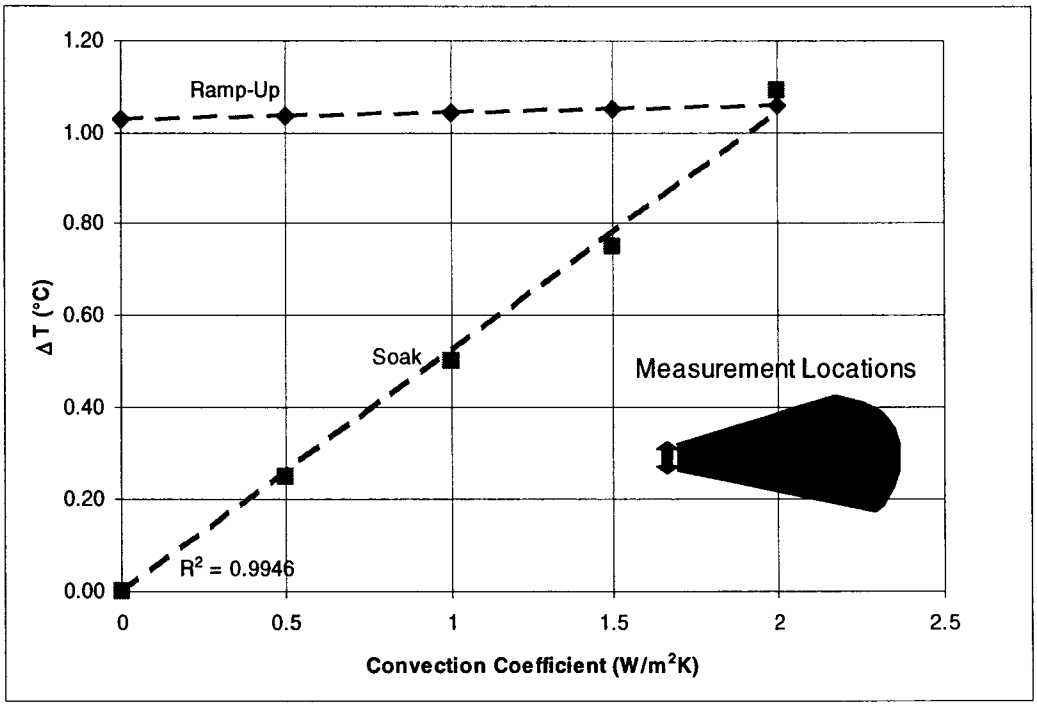

Figure 6-23: Transverse ΔT as a Function of Convection Coefficient

Similarly, convection has little effect on the radial temperature gradient during the ramp-up phase. However, the impact is more pronounced during the steady state phase with radial temperature gradients rising to 2.25 °C at a convection coefficient of 2 W/m^2K (Figure 6-24). There is more impact from convection on the radial temperature gradient than on the transverse temperature gradient (2.25 °C at 2 W/m^2K radially compared to 1.09 °C transversely).

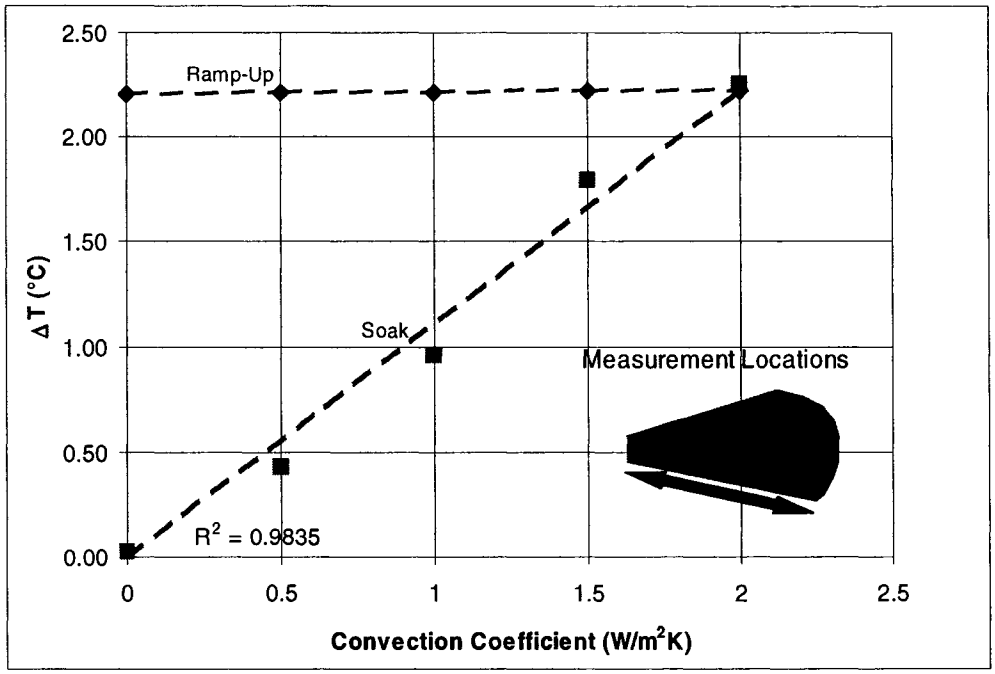

Figure 6-24: In-Plane ΔT as a Function of Convection Coefficient

6.4.2.4 Configuration D (Heater Blanket and Tile, Convection)

The results for configuration D are given in Table 6-8.

Table 6-8: Result Summary for Configuration D Case

Case ID	BC*	Results				
	h	ΔT (°C)				time to soak
		t = 1005s		t = 2205s		(sec)
	(W/m²K)	r = 0 mm	t = 5.04 mm	r = 0 mm	t = 5.04 mm	
D1	0.5	0.784	0.322	0.246	0.113	2905.00

*BC = Boundary Conditions

No further significant trends were observed with the addition of convection to the copper heating tile. The results obtained corroborate the results obtained with the configuration C cases (Figure 6-25).

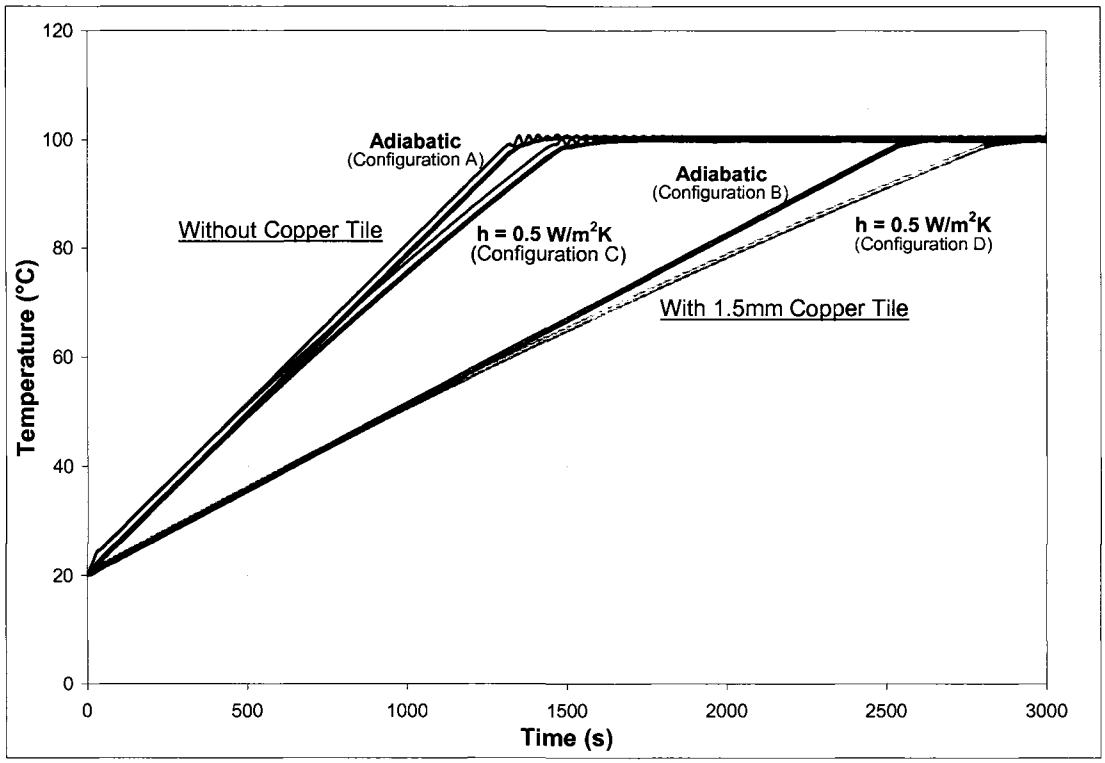

Figure 6-25: Temperature Profiles for Various Copper Tile Thicknesses

6.4.3 Conclusions

In the absence of a copper heater tile and of convection loads, the heat-up rate is only affected by the specific heat of the material. The relationship is quasi-linear with heat-up rates decreasing with increasing specific heat. The addition of the copper tile decreases the achievable heat-up rate; increasing the copper tile thickness causes a

decrease in heat-up rate due to the increase in thermal mass added to the system. Adding convective boundary conditions increases the amount of time required to achieve soak conditions by causing non-linear heat-up rates. The thermal conductivity of the material was not found to have any effect on the heat-up rate of the system.

The transverse temperature gradient in the system is most highly affected by variations in the transverse thermal conductivity of the system. A rapid decrease in transverse temperature gradients is observed for both A and B configurations when increasing the transverse thermal conductivity from 0 W/mmK to 0.0025 W/mmK. The addition of the copper heater tile contributes to lowering the transverse temperature gradient with the highest reduction occurring at the application of the tile. Additional thickness increases to the copper heater tile have little effect on the transverse temperature gradient. It is important to note that without the application of convection, there are no temperature gradients encountered during the soak phase. The application of convective boundary conditions to external surfaces causes a measurable temperature gradient to occur during the soak phase; however, little difference is measured in the heat-up phase temperature gradients.

The radial temperature gradient was found to be most affected by the in-plane thermal conductivity. There is a rapid decrease in radial temperature gradient when increasing the in-plane thermal conductivity from 0 to 0.075 W/mmK; further increase in in-plane thermal conductivity have less impact on the radial temperature gradient encountered. It was found that the copper heater tile addition had little impact on the radial temperature gradient unless the transverse thermal conductivity is low enough to promote homogenisation of the upper surface temperature before any significant heat

transfer can occur in the transverse direction. The radial temperature gradient is then negligible. As with the transverse temperature gradient, convection has little impact on the temperature gradients encountered during the heat-up phase. The addition of the convection causes the radial temperature gradient to increase proportionally to the convection coefficient during the soak phase.

The directional thermal conductivities were found to have the highest influence on the temperature gradients. Low thermal conductivity inputs lead to more sensitive models; as the thermal conductivities get lower, small changes in thermal conductivity lead to higher temperature gradient changes than at higher thermal conductivity values. This was particularly visible in the adiabatic cases. The presence of convection boundary conditions plays a large role in determining the magnitude of the thermal gradient, particularly in-plane. Therefore, although the temperature gradients are dependent on the material properties, they are also highly influenced by the boundary conditions applied. As such the slight changes in thermal conductivity can be offset by the convective boundary condition applied to the model; the exact effect of each will be difficult to assess accurately without extended experimental validations.

It is important to note that an accurate specific heat value is not critical to achieve acceptable modelling of the composite system for heat transfer characteristics as specific heat variations have little effect on the observed temperature gradients. The power input used for the parametric studies was also lower than the value that will be used for the predictive analyses; this was done in order to avoid heat spikes and to obtain observable differences when changing the physical properties. With a significantly higher power input 0.0164 W/mm^3 (268 W/in^3), small thermal

conductivity variations do not show as pronounced an effect due to the high amount of heat input into the material. However, the general trends observed in this parametric study will hold at higher power input values.

6.5 Predictive Analysis

6.5.1 Model Description

Predictive analysis for the thermal problem with heater blanket (shown in Figure 6-26) was carried out using MSC Nastran. In order to model the controlled process accurately, each model was separated into two parts: the ramp-up constituted one part of the model and the soak conditions constituted the second part of the model. The separation of the models into two parts was necessary, as the thermostat control function used to model the heater blanket cannot be made a function of time.

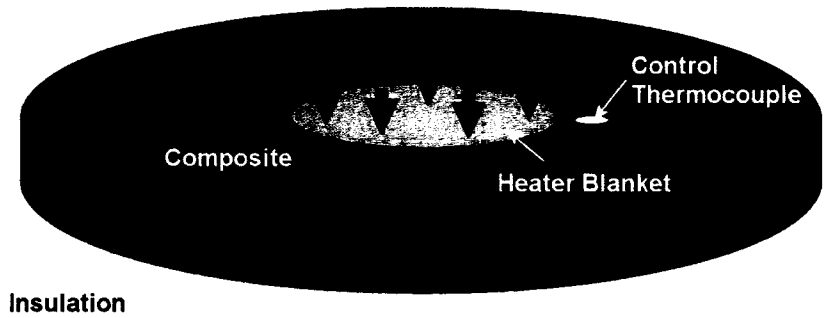

Figure 6-26: Thermal Problem with Heater Blanket

The first part of each model was modelled using a time dependent temperature function applied to the heater blanket. The input used to determine the temperature function is given in Table 6-9.

Table 6-9: Input for FEM Heater Blanket Ramp-Up Temperature Function

Time (sec)	Temperature (°C)
0	25
1800	117

The end temperature was a best estimate made using the following assumptions:

- 80% of the heat provided by the heater blanket was assumed to travel into the substrate. This approximation is based on typical heat exchanger and duct insulation efficiencies found in literature [31][51][52].
- The directional heat fluxes are directly proportional to the directional thermal conductivities.
- The heater blanket has a homogeneous temperature.
- The distance between the control thermocouple and the edge of the heater blanket is 12.7 mm.
- The desired temperature of the control thermocouple at 1800 seconds is 85°C

The calculations were carried out as follows.

Based on the thermal conductivity measurements discussed in section 4.5.2, it was found that k_x = 1.87 W/mK and k_z = 0.57 W/mK, therefore:

$$k_z \cong 0.3k_x \tag{5.1}$$

Assuming that the heat flows within the specimen are directly proportional to the directional thermal conductivities of the material:

$$q_z \cong 0.3q_x \tag{5.2}$$

And assuming 80% of the heat output by the heater blanket is transmitted to the material:

$$\begin{aligned} q_{act} &\cong 0.8q_{input} \\ \therefore q_{act} &\cong 1.3q_x \\ \therefore q_x &\cong \frac{0.8}{1.3} q_{input} \\ \therefore q_x &\cong \frac{0.8}{1.3} \times 0.0082\, W/mm^2 = 0.00505\, W/mm^2 \end{aligned} \tag{5.3}$$

Assuming a one dimensional Fourier's Law application:

$$\begin{aligned} q_x &= k_x \frac{\Delta T}{\Delta x} \\ \therefore T_{HB} &= \frac{q_x \Delta x}{k_x} + T_{CTC} \\ T_{HB} &= \frac{0.00505\, W/mm^2 \times 12.7\, mm}{0.002\, W/mm°C} + 85°C \\ T_{HB} &= 117°C \end{aligned} \tag{5.4}$$

It should be noted that the above is a simple approximation for modelling purposes based on available material properties and on expected heat losses to the surrounding insulation system. The thermal conductivity values used are the experimental values. These values are much lower than the nominal values used for the parametric studies and are also more homogeneous (3:1 vs. 50:1 for k_x/k_z). The ideal ramp-up using a

heater blanket with a homogeneous temperature is not representative of the actual process but gives an approximation of the resulting temperature spread in the material for the soak condition.

The soak phase was modelled using volumetric heat generation within the heater blanket solid. The heater blanket heat generation was controlled using the MSC Nastran thermostat control (CONTRLT) function: this function allows the user to set a temperature dead band above which the heater is turned off and below which the heater is turned on [54]. The end conditions of the ramp-up part of the models were used as initial values for the soak part of the models.

An ideal insulation case was modelled using adiabatic boundary conditions. As this case is not representative of the real system, additional cases were modelled using low convection boundary conditions on the outer surfaces of the substrate and heater blanket to simulate heat losses in the system due to imperfect insulation. Based on the results obtained with the parametric studies and discussed in section 6.4.2.4, convection coefficient values were selected between 0.5 W/m^2K and 1.5 W/m^2K. Cases were also modelled using a volumetric heat generation value equivalent to 80% of the heater blanket's manufacturer specified heat output value. This was conducted to account for the heat losses to the insulation occurring at the top of the heater blanket. A value of 80% was selected based on engineering judgement and on the typical efficiency of heat exchange devices [31][40][41].

The different model configurations are given in Table 6-10:

Table 6-10: Prediction Model Configurations

Configuration	Boundary Condition	Heater Blanket Output
1	Adiabatic	100%
2	Convection h = 0.5 W/m^{2}K	100%
3	Convection h = 1 W/m^{2}K	100%
4	Convection h = 1.5 W/m^{2}K	100%
5	Convection h = 0.5 W/m^{2}K	80%
6	Convection h = 1 W/m^{2}K	80%
7	Convection h = 1.5 W/m^{2}K	80%

The mesh generated for the predictive model is identical to the mesh generated for configurations A and C of the parametric studies, which did not include the copper heat tile. All analyses were conducted using 10-second time steps; the first part of the model contained 180 time steps while the second part contained 300 time steps.

6.5.2 Results

The temperature data for the node locations shown in Figure 6-27 were extracted for the predictive analysis and for comparison to experimental validation data.

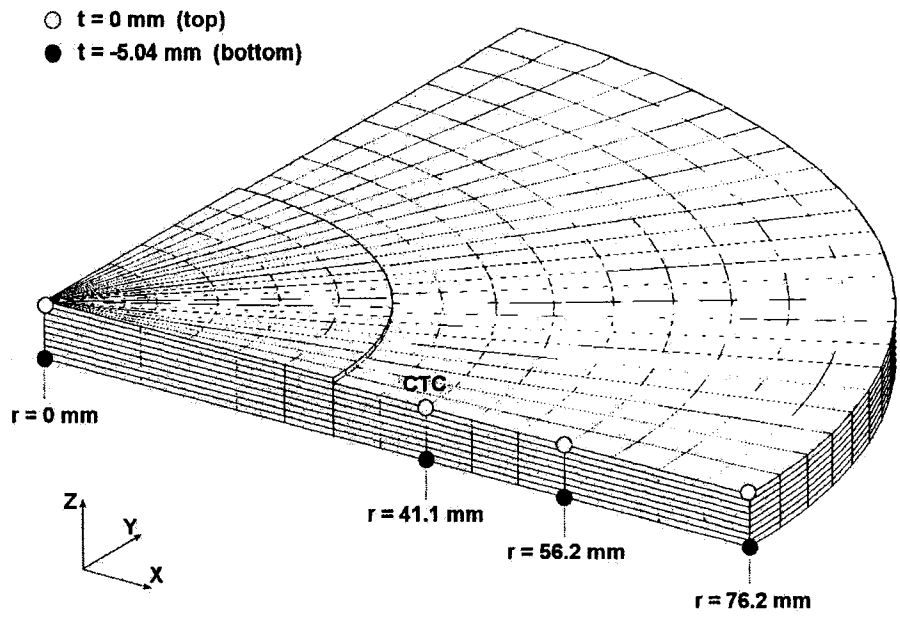

Figure 6-27: Location of Nodes Used for Temperature Data Extraction

The temperature results obtained were plotted as a function of time; these were compared amongst each other in order to evaluate any significant differences between the results. The results obtained are summarized in Table 6-11. The average maximum temperature was calculated based on the soak temperatures at the central radius bottom face node (r = 0, t = -5.04 mm). Similarly, the average maximum temperature was determined for the outer edge nodes (r = 76.2 mm) and these values were used to calculate the temperature gradients along the central axis, bottom face and outer radius of the models. The temperature differentials of interest are primarily the ones on the bottom face, as this is the tool face. It is also important to recall that the temperature under the heater blanket is not readily measured since the presence of a thermocouple wire would impede the intimate contact required between the heater blanket and the

substrate. Therefore only the temperature at the top of the heater blanket can be measured.

Table 6-11: Results Summary for Predictive Analyses

Configuration	ΔT (°C)			Average Maximum Temperature (°C)	Minimum Temperature (°C)
	bottom	outer edge	centre radius		
1	1	0.0	0.3	90	87
2	19	2.5E-03	1.7	103	81
3	35	4.6E-03	3.4	114	76
4	48	6.3E-03	4.9	122	72
5	19	2.5E-03	1.8	101	80
6	34	4.5E-03	2.9	112	75
7	47	6.3E-03	4.6	120	71

It was found that there was little difference between the cases with full heat input and 80% heat input: the maximum difference of 1°C was noted in the temperature gradient along the bottom face of the substrate at a convection coefficient of $1 W/m^2K$ and $1.5 /m^2K$. There is therefore little value in reducing the heat input from the heater blanket to compensate for thermal losses within the system. The results obtained for the adiabatic case and for the $0.5 W/m^2K$ convective coefficient case are unrealistic based on previous experience with heated composite systems. The heat retention within these models is too high; the lack of heat losses in these models means there is little heat input required from the heater blanket over the span of the process time modelled. It can be concluded that the estimated convection coefficient must be higher than $0.5W/m^2K$ for a more realistic representation of the heat transfer process in the system

to be obtained. The temperature profiles obtained for configuration 3 and 4 (Table 6-10) are shown in Figure 6-28 and Figure 6-29.

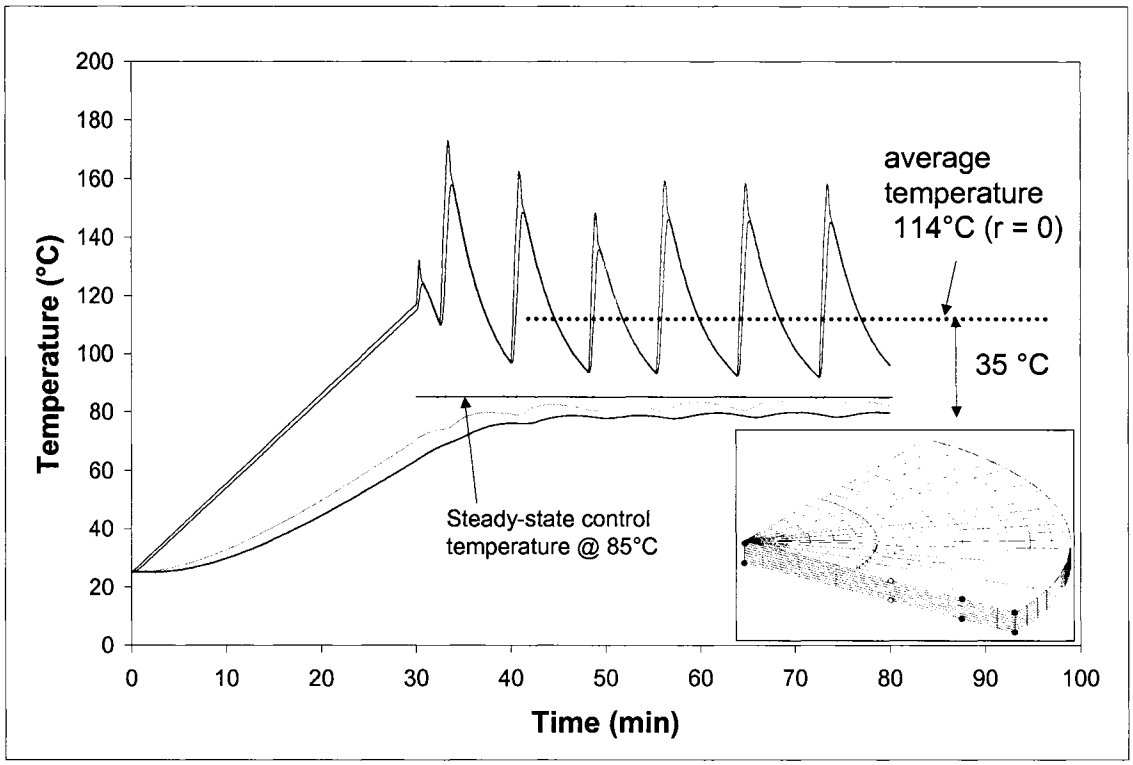

Figure 6-28: Time vs. Temperature Profile for Configuration 3

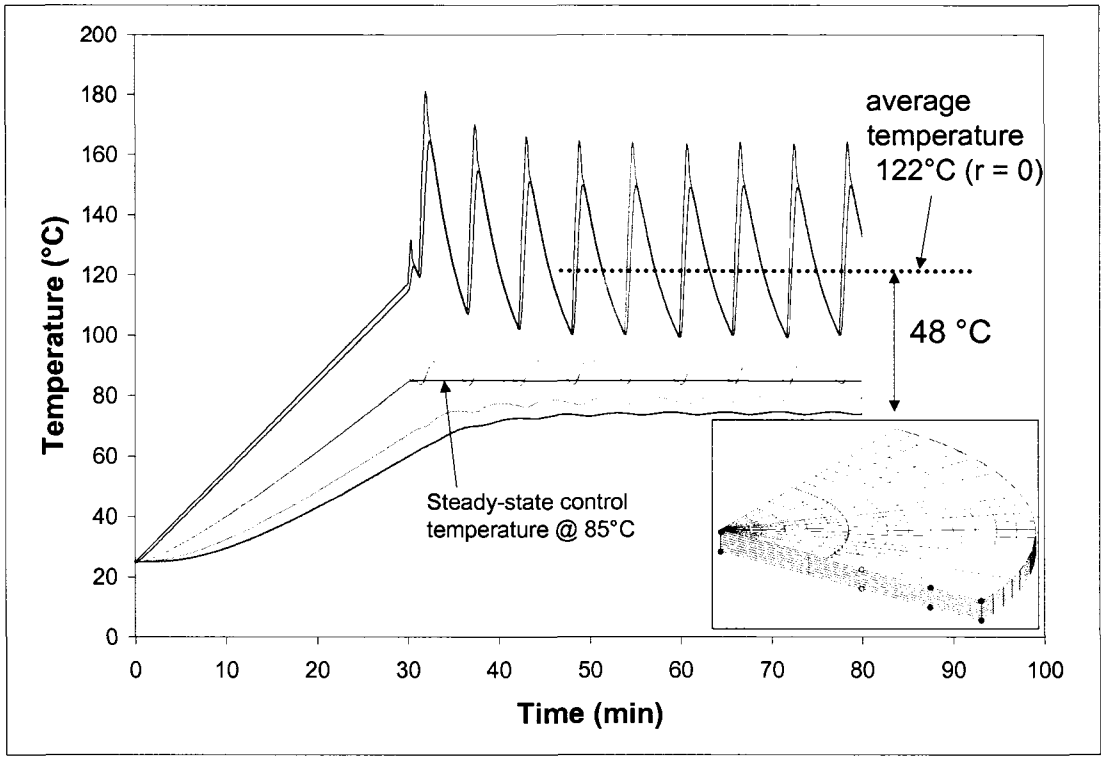

Figure 6-29: Time vs. Temperature Profile for Configuration 4

These results will be compared to the experimental results obtained from the FEM validation experiments.

7 Experimental FEM Validation

The first experimental phase consisted of the thermal conductivity determination. This initial phase was required in order to obtain the thermal conductivity values required for the FEM. The second experimental phase is the FEM validation test, which reproduced the heat transfer problem described in Figure 6-1. This phase consisted of a series of heat transfer tests to verify the results obtained through the FEM predictive analysis.

7.1 Test Setup

A 152 mm, eight-ply composite disk was heated using a 62 mm 24.95 W heater blanket. Eight thermocouples were used to monitor and control the temperature across the composite. The heater blanket was placed at the centre of the top surface of the composite disk and held in place under a vacuum bag. This also ensured proper contact between the heater blanket and the composite. The assembly was placed in insulation to limit possible heat losses from the system (Figure 7-1 and Figure 7-2).

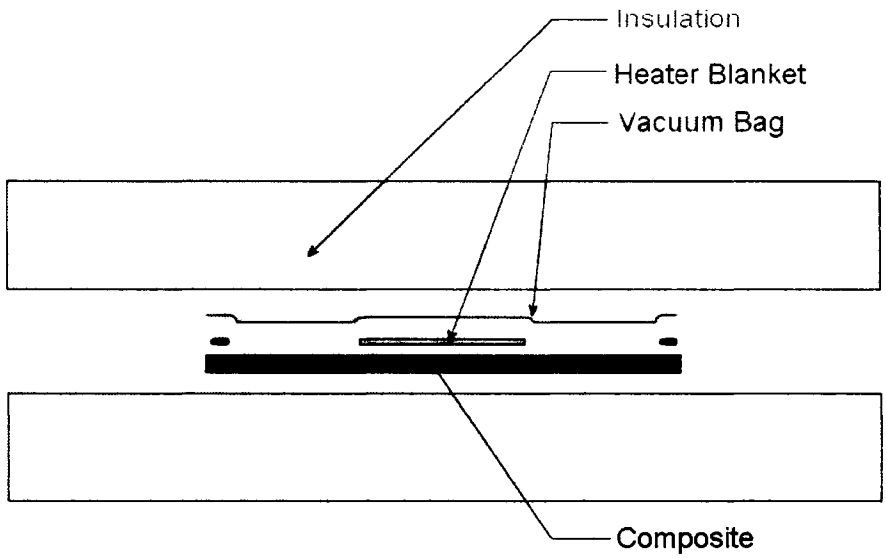

Figure 7-1: FEM Validation Test Setup

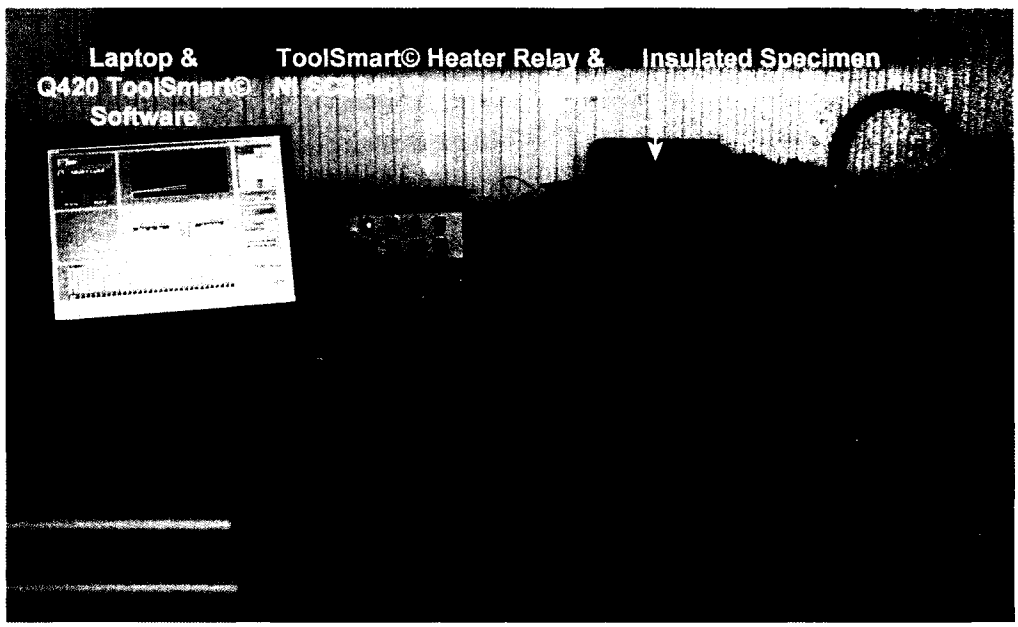

Figure 7-2: Experimental Test Setup

7.2 Temperature measurements

The temperature measurements were taken by means of eight K-type thermocouples. A control thermocouple was placed on the composite 8 mm away from the edge of the heater blanket. A heater thermocouple was placed at the centre of the top surface of the heater blanket in order to prevent the heater blanket from over-heating. Six thermocouples were added in order to monitor the temperature across the surfaces of the composite disk (Figure 7-3 and Figure 7-4). The thermocouple (TC) locations are provided in Table 7-1.

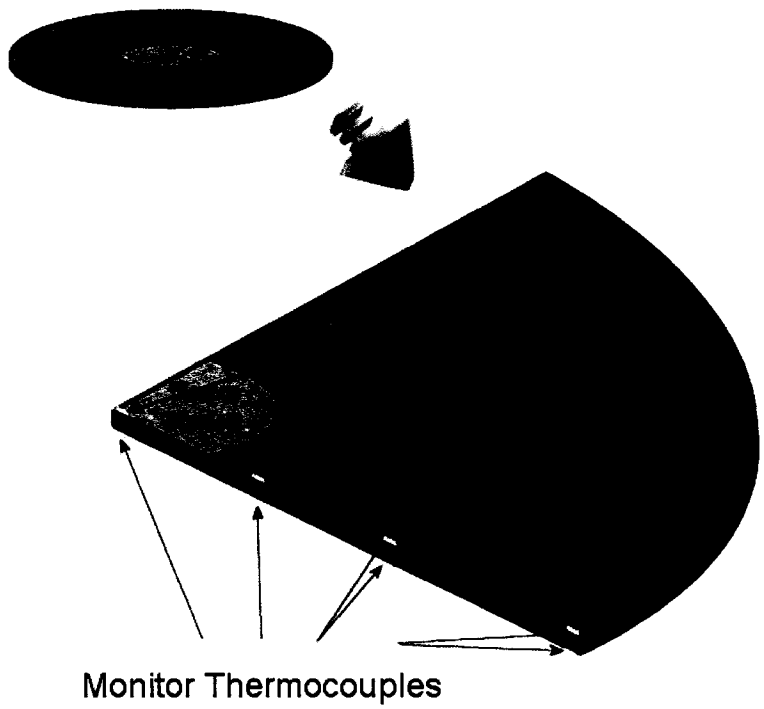

Figure 7-3: Schematic of Thermocouple Placement on the Composite Disk and Heater Blanket

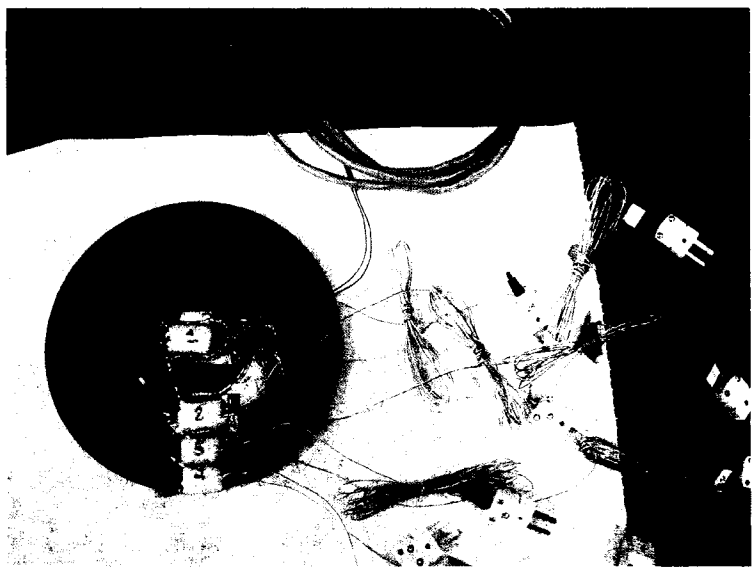

Figure 7-4: Instrumented Top Surface of FEM Validation Specimen

Table 7-1: Radial Location of Thermocouples

	TC#	Radial Location (mm)
Top	1	0.0
	2	38.1
	3	57.1
	4	73.0
Bottom	5	0.0
	6	38.1
	7	57.1
	8	73.0

7.3 Specimen Specifications and Fabrication

The 152 mm composite disk was manufactured using eight plies of ACG LTM-33-CFO-700T carbon fibre tooling prepreg. The procedure followed is identical to that used to manufacture the transverse thermal conductivity specimen (Section 4.3.1) with the exception of the size of the trimmed square specimen; the un-cured layup was

trimmed to a final dimension of 191 mm (7.5in) square and was water-jet cut to a diameter of 152 mm after post-cure.

7.4 Data Acquisition

The data acquisition system used for this experimental phase was identical to that used for the determination of the thermal conductivity of the composite material (section 4.4.1). The temperature profile outlined in Table 7-2 was used for this phase of the experimental work.

Table 7-2: Temperature Profile Settings for the FEM Validation

ramp-up	2°C/min
soak	85°C for 50 mins
cool-down	7°C/min

The results obtained for all experimental tests are discussed in the following section.

7.5 Results

The temperature data obtained from the eight thermocouples was plotted against time and against radial distance to obtain the temperature profiles of each test. The results are shown in Figure 7-5 and Figure 7-6. It is important to note that the central

temperature reading for the top face was taken on the heater blanket and that the radial temperature profiles are given for a time of 80 minutes.

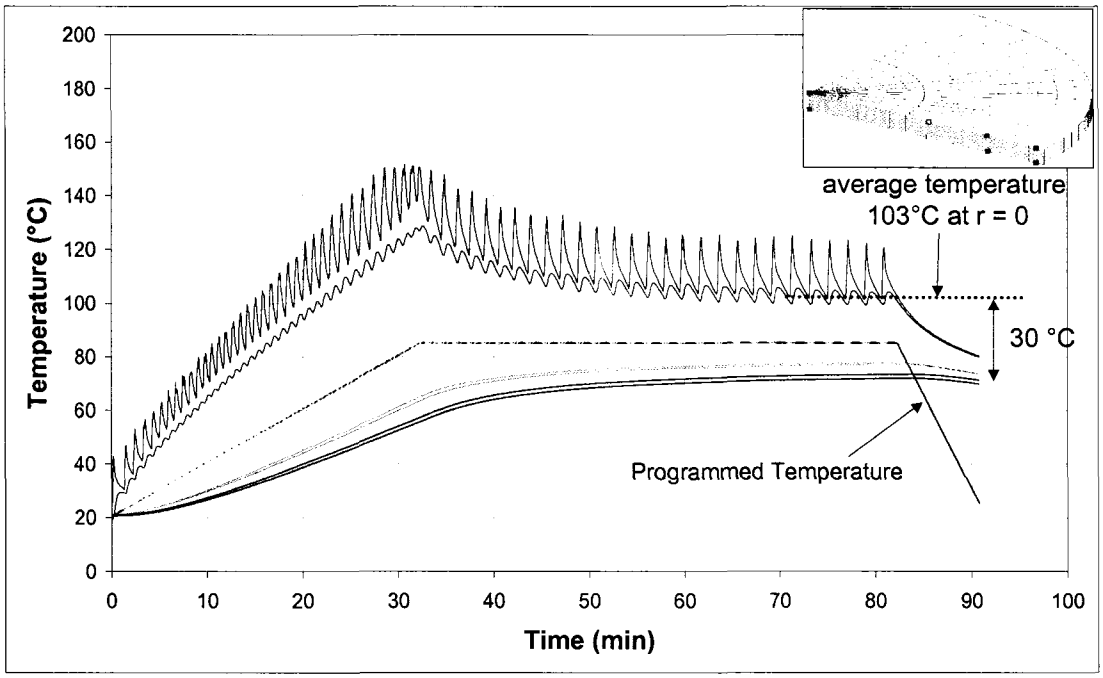

Figure 7-5: Temperature Profile for FEM Validation Test#1

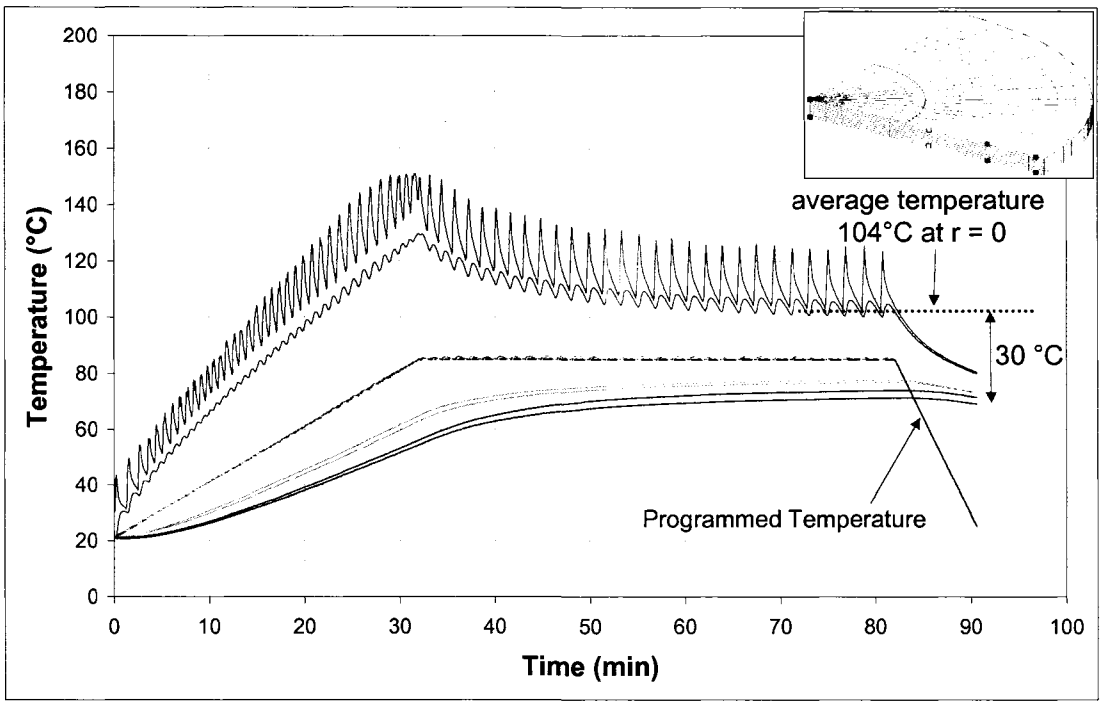

Figure 7-6: Temperature Profile for FEM Validation Test#2

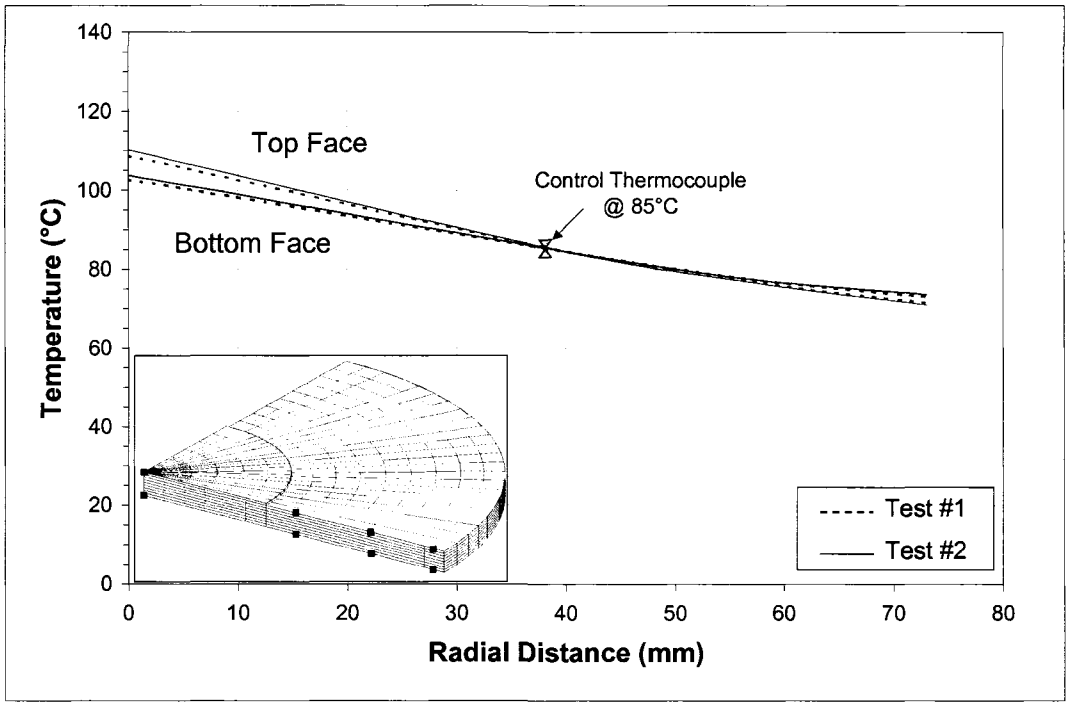

Figure 7-7: Radial Temperature Profiles for FEM Validations Test #1 and #2

In both FEM validation tests it was noticed that the temperature at the outer edge of the specimen was approximately 2°C higher on the bottom face than on the top face (Figure 7-7). This is thought to have been due to a better insulation of the lower face of the specimen; due to the vacuum bag, a vacuum line was connected to a vacuum bag protruding from the edge of the specimen. A tight cut-out was made in the insulation in order to provide for this contingency; this could have contributed to an increase in edge effects on the upper surface leading to a lower temperature.

Both trials showed similar bottom face temperature differentials of 30°C between the central axis ($r = 0$) and the outer edge.

The experimental results were compared to the FEM results obtained for convection coefficients of 1 W/m^2K and 1.5 W/m^2K. The results are shown in Figure 7-8 to Figure 7-12.

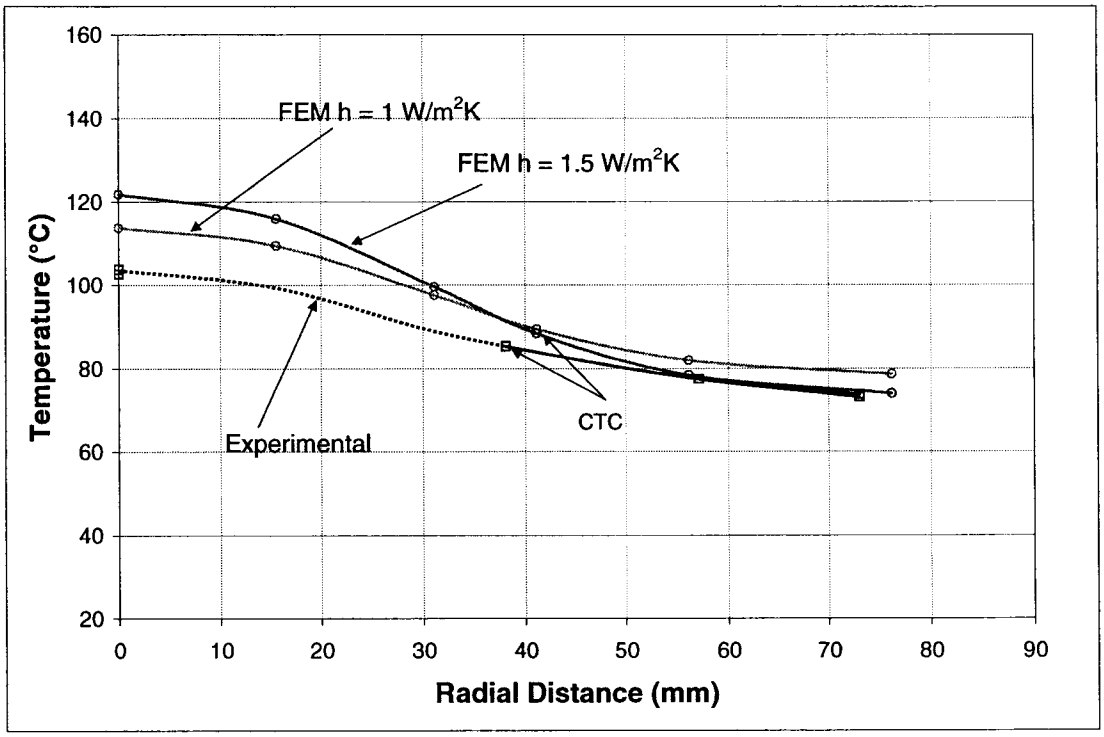

Figure 7-8: Radial Temperature Profile Comparison Between FEM and Experimental Results

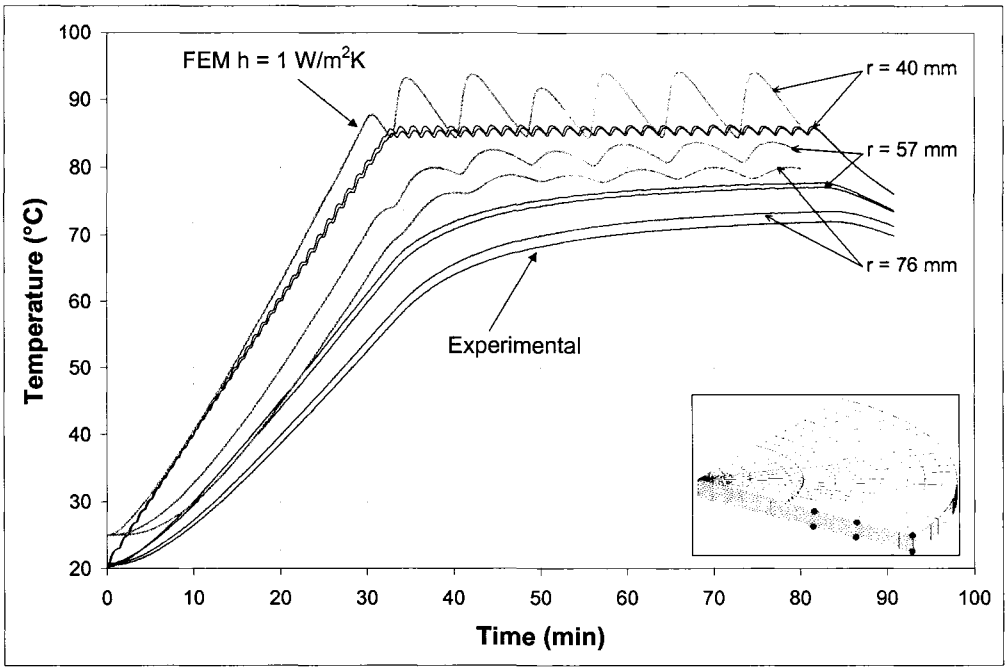

Figure 7-9: Outer Radii Process Temperature Profile Comparison Between Experimental Results and FEM 1 W/m²K Convection FEM Results

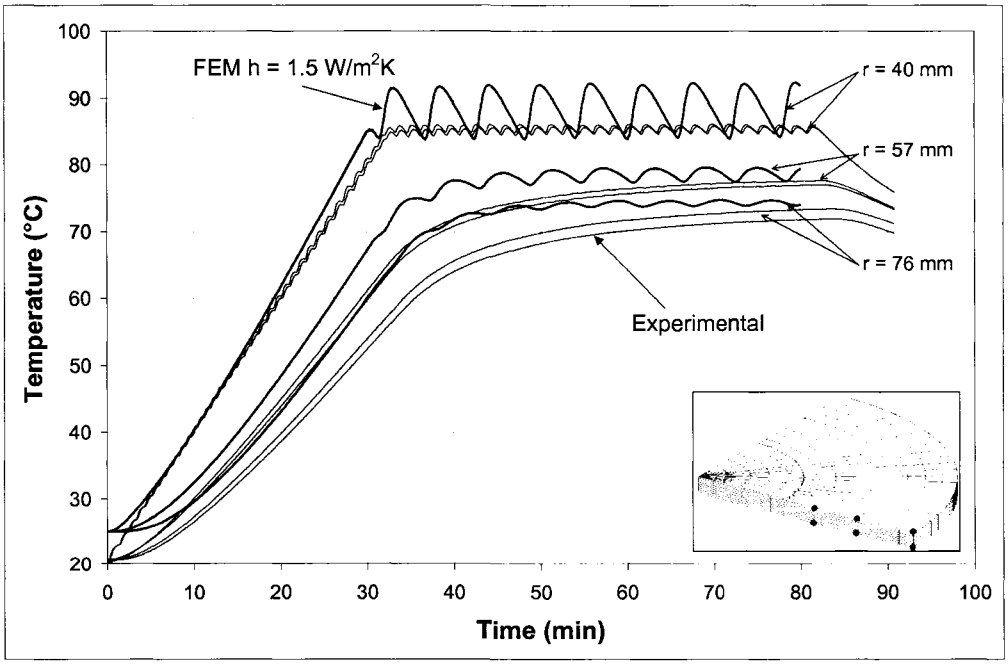

Figure 7-10: Outer Radii Process Temperature Profile Comparison Between Experimental Results and FEM 1.5 W/m²K Convection FEM Results

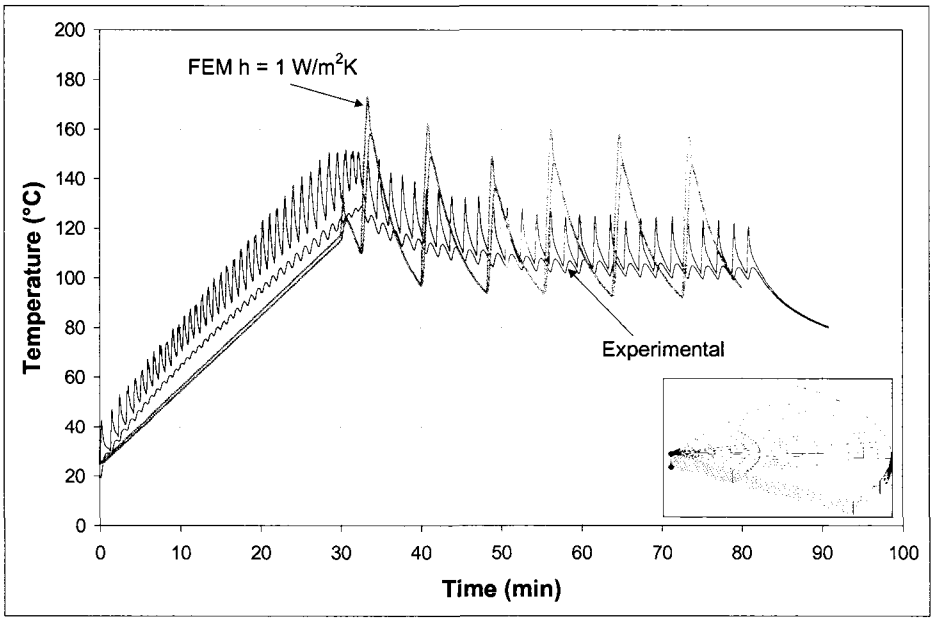

Figure 7-11: Centre Radius Process Temperature Profile Comparison Between Experimental Results and FEM 1 W/m²K Convection FEM Results

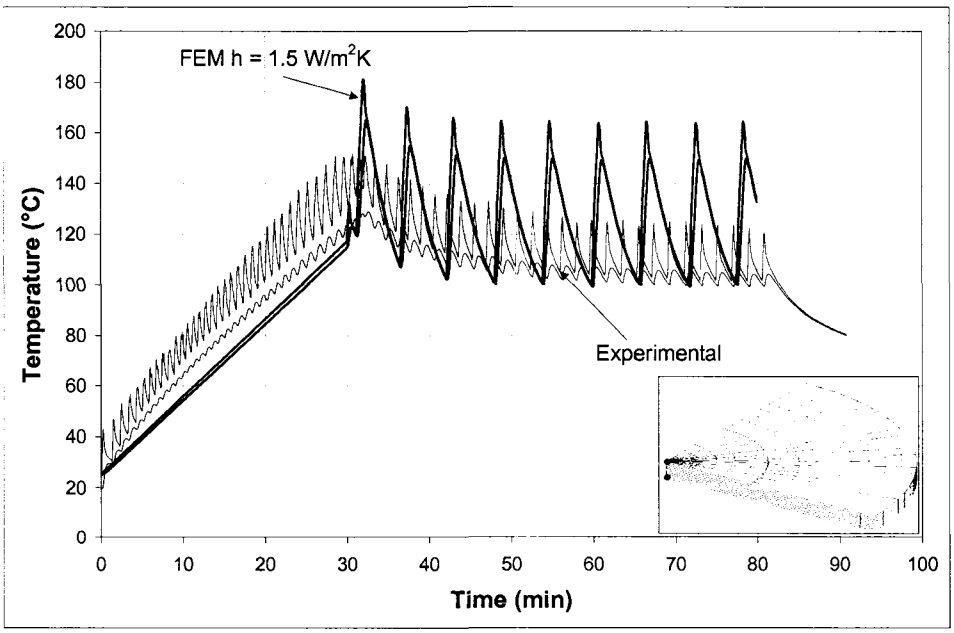

Figure 7-12: Centre Radius Process Temperature Profile Comparison Between Experimental Results and FEM 1.5 W/m²K Convection FEM Results

The radial temperature profiles shown in Figure 7-8 do not appear to have the same shape: this is due to the lack of experimental points available when compared to the FEM. From the data points available, it can be seen that the outer radii data points offer similar results to the FEM data points. The central points do however show a large discrepancy.

In Figure 7-11 and Figure 7-12, the lack of sensitivity of the FEM simulation with regards to heater control is visible when compared to the experimental results. In both cases the peaks of heat when the heater is turned on have a much greater magnitude than those observed experimentally. It is assumed that this is the result of a PID type control issue within the Nastran control function. As a result, the central area of the model has a different thermal response than the physical process. The effects of the central discrepancy diminish with increasing radial distance and the outer radii data points have a similar behaviour to those observed experimentally.

By observation of Figure 7-8 to Figure 7-12, it can be seen that the convection boundary condition of 1.5 W/m^2K offers the best representation of the thermal response in the system. The thermal gradients observed outside the inner radii heat application zone, are similar to those observed experimentally (Figure 7-10). The temperature profiles in the heat application zone differ from the experimental ones in peak magnitudes and in heater input frequency; however, the lower part of the oscillations follow the same general trend as the results obtained experimentally (Figure 7-12), whereas the trends observed for a convection boundary condition of 1 W/m^2K do not (Figure 7-11).

8 Discussion

8.1 Thermal Conductivity Measurement

8.1.1 Thermal Conductivity Tests Conducted Using Al 6061 Standards

It was found that a large difference in thermal conductivities between the specimen and the standards leads to very high errors in the measurements. A number of effects were thought to contribute to this problem. To measure very low thermal conductivity specimens with high thermal conductivity standard, an extremely large temperature gradient would have to be measured across the specimen when compared to the temperature gradient measured across the standards. This is due to the fact that he thermal conductivity k is proportional to the temperature gradient. In the case of the SS 304 specimen and the Al 6061 standards, the thermal conductivity of the standards is approximately 10 times higher than that of the specimen (16 W/mK vs 154 W/mK). As such, assuming the heat is applied to the same cross-sectional area, that the heat flow passing through the two materials is the same and that the standards and the specimen are of equal thickness, the temperature gradient measured across the specimen should be 10 times higher than that measured across the standards. However, the temperature gradient on the SS 304 specimen was on average only three times higher than the top standard temperature gradient (2.8°C) and five times higher than the bottom standard (1.7°C). As the thermal conductivity difference between the standards and the specimen increases, this effect becomes more pronounced. In the case of the HDPE, the

material acts as an insulator within the measurement column; this makes the temperature gradient across the standards very small and difficult to measure accurately (0.5°C to 1.4°C). These small temperature gradients across the standards further contribute to the error as the thermocouples are accurate to ±0.2°C at temperatures of 70°C. Additional tests showed that there is a measurable heat loss to the insulation: the temperature of the insulation surrounding the measurement column increases noticeably during the tests. Two thermocouples were placed in the insulation near, but not adjacent to the measurement column. The thermocouple placement and the temperature profile measured are shown in Figure 8-1. The heat lost to the insulation increases as the specimen becomes less conductive thereby becoming a more difficult path for the heat to flow through. This contributes to the smaller temperature gradients observed across specimens with thermal conductivity that is significantly lower than that of the standards.

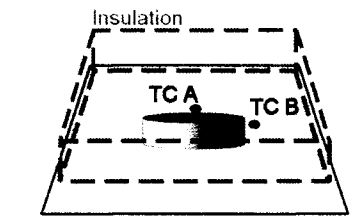

TC A: approximately 0.18 inch from top of measurement column, along central axis

TC B: 0.5 inch from edge of measurement column

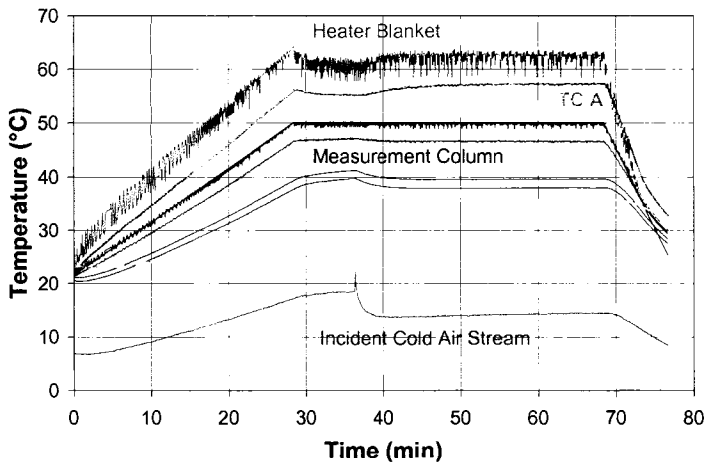

Figure 8-1: Thermal Measurements in Insulation Adjacent to Measurement Column

Small amounts of parasitic heat transfer in the form of radiation and convection are also assumed to occur: the direct effects of these are difficult to measure but are assumed to be minimal compared to the parasitic conduction occurring through the insulation.

Despite the difficulties encountered with the lower conductivity specimens, the Al 6061 specimen results indicate that the apparatus is reliable for specimens with a thermal conductivity that is similar to that of the standards. The initial error obtained with respect to the expected value was high (-31%); after the insulation around the measurement column was improved the error was reduced to a range of –14% to –20%. According to the ASTM E 1225-04 the error can be reduced to achieve a precision of 6.8% using a guarded apparatus [45]: as such the error obtained with insulation is deemed reasonable.

A large discrepancy was observed between the heat flows measured by the top and bottom Al 6061 standards. During experiments on the Al 6061 specimen the heat flow measured on the bottom standard was found to be 17% to 28% lower than the heat flow measured on the top standard. The lower heat flow measured in the lower standard is thought to be due to the large heat sink the base plate represents. The aluminum base plate effectively draws the heat out of the standard in both the transverse and radial directions. The presence of the base plate also prevents perfect insulation of the bottom standard as the standard cannot be fully insulated and heat loss occurs between the bottom of the insulation and the base plate. The difference in heat flow measured between the top and bottom standards has a high effect on the thermal conductivity

value measured. The thermal conductivity values calculated from the top standard for the Al 6061 specimen were within a 1% to 10% error from the expected value, whereas the thermal conductivity values obtained from the bottom standard had larger errors (24% to 30%). Though similar experiments using a guarded apparatus have yielded good results using an average of values calculated from the top and bottom standards, the use of the average in the current case may not provide the best data. Further experiments would be required to confirm this; however, it is foreseeable that the best results would be obtained using only the thermal conductivity values obtained from the measurements taken across the top standard. This would only be valid if the specimen and standard were of similar thermal conductivities.

8.1.2 Thermal Conductivity Tests Conducted Using SS 304 Standards

The measurements taken with the SS 304 standards further confirm that as the materials present in the column become less conductive, more heat is lost to the surrounding insulation. The minimum error achieved for the SS 304 specimen thermal conductivity measurement using the SS 304 standards was 30% low. The thermal conductivity readings obtained with the SS 304 also confirm that the apparatus is only accurate with materials of similar thermal conductivity as the Al 6061 thermal conductivity obtained showed an error of 81% low and the HDPE had an error of 50% high. The error on the HDPE is seven times lower than the one calculated with the Al 6061 standards.

The thermal conductivity values measured experimentally for the CF/Ep laminate (0.57 W/mK and 1.87 W/mK) were lower than those found in literature (2 W/mK and

100 W/mK) but the transverse thermal conductivity value was found to be in agreement with predictions from transverse thermal conductivity models found in literature. The in-plane thermal conductivity was much lower than values found in literature (~ 100 W/mK); it is assumed that these values were based on unidirectional prepreg and on raw carbon fibre material values.

It should be noted that the thermal conductivity values used seemed to provide acceptable results. Although there may be some source of error due to the values entered, the general trends observed in all FEM models carried out are similar to those observed on the physical model. Therefore, despite the large errors encountered, if the apparatus is calibrated correctly, it is possible to obtain thermal conductivity values that yield good modelling results.

Though the thermal conductivity results obtained were adequate for modelling purposes, more accurate results are possible. This would be achievable with a stronger heat sink and heat source. A more efficient means of containing the heat within the column, such as the use of a guard heater, would also provide increased accuracy.

8.2 FEM Validation

Based on temperature outside the central heat input zone, it would seem that the best modelling approximation is provided by assuming a convection factor of 1.5 W/m^2K to account for the minor heat losses that occur in the system. As explained in section 6.5.2, the lower convection coefficients tested do not provide realistic representations of the physical model; the material retains too much heat making the process too ideal and unrealistic.

The major difference observed between the time/temperature profiles of the FEM and of the physical model lies in the cyclical aspect of the heating; the frequency of the cycling is much lower in the FEM models than it is on the physical model. The amplitude of the heater blanket temperature cycling is also much higher than that of the physical model.

The central parts of the physical model and of the FEM have similar temperature; however, the experimental data tends to suggest stronger edge effects are present than what is modelled by the FEM for a fixed convective load boundary condition. The edge effects are thought to have been due to the vacuum line attached close to the edge of the specimen. As a hole had to be made in the insulation to accommodate the vacuum line, the insulation on the top surface was not as complete as that of the bottom surface.

Though the model and the validation data show similar trends, MSC Nastran does not offer adequate control of volumetric heat loads to allow the type of predictive modelling required to match the behaviour of a heater blanket. The results obtained by using the method described in this thesis (Chapter 6) provide results that would be adequate to carry out a preliminary assessment of a complex apparatus that is expected to be held at a fixed temperature for a specified amount of time. However, cases with short ramp-up and soak times would not necessarily lead to acceptable FEM models because the thermostat control function cannot be made a function of time in the current version of MSC Nastran. The temperature of the heater blanket at the end of the ramp-up must be estimated; if the time at soak is long enough, the volumetric heat load will compensate for slight errors occurring in the ramp-up temperature estimates. A short

soak time will not allow this to occur. The most restricting factor for the use of MSC Nastran to model a full ramp-up and soak process comes from the ramp-up function, which is estimated based on the physical properties of the material and on the known heat input. Although such estimates can be carried out for simple geometries such as the one used in this thesis, it is unlikely that such a process could be used with a complex geometry and multiple heater configurations.

The extension of the modelling to a heater tile configuration using the determined thermal properties of the CF/Ep composite could provide information of value to the conceptual design or trade-off studies. As the model without a heater tile yields acceptable results for initial design purposes, it can be assumed that the addition of the heater tile in the FEM is possible without further loss of data or profile accuracy. The results obtained for the heater tile configuration in the FEM parametric studies agrees with what researchers at IAR have experienced. Amongst other results obtained with the heater tile analyses, the effective copper thickness issue has been widely observed; it is a known factor among the concerned researchers that if the copper tile is too thin, it will not function as expected. This is thought to be due to the large thermal mass that the composite then constitutes when compared to the heater tile. FEM could then be used as a tool to determine the adequate copper tile thickness required for a specific composite tooling system.

9 Conclusions and Recommendations

9.1 Conclusions

The reviewed literature does not provide the means required to develop a simple analytical solution to the transient heat conduction in a realistic CF/Ep woven laminate tool. This is due to the high non-linearity of the problem as well as to limited knowledge regarding the boundary conditions which are applied to the system. In order to obtain the temperature distribution within the material, numerical methods must be applied. FEM was the selected numerical method for this research; MSC Nastran was used as the analysis code and MSC Patran was used as pre- and post-processor.

The thermal properties of the material were required for input into the model of the physical heat transfer problem studied in this research. The specific heat was provided by the composite prepreg manufacturer, however, the directional thermal conductivities were determined experimentally using a comparative test method. The experimental method devised produced thermal conductivity values of 0.57 W/mK for the transverse thermal conductivity and of 1.87 W/mK for the in-plane thermal conductivities. The thermal conductivity values measured produced results comparable to experimental results when implemented into the FEM but large errors were encountered within the comparative test apparatus while taking measurements. It was found that best results with the comparative test apparatus were obtained with materials of higher conductivity but more importantly with materials with thermal conductivity similar to that of the

standards used. A better heat containment method must be used to limit the heat loss of lower conductivity materials and to obtain less error.

The FEM carried out to predict the thermal response behaviour showed trends that are similar to those found through the validation experiments. However, the lack of control over the volumetric heat generating loads in MSC Nastran limits the predictive capabilities of the software. Though the results of analyses, similar to that carried out in this research, may be used as a tool for conceptual design or preliminary trade-off studies, they could not be used as a final design tool. The many assumptions made for the initial ramp-up phase imply that testing would be required to ascertain that these assumptions are valid. Therefore, though the results obtained may be used in initial design phases, they do not offer enough accuracy to be used in advanced stages of design of integrally heating composite tooling systems.

9.2 Recommendations

In order to properly apply the FEM, more heat loss control is required during the thermal conductivity determination. In order to limit heat losses, the apparatus would have to be modified to either be used in a vacuum environment or to have an integrated guard heater. This would effectively limit the heat losses, particularly when determining the thermal conductivity of materials with thermal conductivities below approximately 20 W/mK.

Other commercial FEM software packages should be investigated to determine if they offer the flexibility of control required to model a control ramp-up followed by a soak period. Software such as ABAQUS or ANSYS may provide the extra flexibility

not offered by MSC Nastran, through existing functions or user implemented subroutines. MSC Nastran does not offer the user the possibility of defining sub-functions, thereby restricting the control possibilities within the model.

Further work should be carried out to evaluate the accuracy of the predictive modelling for composite tools using copper heater tiles. A copper tile could be bonded to the FEM validation specimen and used to run experiments to be compared to results obtained with FEM. The effectiveness of copper tiles for heat distribution is an asset when heating composite tools since fewer heaters would be required to heat large areas. A tool capable of adequately modelling the cure process (ramp-up and soak) could be used to optimize the heat usage in the system thereby allowing a power saving and reduced costs. Comparative work with technologies currently used would also be an asset in such a project as it would allow direct comparison between known methods and quantities.

The possibility of using woven material micro-geometry (fibre sizes, gaps, and fibre angles) to produce a geometry based model to determine the thermal conduction properties of a material should also be investigated further. This would require the development of a method that would allow the easy determination of the geometric properties of each type of weave encountered. Currently, in order to obtain this information, several microscope observations of the material must be carried out. If a simple method could be found that could provide the information required, the thermal conductivity of any weave could be determined based solely on its geometrical properties.

REFERENCES

[1] Jones, H. N., Keller, T.M., "High-Temperature Tensile Properties of Graphite Fiber-Phthalonitrile Composites", *NRL Review: Featured Research*, US Naval Research Laboratory, Washington, May 2002.

[2] Black, S., "Composite nacelles: Flying toward new horizons", *High Performance Composites*, **12**, No. 3, Ray Publishing, May 2004.

[3] Johnston, A., *Introduction to Composites,* Course Notes, Fall 2004, Carleton University, Ottawa, 2004.

[4] Griffiths, B., "Boeing sets pace for composite usage in large civil aircraft", *High Performance Composites* available online: http://www.compositesworld.com/hpc/issues/2005/May/865, Ray Publishing, May 2005.

[5] Piasecki, N., "Defining the Future of Commercial Aviation with the Boeing 7E7 Dreamliner", presented at the Fall Business Advisory Committee Meeting, Northwestern University Transportation Center, October 2004.

[6] Pora, J., "Advanced materials and technologies for A380 structure, technology platform for future developments", *FAST*, **32**, Airbus, July 2003, pp 3-8.

[7] Burke, S., "Low Cost Tooling For Composites: A Real World Analysis of Tooling," *SAMPE Journal*, **39**, No. 1, January/February 2003, pp. 46-50.

[8] Barlow, d., Howe, C., Clayton, G., Brouwer, S., "Preliminary study on cost optimization of aircraft composite structures applicable to liquid moulding technologies", *Composite Structures*, **57**, Elsevier Science Ltd., 2002, pp. 53-57.

[9] Raizenne, D., Brown, Y., "Projection Heating for Composite Repair", *Fourth International Canadian Conference on Composites – Cancom 2003, Ottawa,* August 19-22, 2003.

[10] Milovich, D., "Tooling and equipment for net shape composites manufacturing", *SME Technical Paper*, **EM93-114**, Society of Manufacturing Engineers, 1993.

[11] Rice, E. V., Owen, M. J., Pickering, S. J., "Simultaneous engineering of components and tooling for resin transfer moulding (RTM) composites", *Engineering Systems Design and Analysis,* **64-2**, ASME, New York, 1994, pp. 269-283.

[12] Venisse, P., Hind, S., Raizenne, D., Smart Tooling Literature Review, in-progress, NRC, Canada, July 2004.

[13] Fontana, Q. P. V., "Viscosity: thermal history treatment in resin transfer moulding process modelling," *Composites Part A*, **29A**, Elsevier Science Limited, Great Britain, 1998, pp. 153-158.

[14] Li, C., *Simulation of Process-Induced, Residual Stresses in Thick Filament Wound Tubes*, Ph. D. Thesis, Department of Aerospace Engineering, University of Bristol, 2003.

[15] Johnston, A. A., *An Integrated Model of the Development of Process-Induced Deformation in Autoclave Processing of Composite Structures*, Ph. D. Thesis, Department of Metals and Materials Engineering, University of British Columbia, 1997

[16] Joshi, S. C., Liu, X. L., Lam, Y. C., "A numerical approach to the modeling of polymer curing in fibre-reinforced composites," *Composites Science and Technology*, **59**, Elsevier Science Limited, 1999, pp.1003-1013.

[17] Tucker, C. L., "Heat Transfer and Reaction Issues in Liquid Composite Molding," *Polymer Composites*, **17**, No. 1, February 1996, pp. 60-72.

[18] Mijovic, J., Wang, H. T., "Modelling of Processing of Composites Part II – Temperature Distribution During Cure," *SAMPE Journal*, **24**, No. 2, March/April 1988, pp. 42-55.

[19] LeGrand, M., Bellenger, V., "The Cure Optimisation of Carbon/Epoxy Prepregs," *Composites Science and Technology*, **58**, Elsevier Science Ltd., 1998, pp. 639-644.

[20] Farmer, J. D., Covert, E. E., "Transverse Thermal Conductance of Thermosetting Composite Materials During Their Cure," *Journal of Thermophysics and Heat Transfer*, **8**, No. 2, AIAA, 1994, pp. 358-365.

[21] Auriault, J.-L., Ene, H. I., "Macroscopic modelling of heat transfer in composites with interfacial thermal barrier," *International Journal of Heat Mass Transfer*, **37**, No. 18, Elsevier Science Ltd, Great Britain, 1994, pp. 2885-2892.

[22] Graham, S., McDowell, D. L., "Numerical Analysis of the Transverse Thermal Conductivity of Composites with Imperfect Interfaces," *Journal of Heat Transfer*, **125**, ASME, 2003, pp. 389-393.

[23] Farmer, J. D., Covert, E. E., "Thermal Conductivity of a Thermosetting Advanced Composite During It's Cure," *Journal of Thermophysics and Heat Transfer*, **10**, No. 3, AIAA, July-September 1996, pp. 467-475.

[24] Cha, W., Beck, J. V., "Numerical Study of Thermal Conductivity of Fiber-Matrix Composite Materials," *Design and Manufacturing of Advanced Composites: Proceedings of the Fifth Annual ASM/ESD Advanced Composites Conference,* ASM International, 25-28 September 1989, pp 219-225.

[25] Ning, Q.-G., Chou, T.-W., "Closed-Form Solutions of the In-Plane Effective Thermal Conductivities of Woven-Fabric Composites," *Composites Science and Technology*, **55**, Elsevier Science Limited, Northern Ireland, 1995, pp. 41-48.

[26] Ning, Q.-G., Chou, T.-W., "A Closed-Form Solution of the Transverse Effective Thermal Conductivity of Woven Fabric Composites," *Journal of Composite Materials*, **29**, No. 17, Technomic Publishing Co. Inc., 1995, pp. 2280-2294.

[27] Zou, M., Yu, B., Zhang, D., Ma, Y., "Study on Optimization of Transverse Thermal Conductivities of Unidirectional Composites," *Journal of Heat Transfer*, **125**, No. 6, ASME, December 2003, pp. 980-987.

[28] Kaminski, M., "Homogenization of transient heat transfer problems for some composite materials", *International Journal of Engineering Science*, **41**, Elsevier Science Limited, 2003, pp. 1-29.

[29] Roberts, J. C., Luesse, M. H., Magee, T. C., "A Technique for Locally Increasing Surface Heat Spreading and Through-Thickness Thermal Conductivity of Graphite/Epoxy Laminates," *Journal of Composite Materials*, **30**, No. 2, Technomic Publishing Co. Inc., 1996, pp. 231-247.

[30] James, B. W., Wostenholm, G. H., Keen, G. S., McIvor, S. D., "Prediction and measurement of the thermal conductivity of composite materials," *Journal of*

Physics D: Applied Physics, **20**, IOP Publishing Ltd., United Kingdom, 1987, pp. 261-268.

[31] Holman, J. P., Heat Transfer, 8th Edition, McGraw Hill, USA, 1997.

[32] Hashin, Z., "Analysis of Composite Materials – A Survey," *Journal of Applied Mechanics*, **50**, ASME, 1983, pp. 481-505.

[33] Halpin, J. C., Primer on Composite Materials Analysis, Second Edition, Revised, Technomic Publishing Company Inc., USA, 1992.

[34] Lord Rayleigh, W., "On the Influence of Obstacles Arranged in Rectangular Order upon the Properties of a Medium," *Philosophical Magazine*, **34**, No. 4, 1892, pp. 481-503.

[35] Dasgupta, A., Agarwal, R. K., "Orthotropic Conductivity of Plain-Weave Composites Using a Homogenization Technique," *Journal of Composite Materials*, **26**, No. 18, Technomic Publishing Co. Inc., 1992, pp. 2736-2758.

[36] Incropera, F. P., DeWitt, D. P., Fundamentals of Heat and Mass Transfer, Fourth Edition, John Wiley & Sons, Toronto, Canada, 1996.

[37] Han, L. S., Boyee, W. F., Glower, L., "Directional Thermal Conductivities of Graphite/Epoxy Composites: 0/90 and 0/±45/90", *AIAA 20th Thermophysics Conference, Williamsburg, Virginia*, AIAA, June 1985.

[38] Hsu, S. T., Engineering Heat Transfer, D. Van Nostrand Company, Inc., Princeton, USA, 1963

[39] Twardowski, T. E., Lin, S. E., Geil, P. H., " Curing in Thick Composite Laminates: Experiment and Simulation", *Journal of Composite Materials*, **27**, No 3, Technomic Publishing Co. Inc., 1993.

[40] Poulikakos, D., Conductive Heat Transfer, Prentice-Hall, Inc., Englewood Cliffs, NJ, USA, 1994.

[41] Kutateladze, S. S., Borishanskii, V. M., A Concise Encyclopedia of Heat Transfer, Pergamon Press Ltd., Oxford, England, 1966.

[42] Hào, D. N., "Methods for inverse heat conduction problems", *Methoden und Verfahren der mathematischen Physik,* **BD 43**, Peter Lang GmbH, Frankfurt am Main, Germany, 1998.

[43] Ang, D.D., Gorenflo, R., Le, V. K., Trong, D.D., Moment theory and some inverse problems in potential theory and heat conduction, Springer – Verlag Berlin Heidelberg, Germany, 2002.

[44] NRC, ToolSmart™ Real Time Active Control and Q420© Control Software, Version Comtek 1.0, User Manual, National Research Council of Canada, Ottawa, September 2004.

[45] ASTM, E 1225-04 Standard Test Method for Thermal Conductivity of Solids by Means of the Guarded-Comparative-Longitudinal Heat Flow Technique, *ASTM Book of Standards*, ASTM International, USA, 2004.

[46] ACG, PDS2053/01.99/1 ACG LTM33 Tooling Prepreg, The Advanced Composite Group, Derby, England, 1999.

[47] ACG, TDS1001/01.99/5 Manufacturing Procedure for LTM Prepreg Mould Tools, The Advanced Composites Group Ltd, Derby, England, 1997.

[48] ACG, TDS1019/06.00/2 User's Manual for LTM Prepregs and Adhesive Films, The Advanced Composites Group Ltd., Derby England, 2000.

[49] Fontana, Q. (Qfontana@acg.co.uk), RE: Request for material properties, November 10, 2004. Email to: Magali Duval (Magali.Duval@nrc-cnrc.gc.ca).

[50] ACG, PDS1005/03.99/4 ACG LTM10, LTM12 and LTM16 Tooling Prepregs, The Advanced Composites Group Ltd, Derby, England, 1999.

[51] Vila, B., "Insulation For Home Comfort", Available online: http://www.bobvila.com/ArticleLibrary/Subject/Energy_Efficiency/InsulationOverview.html, Bob Vila.com, 2001.

[52] EPA, "Duct Insulation, Air distribution system improvements, EPA 430-F-97-028", United States Environmental Protection Agency, December 2000.

[53] Chainyk, M., MSC Nastran Thermal Analysis User's Guide V68, MSC Software Corporation, 2001.

[54] MSC Software, MSC Nastran 2005, Quick Reference Guide: Volume II, MSC Software Corporation, USA, 2004.

BIBLIOGRAPHY

Achmatowicz, S., Wyzkiewicz, I, Zwierkowska, E, Lobodzinski, W., "New approach to thermal conductivity of thin films measurements by means of a comparative method", *Proceedings of SPIE the International Society for Optical Engineering; 2003 International Symposium on Microelectronics*, **5288**, SPIE, 2003, pp. 655-660.

"ASTM E 220- 02, Standard Test Method for Calibration of Thermocouples By Comparison Techniques", *Annual Book of ASTM Standards*, ASTM International, USA, September 2002.

"ASTM E 563 – 97, Standard Practice for Preparation of an Ice-Point Bath as a Reference Temperature", *Annual Book of ASTM Standards*, ASTM, USA, April 1998.

"ASTM E 1269-01, Standard Test Method for Determining Specific Heat Capacity by Differential Scanning Calorimetry", *Annual Book of ASTM Standards*, **14**, No. 2, ASTM International, USA, 2001.

Bendada, A., Bastale, J. C., "Approximate Solutions to 3D Unsteady Heat Conduction Through Plane Flaws Within Anisotopic Media Using a Perturbation Method", *IMI (series)*, National Research Council Canada, Industrial Materials Institute, 2000.

Bialecki, R., Divo, E., Kassab, A., "The time-to-arrival problem for reconstruction of multidimensional heat flux", *Inverse Problems in Engineering Mechanics III: International Symposium on Inverse Problems in Engineering Mechanics (ISIP 2001)*, Elsevier Science, 2002, pp. 29-39.

Calibration of Thermocouples, EAL-G31, European cooperation for Accreditation of Laboratories, October 1997.

Carson, J. K., Lovatt, S. J., Tanner, D. J., Cleland, A. C., "Experimental measurements of the effective thermal conductivity of a pseudo-porous food analogue over a range of porosities and mean pore sizes", *Journal of Food Engineering*, **63**, Elsevier Ltd., 2004, pp. 87-95.

Cassel, R. B., "How Tzero™ Technology Improves DSC Performance, Part III: The Measurement of Specific Heat Capacity", TA Instruments Applications Note TA279.

Chen, C.-K., Chen, T.-M., "New Hybrid Laplace Transform/Finite Element Method for Three Dimensional Transient Heat Conduction Problem", *International Journal for Numerical Methods in Engineering*, **32**, John Wiley & Sons Ltd., 1991, pp 45-61.

Chen, D.-J., Wu, S. –C., Xiang, Y.-B., Li, M.-Q., "Simulation of three dimensional transient temperature field during laser bending of sheet metal", *Materials Science and Technology*, **18**, IoM Communications Ltd., February 2002, pp. 215 -218.

Chen, P. C., Ramkumar, R. L., "RAMPC – An integrated three-dimensional design tool for processing composites", *33rd International SAMPE Symposium*, SAMPE, March 7-10, 1988, pp. 1697-1708.

Clarke, S., *Field Repair of Composite Plates Using Fibre Metal Laminates*, M.A.Sc. Thesis, Department of Mechanical and Aerospace Engineering, Carleton University, Ottawa, Canada, 2002.

Dennis, H. B., Dulikravich, G. S., "A 3-D finite element formulation for the determination of unknown boundary conditions in heat conduction", *Inverse*

Problems in Engineering Mechanics III: International Symposium on Inverse Problems in Engineering Mechanics (ISIP 2001), Elsevier Science, 2002, pp. 67-77.

Kaminski, M., "Homogenization technique for transient heat transfer in unidirectional composites", *Communications in Numerical Methods in Engineering*, **19**, No. 7, John Wiley & Sons, Ltd., 2003, pp. 503-512.

Großmann, K., Mischke, M., "A non-steady-state probe measurement method to determine heat conductivity, heat capacity as well as moisture in solids and bulk materials", *Measurement*, **14**, Elsevier Science B. V., 1995, pp. 191-197.

Gustafsson, S. E., Karawacki, E., Khan, M. N., "Determination of the thermal-conductivity tensor and the heat capacity of insulating solids with the transient hot-strip method", *Journal of Applied Physics*, **52**, No. 4, American Institute of Physics, April 1981, pp. 2596-2600.

Hasselman, D. P. H., Johnson, L. F., "Effective Thermal Conductivity of Composites with Interfacial Thermal Barrier Resistance", *Journal of Composite Materials*, **21**, Technomic Publishing Co., Inc., June 1987, pp. 508-515.

James, B. W., Keen, G. S., "A nomogram for the calculation of the transverse thermal conductivity of uniaxial composite lamina", *High Temperatures –High Pressures*, **17**, Pion, Great Britain, 1985, pp. 477-480.

Krejsa, J., Sláma, L., Horský, J., Raudenský, M., Pátíková, B., "A comparison of traditional and non-classical methods for solving inverse heat conduction problem", *Fourth International Conference on Advanced Computational Methods in Heat Transfer*, Computational Mechanics Publication, 1996, pp. 451-461.

Ling, J. P. C. W., Ireland, P. T., Turner, L., "A Technique for Processing Transient Heat Transfer, Liquid Crystal Experiments in the Presence of Lateral Conduction", *Journal of Turbomachinery*, **126**, ASME, April 2004, pp. 247-258.

Lloyd, G., Kim, K.J., Razani, A., Feldman, K. T., "Thermal conductivity measurements of metal hydride compacts for high-power reactors", *Journal of Thermophysics and Heat Transfer*, **12**, No. 2, American Institute of Aeronautics and Astronautics, Inc., 1998, pp. 132-137.

Lundblad, W. E., Starrett, H. S., Wanstall, C. W., "Thermal conductivity test technique for thermal management composite materials", *26th International SAMPE Technical Conference*, SAMPE, October 17-20, 1994, pp. 774-778.

Mahishi, J. M., Chandra, R., Murthy, M. V. V., "Transient heat conduction analysis of laminated composite nose cone", *The Journal of the Aeronautical Society of India*, **32**, Aeronautical Society of India, 1980, pp. 77-84.

Matsumoto, K., Zako, M., "Study on three dimensional transient thermal stress analysis for laminated composite materials", *Composites for the Pressure Vessel Industry*, **302**, ASME – PVP publication, 1995, pp. 75-80.

MIL-HDBK-17F, Composite Materials Handbook, Volume 3, Polymer Matrix Composites, Materials Usage, Design and Analysis, Department of Defense, USA, 17 June 2002.

Pantano, A., Averill, R. C., "An improved thermal lamination model for analysis of heat transfer in composite structures", *Journal of Composite Materials*, **36**, No. 6, Sage Publications, 2002, pp. 701-719.

Pilling, M. W., Yates, B., Black, M. A., Tattersall, P., "The thermal conductivity of carbon fibre-reinforced composites", *Journal of Materials Science*, **14**, Chapman and Hall Ltd, Great Britain, 1979, pp. 1326-1338.

Progelhof, R. C., Throne, J. L., Ruetsch, R. R., "Methods for Predicting the Thermal Conductivity of Composite Systems: A Review", *Polymer Engineering and Science*, **16**, No. 9, September 1976, pp. 615-625.

Rasekh, A., Vaziri, R., Poursartip, A., "Simple Techniques for Thermal Analysis of the Processing of Composite Structures", SAMPE, 2004.

Roberts, J. C., Luesse, M. H., Magee, T. C., "A technique for locally increasing surface heat spreading and through-thickness thermal conductivity of graphite/epoxy laminates", *Journal of Composite Materials*, **30**, No. 2, Technomic Publishing Co., Inc., 1996, pp. 231-247.

Rudd, C. D., Middleton, V., Owen, M. J., Long, A. C., McGeehin, P., Bulmer, L. J., "Modelling the processing and performance of performs for liquid moulding processes", *Composites Manufacturing*, **5**, No. 3, Butterworth-Heinemann Ltd., 1994, pp 177-186.

Singh, A. K., Mazumdar, D., "Mathematical modelling of thermal fields in some heat treatment operations", *Steel Research*, **63**, No. 5, 1992, pp. 194-200.

Stephenson, D. G., Mitalas, G. P., "Calculation of Heat Conduction Transfer Functions for Multi-layer Slabs", *Research Paper of the Division of Building Research*, **610**, Division of Building Research, National Research Council, Ottawa, Canada, 1971.

Sutradhar, A., Paulino, G. H., Gray, L. J., "Three-Dimensional Transient Heat Conduction in Functionally Graded Materials", *IABEM 2002, International Association for Boundary Elements Methods, UT Austin, Texas*, May 28-30, 2002.

Tamma, K. K., Yurko, A. A., "Finite-element thermal modeling/analysis formulations for layered composite materials", *Numerical Heat Transfer, Part B*, **15**, Hemisphere Publishing Corporation, 1989, pp. 73-97.

Tsai, C. F., Nixon, G., "Transient Temperature Distribution of a multilayer composite wall with effects of internal thermal radiation and conduction", *Numerical Heat Transfer*, **10**, Hemisphere Publishing Corporation, pp. 95-101.

Traceability of Temperature Measurement; Platinum Resistance Thermometers, Thermocouples, Liquid-in-glass Thermometers and Radiation Thermometers, Ref: LAB 11, UKAS Publication, September 2000.

Tucker, C. L., Dessenberger, R. B., "Chapter 8; Governing equations for flow and heat transfer in stationary fiber beds", Flow and Rheology in Polymer Composites Manufacturing edited by Advani, S. G., Elsevier Science B. V., 1994, pp. 257-323.

Wang, Y. R., Chou, T.-W., "Three-Dimensional Transient Interlaminar Thermal Stresses in Angle-Ply Composites", *Journal of Applied Mechanics*, **56**, No. 3, ASME, September 1989, pp. 601 -608.

APPENDIX A: PREDICTIVE FEM RESULTS

List of Figures

List of Tables

In this appendix the results for all the predictive FEM cases are given. The results are provided in the form of time and radial temperature profiles. The configurations used for this study are given in the following table:

Table A- 1: Summary of Predictive Simulation Configurations

Configuration	Boundary Condition	Heater Blanket Output
1	Adiabatic	100%
2	Convection h = 0.5 W/m^2K	100%
3	Convection h = 1 W/m^2K	100%
4	Convection h = 1.5 W/m^2K	100%
5	Convection h = 0.5 W/m^2K	80%
6	Convection h = 1 W/m^2K	80%
7	Convection h = 1.5 W/m^2K	80%

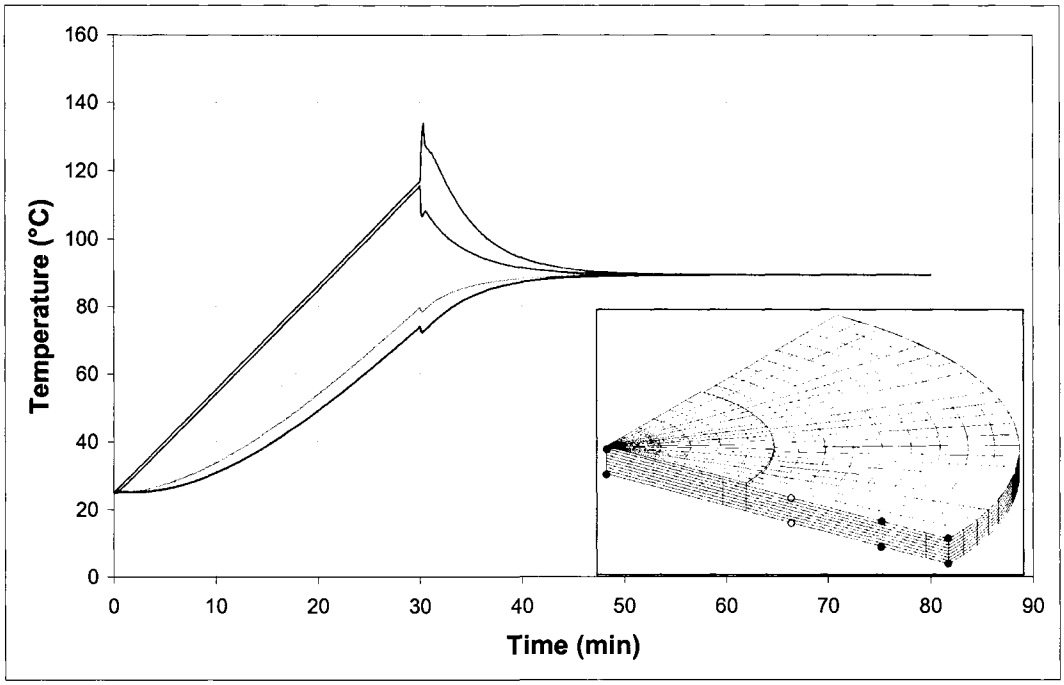

Figure A-1: Process Temperature Profile for Configuration 1

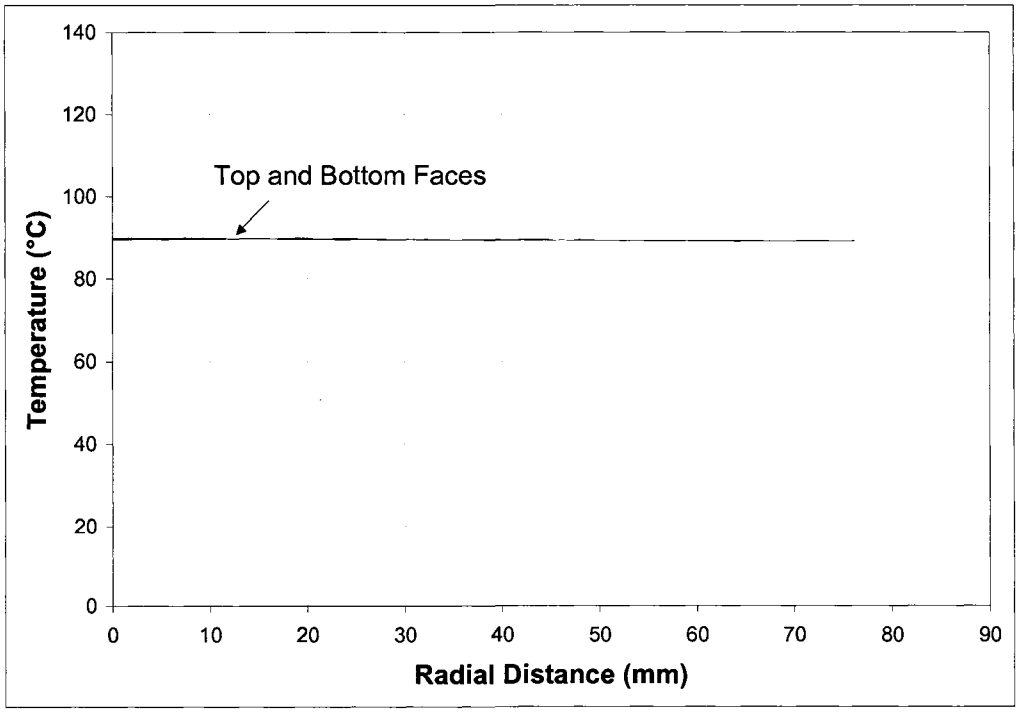

Figure A- 2: Radial Temperature Profile for Configuration 1

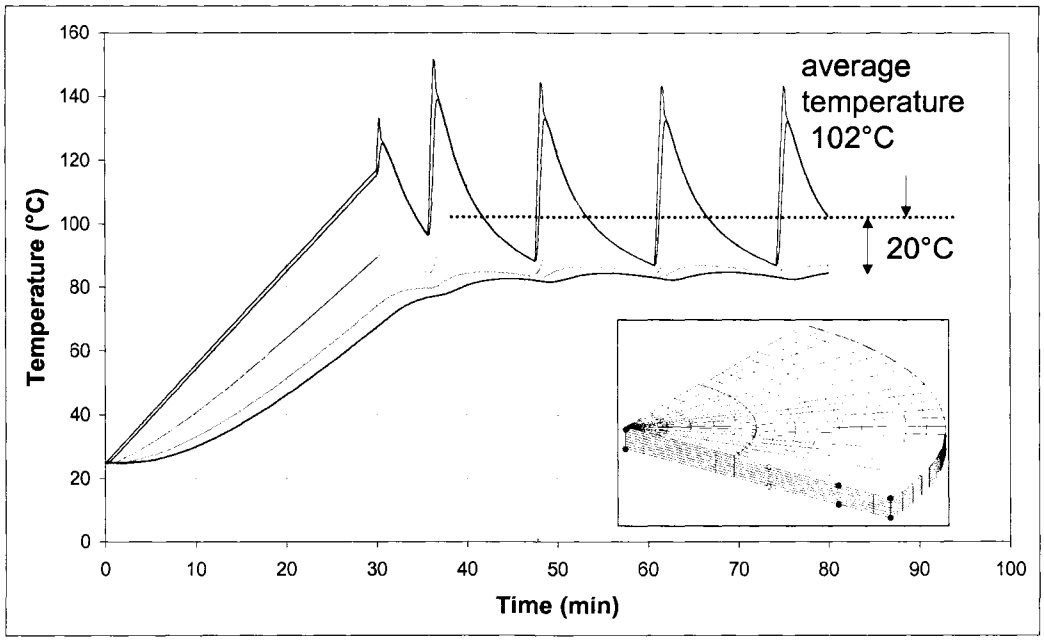

Figure A- 3: Process Temperature Profile for Configuration 2

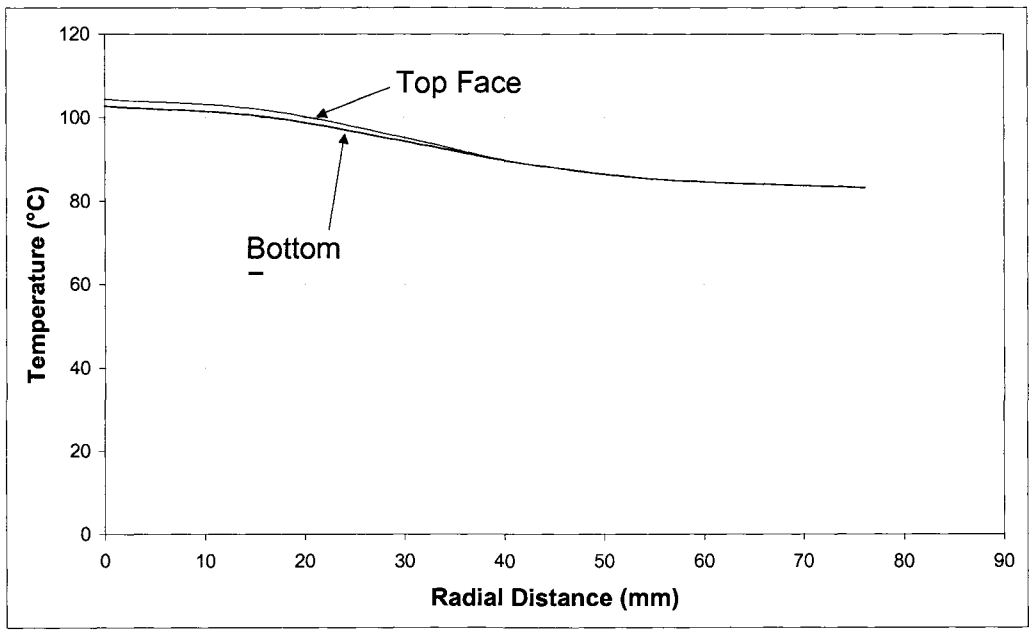

Figure A- 4: Radial Temperature Profile for Configuration 2

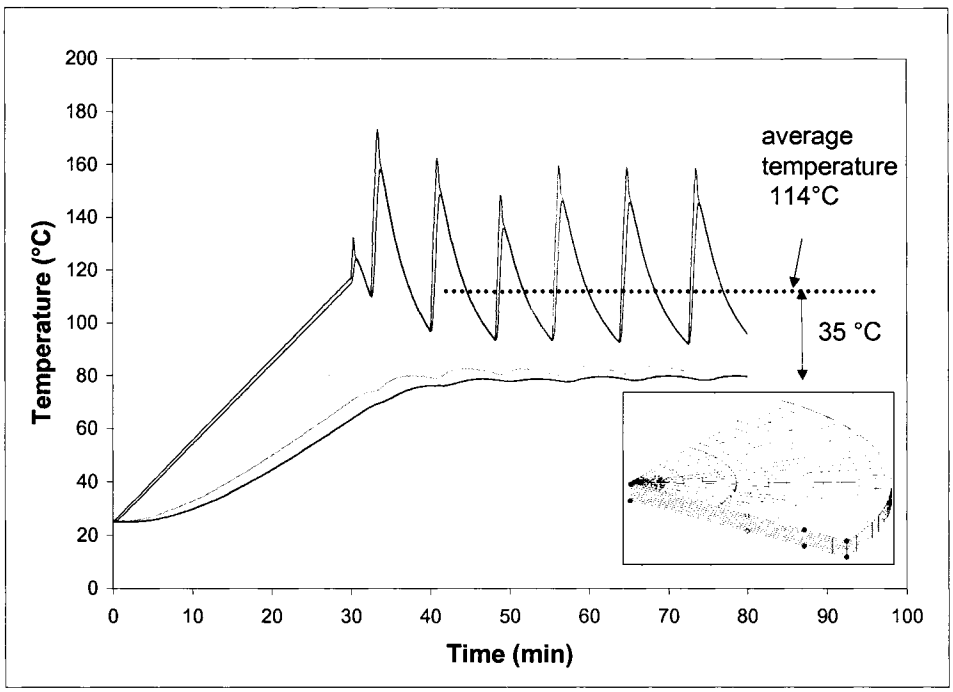

Figure A- 5: Process Temperature Profile for Configuration 3

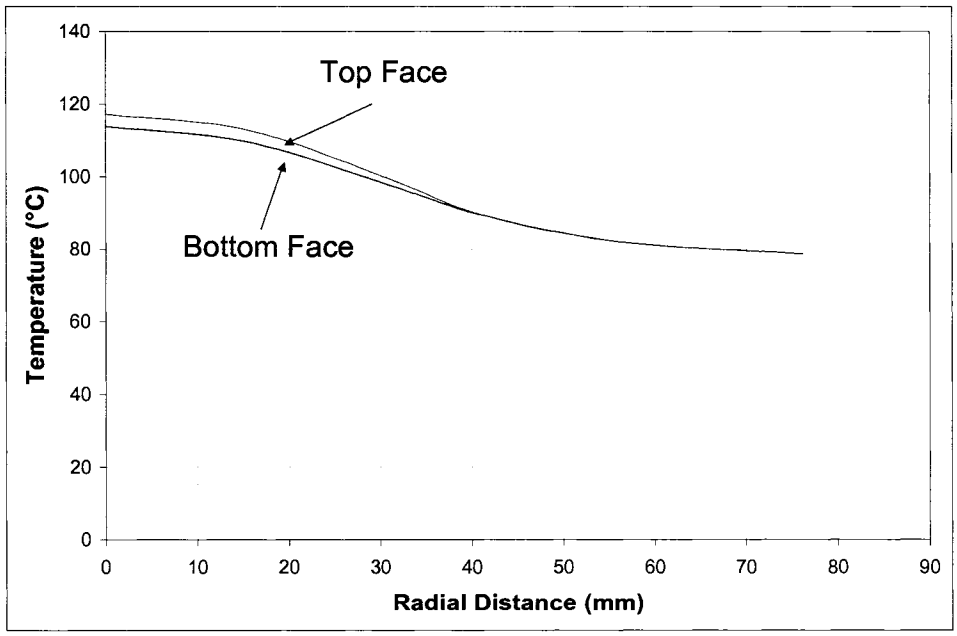

Figure A- 6: Radial Temperature Profile for Configuration 3

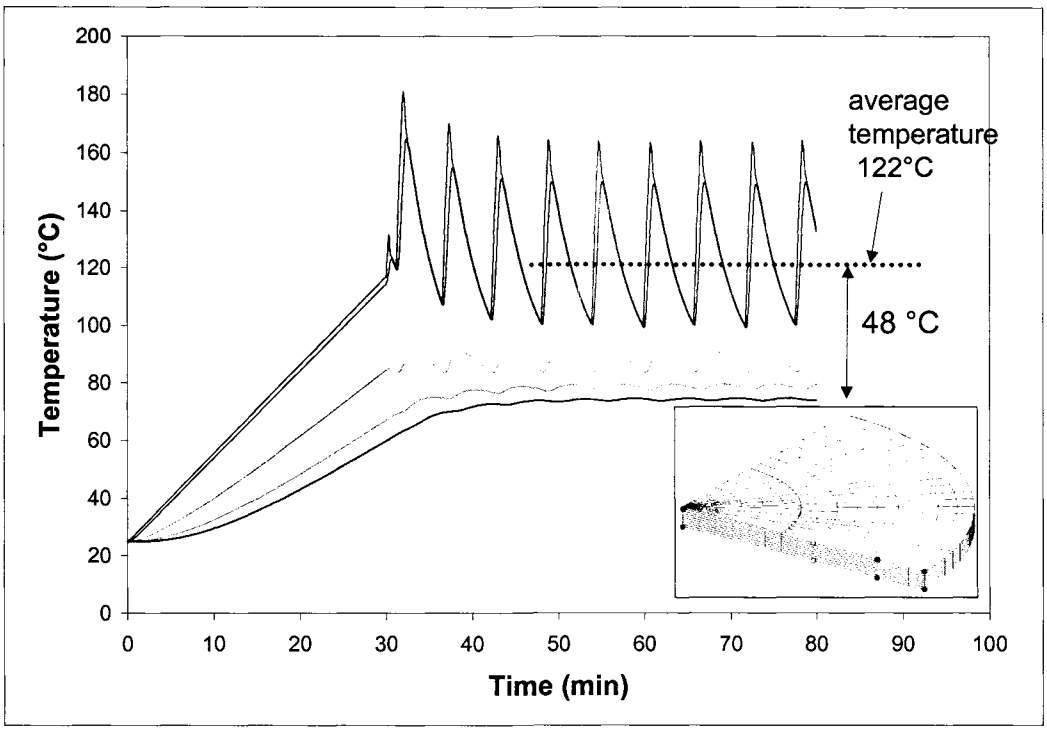

Figure A- 7: Process Temperature Profile for Configuration 4

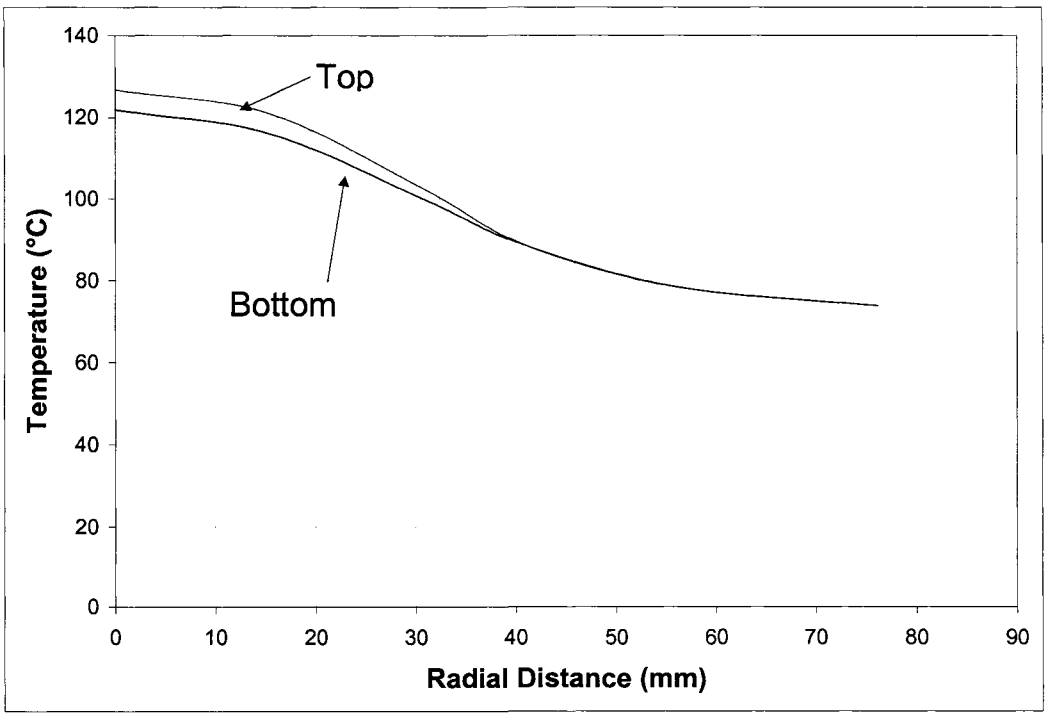

Figure A- 8: Radial Temperature Profile for Configuration 4

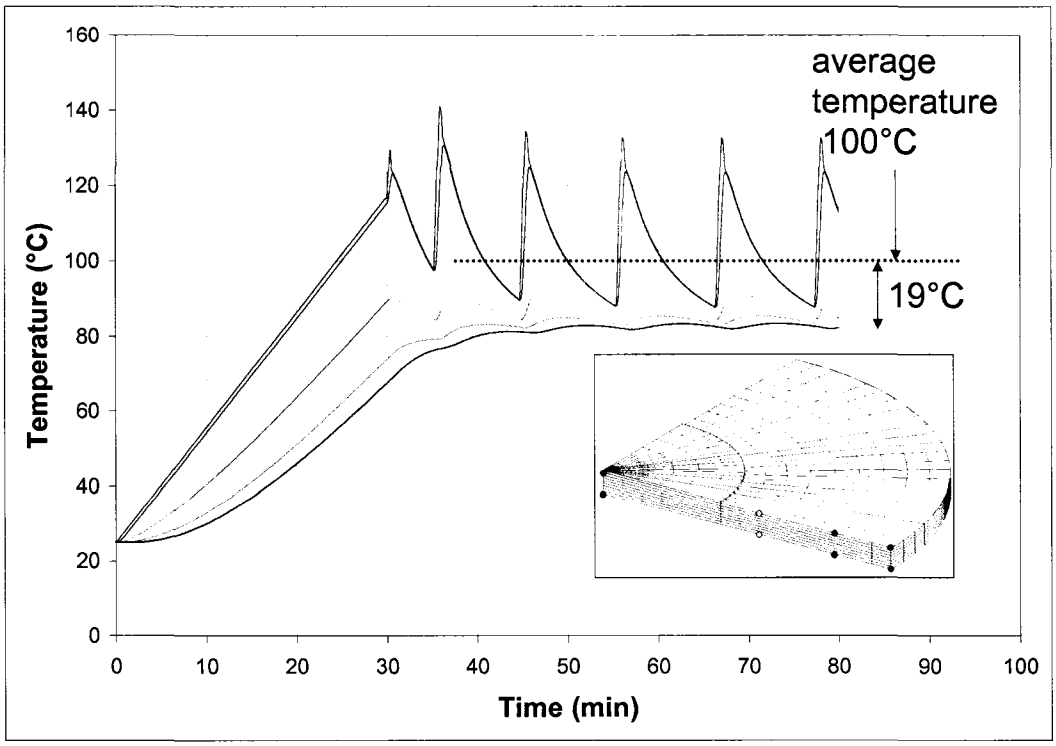

Figure A- 9: Process Temperature Profile for Configuration 5

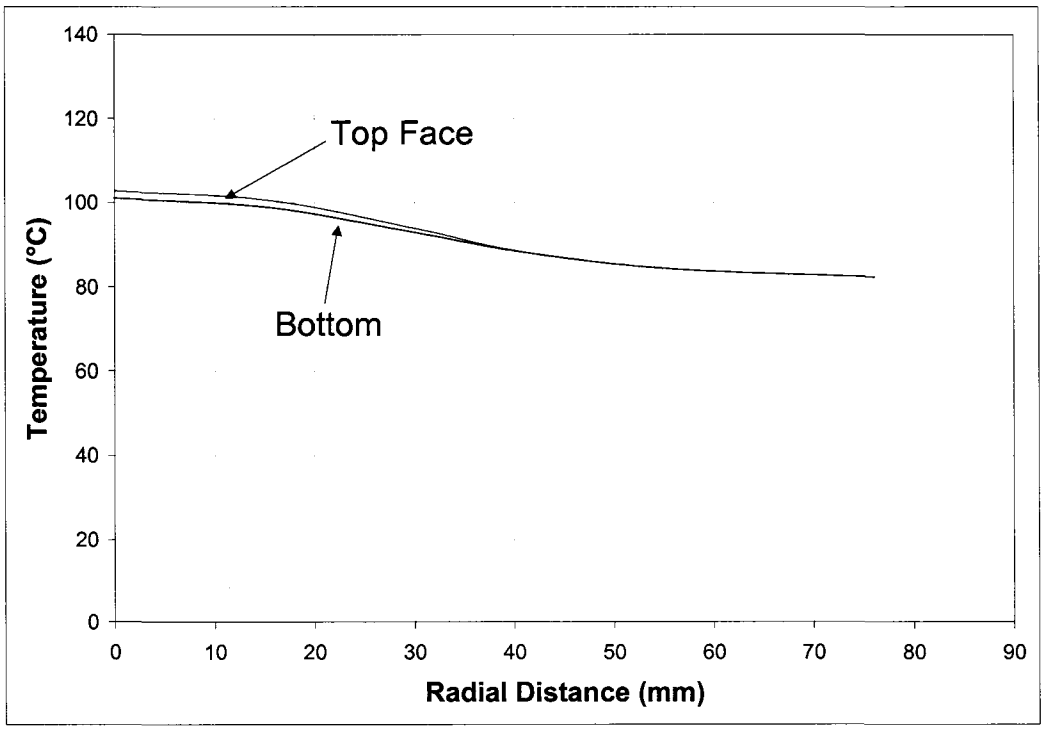

Figure A- 10: Radial Temperature Profile for Configuration 5

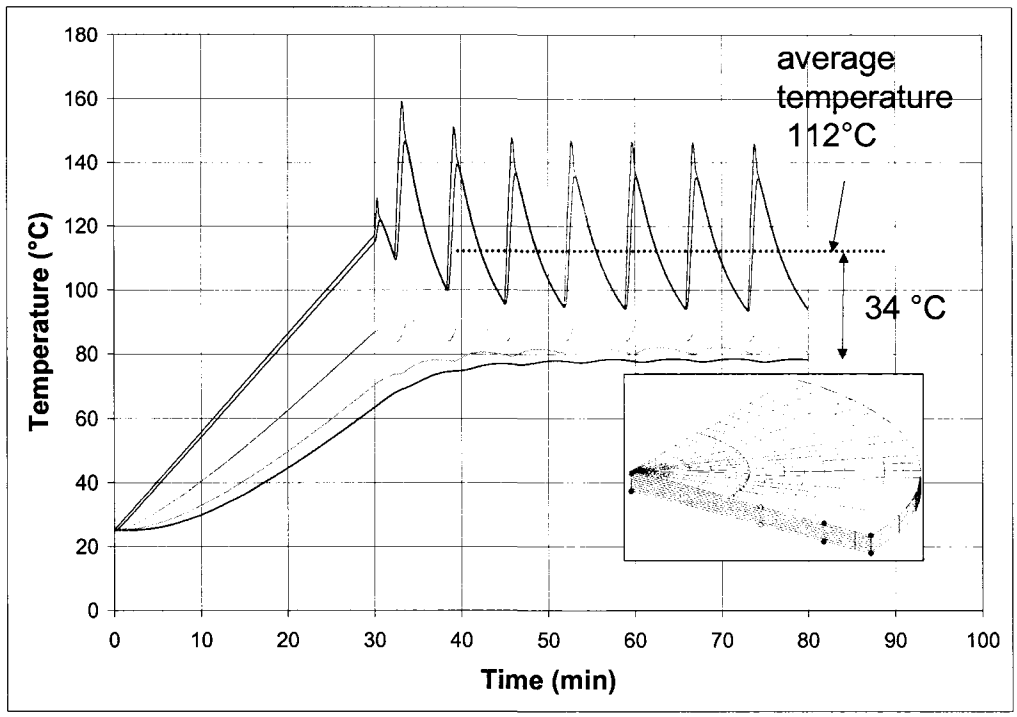

Figure A- 11: Process Temperature Profile for Configuration 6

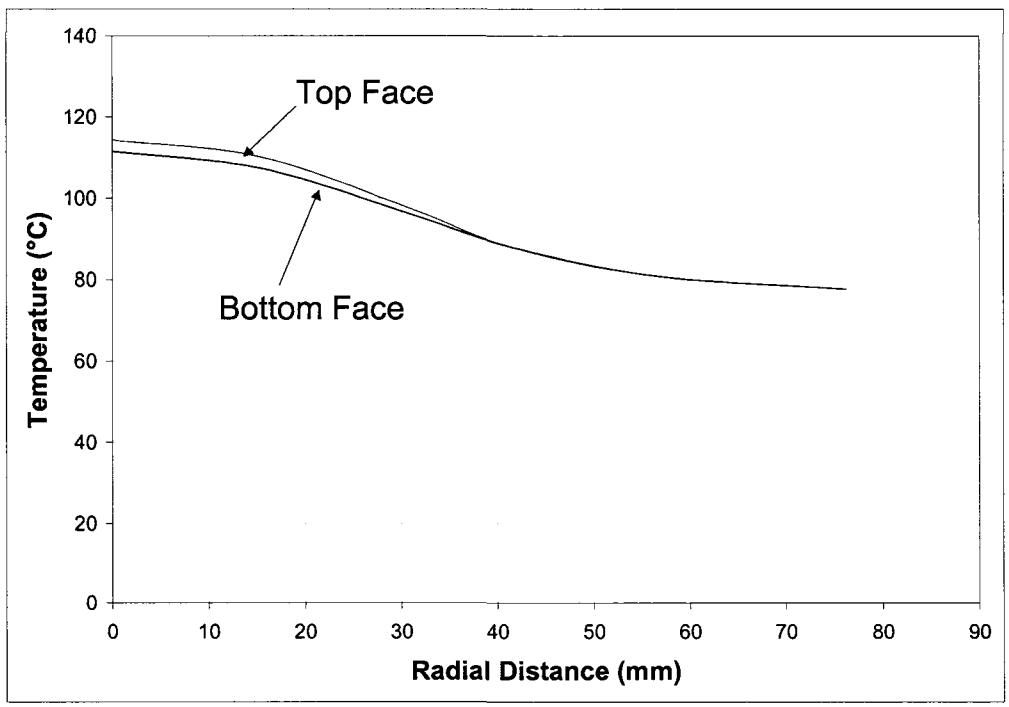

Figure A- 12: Radial Temperature Profile for Configuration 6

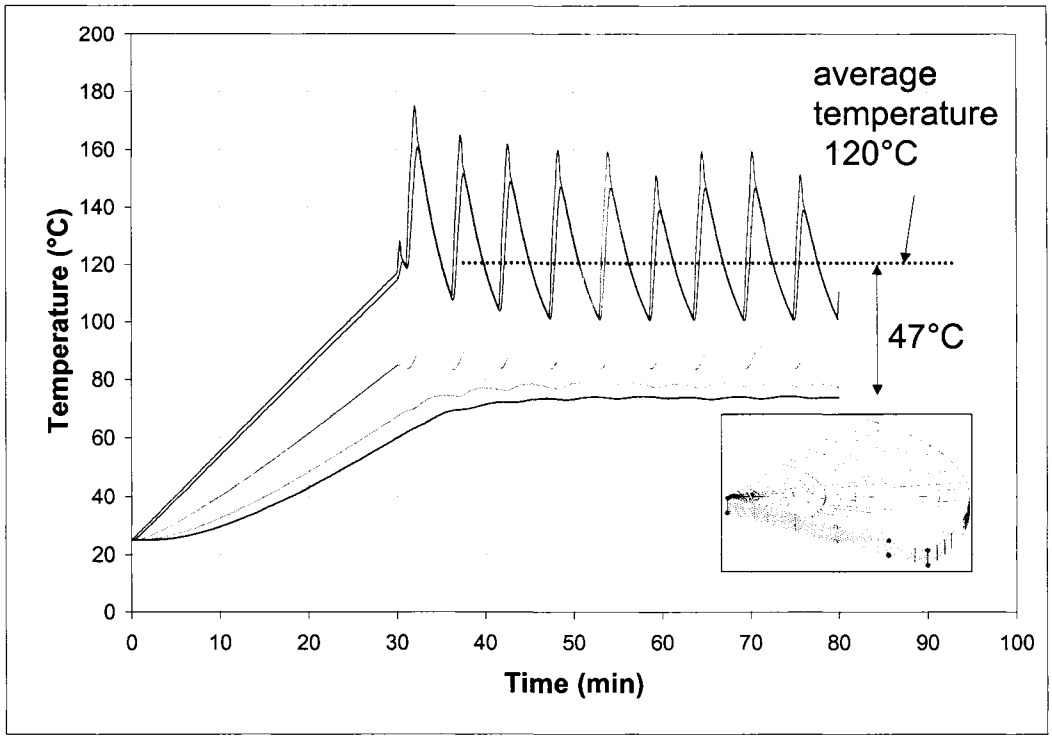

Figure A- 13: Process Temperature Profile for Configuration 7

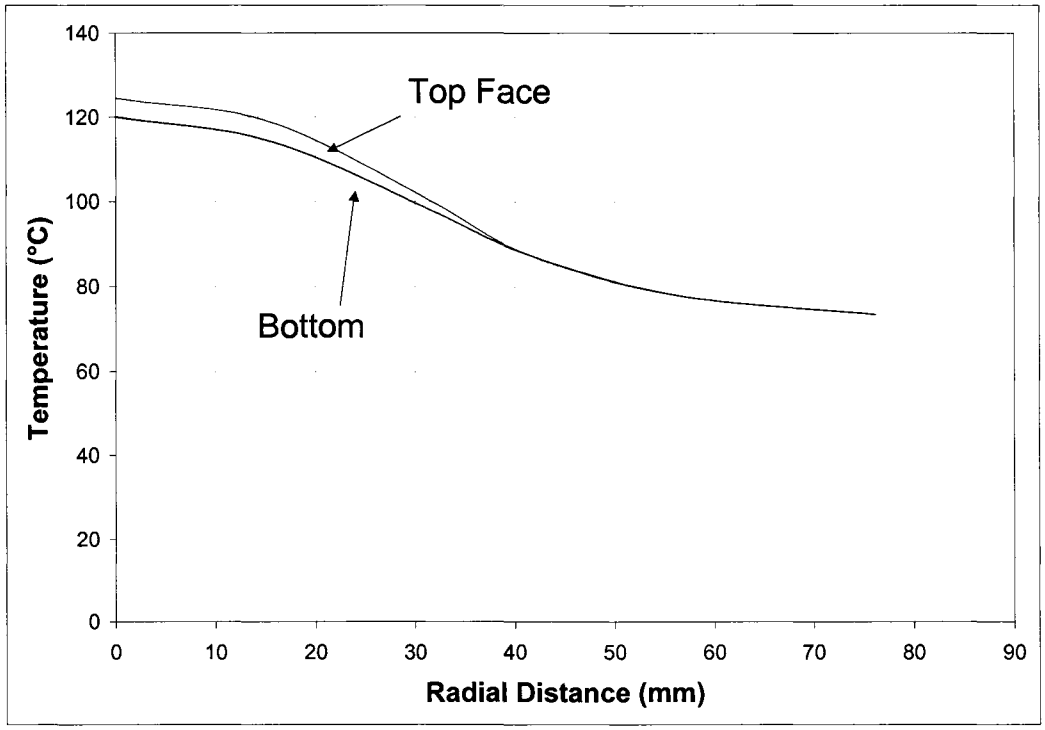

Figure A- 14: Radial Temperature Profile for Configuration 7